Sedimentary cycles in coal and evaporite basins and the reconstruction of Palaeozoic climate

F.J.G. van den Belt

Utrecht Studies in Earth Sciences

Mededelingen van de
Faculteit Geowetenschappen
Universiteit Utrecht

No. 21

Members of the dissertation committee

Prof. dr. S.A.P.L. Cloetingh
Tectonics Research Group
Department of Earth Sciences, University of Utrecht

Prof. dr. C.G. Langereis
Paleomagnetic Laboratory 'Fort Hoofddijk'
Department of Earth Sciences, University of Utrecht

Prof. dr. L.J. Lourens
Stratigraphy and Palaeontology Research Group
Department of Earth Sciences, University of Utrecht

Prof. dr. F. Roure
Institut Français du Pétrole Energies Nouvelles
Rueil-Malmaison, France

Prof. dr. M.E. Tucker
School of Earth Sciences
University of Bristol, United Kingdom

ISBN 978-90-6266-307-1
Sedimentary cycles in coal and evaporite basins and the reconstruction of Palaeozoic climate, viii + 100 p., 6 tables, 43 illustrations. This is Publication 21 of *Utrecht Studies in Earth Sciences*.

Author contact details: F.J.G. van den Belt, Timmermeesterslaan 24, 8014 EL Zwolle, Netherlands
E-mail: f.j.g.vandenbelt@uu.nl, fvdbelt@gmail.com

Printed by Wöhrmann Print Service (Zutphen) in an edition of 200 copies.

Cover photo: Road cuts in the Middle Pennsylvanian Pikeville Fm. (Breathitt Group) near the town of Sidney, Kentucky (USA) along the westbound lane of US-119 between Pikeville (KY) and Williamson (WV). Coal-bearing facies in foreground comprise Upper Elkhorn no. 3 Sandstone, overlain by Upper Elkhorn no. 3 coastal-plain succession, Elfins Fork Shale and Amburgy Sandstone; the overlying dark grey Kendrick Shale (Base Hyden Fm.) is visible at far right. Photo taken on 15 April 2012.

Sedimentary cycles in coal and evaporite basins and the reconstruction of Palaeozoic climate

Sedimentaire cycli in kool- en evaporietbekkens
en de reconstructie van het klimaat tijdens het Paleozoïcum

(met een samenvatting in het Nederlands)

PROEFSCHRIFT

ter verkrijging van de graad van doctor aan de Universiteit Utrecht
op gezag van de rector magnificus, prof.dr. G.J. van der Zwaan,
ingevolge het besluit van het college voor promoties
in het openbaar te verdedigen op

vrijdag 12 oktober 2012 des middags te 16.15 uur

door

Franciscus Joannes Gerardus van den Belt
geboren op 2 november 1969 te Zwolle

Promotor:

Prof. dr. P.L. de Boer

Voor Heleen, Lucas en Mijntje

Once you were tethered
Now you are free
That was the river
This is the sea

(M. Scott, 1985)

CONTENTS

Chapter 1

INTRODUCTION : SEDIMENTARY CYCLES IN COAL AND EVAPORITE BASINS AND THE RECONSTRUCTION OF PALAEOZOIC CLIMATE

F.J.G. van den Belt

The Palaeozoic era lasted from ~542 to ~251 Ma (Gradstein et al. 2004). Its beginning is marked by the Cambrian explosion of life and its end by the greatest mass extinction in Earth history. Other mass-extinction events occurred at the end of the Cambrian, Ordovician, Silurian and Devonian (Raup and Sepkoski 1982). The only boundary that is not associated with a mass extinction is the Carboniferous to Permian transition. However, at that time a major floral reorganization took place with 'coal swamps' relocating from equatorial positions to high latitudes concurrent with equatorial drying (DiMichele et al. 2001).

Besides this evolutionary punctuation, the Palaeozoic periods were characterized by certain dominant modes of sedimentation (Stanley 1986). For instance, shallow-water carbonates are very common in the Cambrian rock record and Ordovician-Silurian rocks are at many places characterized by marine (black) shales of deeper-water origin.

Evaporite deposits occur throughout the Palaeozoic. They are abundant in Cambrian, Devonian and Permian rocks and rare in the intervening Ordovician, Silurian and Carboniferous (Zharkov 1981). Coal-bearing rocks are present from the Middle Devonian onwards, which is related to the evolution of land plants during the Silurian-Devonian (Davies and Gibling 2010). Coals are abundant in Upper Carboniferous strata in basins along the palaeoequator, and are common throughout the Permian as well. These Permian coals were formed at high latitudes (Michaelsen and Henderson 2000).

Both the evolutionary and the sedimentological history of the Palaeozoic point at a strong influence of climate (Frakes et al. 1992, Davies and Gibling 2010) with major climate changes marking the period boundaries. The abundance of coal during the Late Carboniferous and Permian has since long been attributed to glacio-eustatic sea-level fluctuations associated with widespread southern-hemisphere glaciation during the Late Palaeozoic (Veevers and Powell 1987). Another glaciation occurred during the Ordovician-Silurian, but it predates the rise of land plants (Davies and Gibling 2010).

The three main phases of evaporite precipitation occurred during greenhouse periods and are (largely) out of phase with the two Palaeozoic glacial episodes. Only during the Permian, glacial conditions were contemporaneous with widespread evaporite deposition (Frakes et al. 1992). In this thesis the focus is on evaporites and coal-bearing rocks as the sedimentary reflections of two climate extremes: greenhouse and icehouse. At the same time it chronologically discusses the Late Palaeozoic depositional history of northwestern Europe: from coal-bearing fluvio-deltaic deposition during the Late Carboniferous (Pennsylvanian) followed by aeolian-dune and desert-lake deposition in a continental, proto-evaporite basin during the Early Permian (Rotliegend) to evaporite precipiation in a restricted marine basin during the Late Permian (Zechstein).

Sedimentary cycles in coal and evaporite basins

The strata in coal and evaporite basins are both characterized by distinct sedimentary cyclicity, although on a different scale. Coal-clastic cycles, also known as 'cyclothems', are metre- to decametre-scale alternations of (marginal) marine shales and terrestrial shales, sands and coal beds (Weller 1930, Greb et al. 2008). These cycles have since long been attributed to glacio-eustatic sea-level fluctuations in the Milankovitch frequency band (Veevers and Powell 1987, Klein and Willard 1989), but orbital control has not been unambiguously demonstrated and remains to be challenged (Wilkinson et al. 2003).

Evaporite cycles are thicker and less numerous than coal cycles. They are typically a few tens to hundreds of metres thick and comprise precipitation successions of calcium sulphate (gypsum/anhydrite), followed by halite and various 'potash' salts (Hardie 1991, Kendall 1992). The origin of such cycles is still debated, partly because there are no present-day analogues. They are variably attributed to glacio-eustatic sea level (Tucker 1991, Warren 2010) and tectonic events (Benson 1972, Krijgsman et al. 1999).

Overview of this thesis

This thesis deals with sedimentary cycles in coal basins (chapter 2 and 3), and sedimentary cycles in evaporite basins (chapters 4-6). In the final chapter 7 coal and especially evaporite deposition throughout the Palaeozoic era are studied in an attempt to analyse their relation with large-scale Palaeozoic climate fluctuations.

In *chapter 2* the emphasis is on the controls of glacio-eustatic sea-level fluctuations on cyclothem formation. A long and continuous core from a high-subsidence area in the Netherlands is analysed quantitatively and compared with a time-equivalent succession from a medium-subsidence area in Kentucky, USA. The study demonstrates that eccentricity signals can be revealed from cyclothem sequences based on facies ratios in subsequent cycles.

In *chapter 3* a cyclothem succession from the Carboniferous of Poland is analysed. The succession is from an area where syndepositional block faulting influenced sedimentation. A quantitative analysis of sediment distribution is used to unravel how tectonics influenced sedimentation.

Chapter 4 deals with the origin of gas-bearing aeolian cycles from the 'proto-evaporite' Rotliegend (Permian) Basin. The cycles formed at the margin of a hypersaline lake, that contracted and expanded repeatedly. The internal architecture and the thickness of these cycles is related to the infilling of palaeotopography overprinted by climate-controlled lake-level changes.

Chapter 5 deals with the role of isostatic subsidence in evaporite basins. Such basins are typically viewed as very deep, dried-out basins. Incorporation of isostatic subsidence in response to the (very fast) precipitation of salts suggests that deposition occurred in much shallower, non-desiccated basins.

Chapter 6 describes an alternative model to explain evaporite-cycle formation, which is fully dependent on processes operating within the evaporite basin. It is based on the idea that sulphate precipitation along a basin margin progressively obstructs the outflow of dense brines and thus leads to increased salinities and accelerated salt precipitation. The mechanism is validated by numerical modelling and compositional data from Palaeozoic evaporite basins.

Chapter 7 deals with long-term trends in coal and evaporite deposition that line up well with Palaeozoic mass extinctions. It is suggested that a regular, long-term climate oscillation operated during the Palaeozoic and possibly continued into the Mesozoic and Cenozoic.

Chapter 2

REVEALING THE HIDDEN MILANKOVITCH RECORD IN PENNSYLVANIAN CYCLOTHEM SEQUENCES; INFERENCES WITH RESPECT TO LATE PALAEOZOIC CHRONOLOGY, GLACIO-EUSTASY AND COAL ACCUMULATION

F.J.G. van den Belt, T.B. van Hoof and H.J.M. Pagnier

The coal-rich Pennsylvanian cyclothem sequences from Euramerica have since long been related to sea-level fluctuations caused by the waxing and waning of southern-hemisphere ice caps. Although many studies have shown that cycle periods are in the Milankovitch range, orbital control has not been demonstrated unambiguously. We show that a sea-level signal cannot be reconstructed based on cyclothem thickness alone, but requires the analysis of compositional variations of subsequent cyclothems.

We analysed a Duckmantian-Bolsovian (Westphalian B-C) sequence from a high-subsidence area in the Netherlands and a Duckmantian sequence from a medium-subsidence area in Kentucky, USA. For each cyclothem we recorded the percentage of subaerial facies and the coal percentage of each subaerial interval, and correlated the two sequences based on well-established marine-band stratigraphy. The overlapping Duckmantian interval shows correlatable patterns for the subaerial ratio and coal percentage. The Kentucky record has a lower resolution because of lower subsidence and the preservation of – on average - only one out of four cyclothems.

The 1728 m thick Dutch record shows a distinct two-fold cyclicity in the subaerial-facies ratio at wavelengths of ~255 m and ~60 m. Based on recent U/Pb ages this yields cycle periods of approximately 395 ky and 93 ky, indicating long and short-eccentricity control. Individual cyclothems have highly variable thicknesses, but all on a sub-eccentricity scale and with an average duration of ~21 ky. This probably reflects the interference of different cycles with a high-enough amplitude for precession to cause splitting of longer-period cycles into subcycles.

Integration of our results with radiometric age datings indicates that the duration of the Westphalian stage is ~7 My and that the ages of the substage bases (U/Pb calibrated) are approximately ~317.6 (Langsettian), ~315.6 (Duckmantian), ~314.4 (Bolsovian) and ~312.4 Ma (Asturian). Based on this, the estimated coal-accumulation rate in the Netherlands was 5-10 m/My for the Late Langsettian and Early Duckmantian and increased abruptly to ~25 m/My at 315.1 Ma. Coal accumulation rates in Kentucky were much lower. However, when standardized to Dutch subsidence, the patterns are identical. This suggests that carbon storage in the Late Palaeozoic terrestrial system was controlled by climate rather than by local sedimentary conditions, and experienced a uniform variation along the Euramerican palaeo-equatorial coal belt.

Introduction

Pennsylvanian cyclothems, deposited in palaeo-equatorial Euramerican basins during the Late Palaeozoic ice-house period, are a classic example of sedimentation controlled by glacio-eustasy, with sea-level fluctuations driven by the waxing and waning of southern-hemisphere ice caps (Veevers and Powell 1987). Apart from controlling the alternation of marine and non-marine sediments, sea-level fluctuations controlled the formation of one or more coal beds in most of these cycles (Flint et al. 1995). Pennsylvanian coal beds constitute the largest reservoir of terrestrial carbon on the globe (Berner 2003). Hence,

when linked with volcanic-ash dates, thick cyclothem successions may not only hold the key to detailed reconstruction of sea-level fluctuations during a major ice age and to the fine-tuning of Late Palaeozoic chronology, but in addition to accurate estimates of global carbon fixation rates in coal swamps.

Although estimated cyclothem periods are in the Milankovitch range (Heckel 1986, Maynard and Leeder 1992) and cyclothem bundling patterns match Milankovitch-cycle ratios (Busch and Rollins 1984, Heckel 1986), orbital control has not been demonstrated unambiguously and lacks a strong quantitative support (Algeo and Wilkinson 1988, Wilkinson et al. 2003). Difficulties in matching data with the Milankovitch model include poor time control (Klein 1990), incomplete sequences (De Boer 1991), non-linear time-sediment relations (Algeo and Wilkinson 1988), and the interference of multiple cycle periods (De Boer 1991). Therefore, the extraction of accurate sea-level records, which could contribute to the understanding of ice-sheet dynamics, terrestrial carbon storage and other aspects of palaeoclimate, remains a challenge.

In older studies Pennsylvanian cycle periods are variably linked with precession (17 ky), obliquity (35 ky) and short and long eccentricity (95-413 ky) (Heckel 1986, Klein 1990, De Boer 1991, Maynard and Leeder 1992, Goldhammer et al. 1994), but the low resolution of the Pennsylvanian time scale hampered detailed cycle determinations (Klein 1990). In various recent studies, however, it is concluded that cyclothem deposition during the Pennsylvanian was forced by short eccentricity (Greb et al. 2008, Eros et al. 2012a, Waters and Condon 2012). The alleged Pennsylvanian dominance of short-eccentricity is not in line with Quaternary insolation models. These predict alternating eccentricity and obliquity control, as well as some influence of precession (Ruddiman 2006), which is reflected in $\delta^{18}O$ records for much of the Quaternary (Hays et al. 1976, Raymo et al. 1990).

Most cyclothem studies have been performed in low to medium subsidence areas in the USA and the UK, where Pennsylvanian successions are relatively thin (~100s m to ~1 km). In high-subsidence areas such as Nova Scotia and continental Europe, Mid-Pennsylvanian sequences are many kilometres thick (Drozdzewski 1993, Falcon-Lang 2001) and cyclothems are so numerous that they must represent shorter time intervals to be consistent with age data. Hence, the interpreted dominance of eccentricity cycles in low to medium subsidence areas could well be preservation-driven. Chesnut (1997) already noted that cyclothems with a ~100 ky duration in the central Appalachian Basin grade into cyclothems with a 400 ky duration towards areas of lower subsidence, indicating that multiple depositional hiatuses and/or erosion surfaces may characterize areas of low accommodation.

In this study we analysed a Langsettian-Bolsovian (Westphalian A-C) cyclothem succession from a high subsidence area in the Netherlands, which is ~1728 m thick and covers 145 cyclothems. The interval was cored completely, allowing us to study the gradual compositional variation of cyclothems over time. This resulted in a much higher resolution cyclicity interpretation than based on cyclothem thickness alone. We compared the succession with a partly overlapping cyclothem succession in a medium-accommodation setting from Kentucky (USA) that we measured in outcrops to see how subsidence rate affected deposition and the preservation of cyclothems. Results are used to refine Middle Pennsylvanian chronology and to determine carbon-storage rates for coal basins.

Periodicity in cyclothem records

Thickness and average cycle length have been the primary data source in cyclothem analysis. Thus far this has not yielded conclusive evidence in terms of cycle periods. This may be related to the above mentioned problems, such as poor time control, but may be intrinsic to the method as well. Counterintuitively cyclothem boundaries are not typically created at sea-level highstand or lowstand. For example, it may take many thousands of years before rising sea level causes flooding of the land and before deposition of marine shales on top of a previous cycle starts. This is illustrated by the example in Figure 1, which is based on the theoretical depositional model of Jervey (1988). It assumes that subaqueous facies are deposited when base level is above the land surface, followed by non-deposition (or local erosion) when it falls below the land surface, fol-

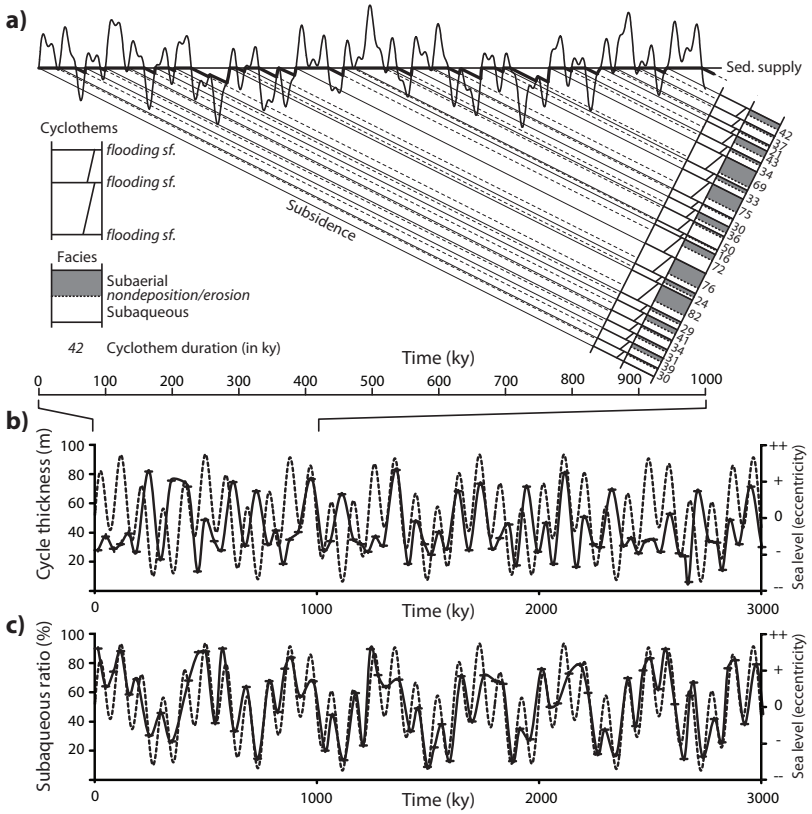

Figure 1 a) Calculated cyclothem sequence based on the deposition model of Jervey (1988). Sea-level curve based on superimposed precession (17 ky), obliquity (35 ky) and short and long eccentricity (95, 413 ky) with relative amplitudes of 0.5, 1, 1, 0.5. **b)** Comparison of the thickness of stacked cyclothems with the input eccentricity signal. **c)** Comparison of the percentage of subaqueous sediment in subsequent cyclothems ('subaqueous ratio') with the input eccentricity signal, showing a much better relation than cyclothem thickness.

lowed by subaerial deposition when rising base-level meets the land surface again and as long as it is balanced by sediment supply. The synthetic sea-level curve in Figure 1 combines precession (17 ky), obliquity (35 ky) and short eccentricity (95/413 ky) cycles (Pennsylvanian cycle periods after Berger and Loutre (1994) and relative amplitudes of 0.5, 1, 1, and 0.5). The resulting cyclothem sequence displays thicknesses as well as the composition of cyclothems in terms of subaqueous and subaerial facies.

The individual cyclothems have a predicted duration between 9 and 82 ky (Fig. 1b). None of the basic input cycles stands out, but with ~50% of the cycles in the 29-39 ky range the record suggests obliquity dominance, although the input sea-level amplitudes for obliquity and short eccentricity were equal. Short eccentricity is represented as trimmed cycles shorter than 82 ky and long eccentricity is faintly present as a long-term fluctuation of cyclothem thickness. A comparison with the eccentricity components of the input sea-level signal shows that the cyclothem thickness fluctuations are locally in phase with sea-level change, but mostly out of phase (Fig. 1b). From the experiment it appears that input sea level can be more accurately reconstructed on the basis of the fluctuation of the percentage of subaqueous facies in subsequent cyclothems (Fig. 1c), which we refer to as the 'subaqueous-

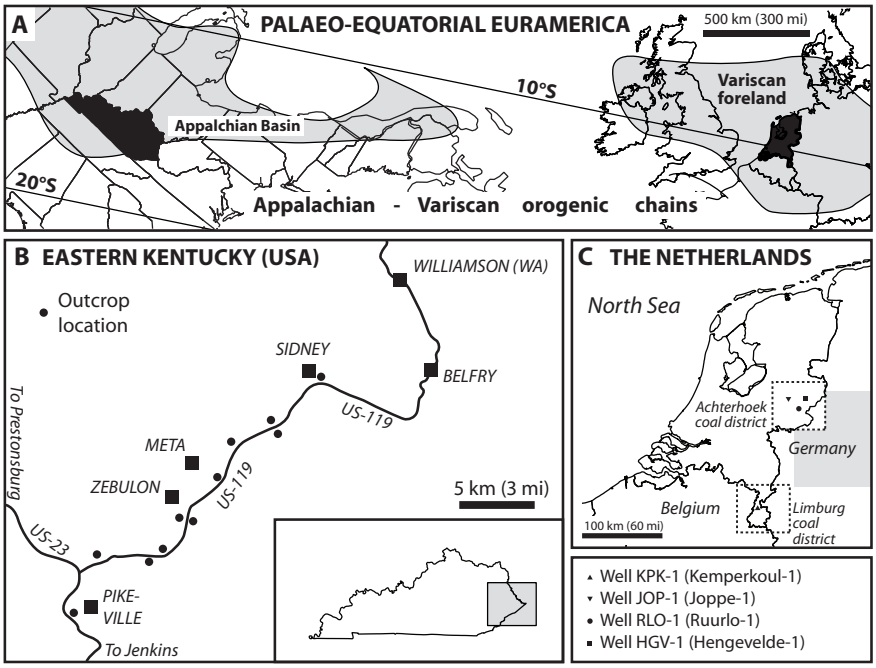

Figure 2 Maps of the two study areas. **a)** Palaeogeographic reconstruction of palaeo-equatorial coal-basins of Euramerica, with the Netherlands and Kentucky (USA) indicated in black (Blakey 2012). **b)** Location of road cuts along US-119 between Pikeville and Sidney, eastern Kentucky. **c)** Well locations in the Netherlands. Grey shaded area in Germany is the study area of Drozdzewski (1993) mentioned in the text.

facies ratio'. In that signal, both the 95 ky and the 413 ky stand out prominently, and a comparison with input sea level shows that peaks line up well with the eccentricity signal (Fig. 1c).

The above experiment may explain why cyclothem-thickness records so far have not yielded conclusive evidence of Milankovitch control, and it indicates that results may be better if the composition of cyclothems is taken into account. Besides the subaqueous-facies ratio we looked at variations of the percentage of coal within the subaerial parts of cyclothems.

The Pennsylvanian of Euramerica

The studied Dutch wells are from the northwest European thermal-sag basin north of the Variscan orogenic chain (Fig. 2), which contains an up to 3-4 km thick Pennsylvanian succession with only gradual thickness variations over relatively great distances throughout most of the basin (Drozdzewski 1993). The studied Kentucky interval is from the central Appalachian Basin, a narrow foreland basin with an up to 1.5 km thick Pennsylvanian succession that rapidly thins westward. Both basins were located near the palaeoequator at latitudes of ~10°S and ~15°S, and were separated by some three thousand kilometres (Blakey, 2012).

In both areas the coal-bearing sequence spans the Langsettian to Bolsovian (Westphalian A-C; Fig. 3) and comprises stacked cyclothems, mostly 10-25 m thick, of alternating (marginal) marine shales and coal-bearing coastal-plain deposits. The lower ~2 km of the Dutch interval is shale-dominated; 10-20 m thick fluvial sandstone bodies only become prominent in the Upper Bolsovian. In Kentucky such sandstone bodies are present throughout the sequence and constitute the basal parts of cyclothems (Aitken and Flint 1995), commonly overlying regionally extensive

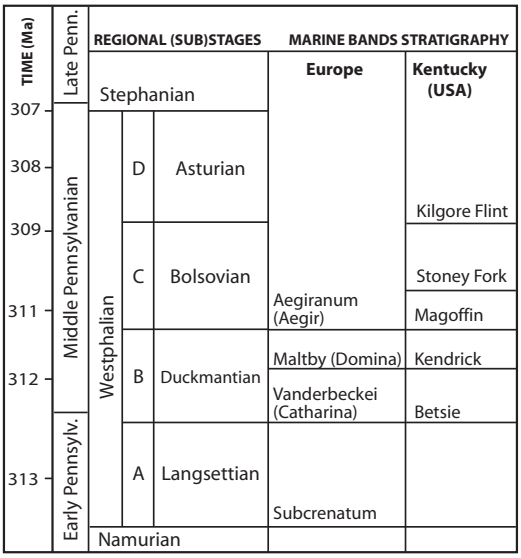

Figure 3 Pennsylvanian stratigraphy in the study areas. Time after Gradstein et al. (2004). Regional stratigraphy based on marine bands, which are correlatable between basins (Riley and Turner, 1995).

erosion surfaces that cut down into underlying strata.

In both areas fossiliferous marine shales are present at the base of the Duckmantian (Vanderbeckei/Betsie) and Bolsovian (Aegiranum/Magoffin), and at approximately 40% below the top of the Duckmantian (Maltby/Kendrick) (Fig. 3). These 'marine bands' are attributed to highstands of global sea level and can be correlated between the basins (Riley and Turner 1995).

Analysis

More than 2.5 km of continuous core from the Pennsylvanian in wells RLO-1, HGV-1, JOP-1 and KPK-1 from the Netherlands were studied (Fig. 2). A 1728 m long composite was built spanning the Late Langsettian-Late Bolsovian (Van der Laar and Fermont 1989). KPK-1 was drilled ~140 km south of the other wells, but regional thickness differences are small (Van der Laar and Fermont 1989). For comparison we recorded a composite sedimentary section from road cuts along highway US-119 in eastern Kentucky, spanning the Duckmantian (Westphalian B), which is only 320 m thick due to a more limited stratigraphic coverage and a lower subsidence rate (~35%).

We recorded cyclothem successions as alternations of subaqueous deposits (laminated/bioturbated shales and mouthbar sands) and subaerial deposits (coals, rooted shales and fluvial sands) and defined cyclothem boundaries as the base of the subaqueous interval. The Dutch succession has been little disturbed by fluvial incision. In the few cases where the presence of thick fluvial sandstone bodies is associated with unconventionally thick cyclothems, we interpreted this to be the result of erosion of the subaqueous part of a cyclothem due to fluvial erosion during lowstand (Aitken and Flint 1995). In such cases a cyclothem boundary was interpreted halfway the composite cycle. In the Kentucky sequence thick fluvial sandstones are so numerous that this was not considered feasible and fluvial sands were included in the subaerial part of cyclothems probably resulting in a less accurate record.

The Dutch wells were merged into a composite sequence based on palynology by Van der Laar and Fermont (1989), and the correlation was fine-tuned using the cyclothem data. The Kentucky section was matched with the Dutch composite using the marine bands at base of the

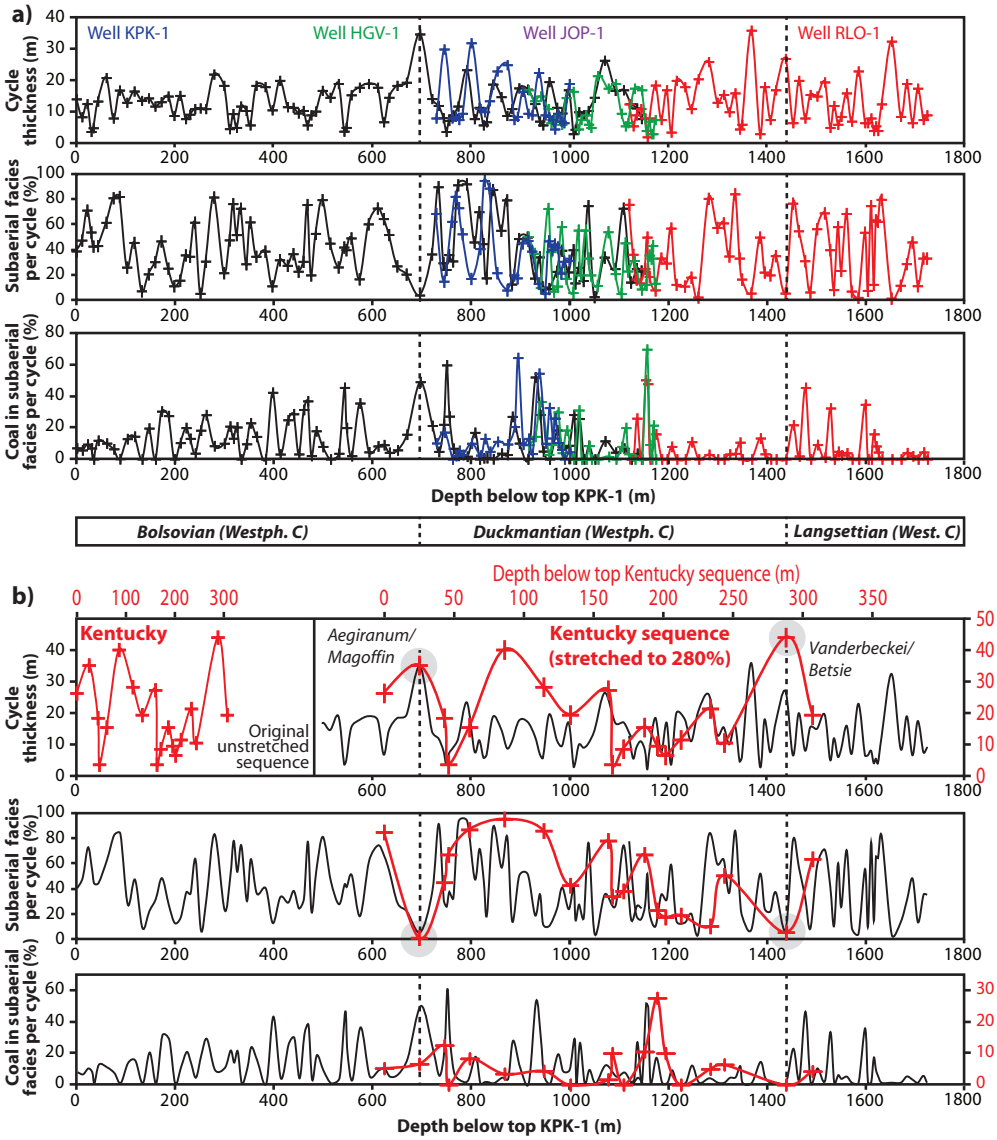

Figure 4 a) Correlated datasets for wells KPK-1, HGV-1, JOP-1 and RLO-1 plotted versus reference depth of KPK-1, all in the Netherlands. Correlation based on palynology by Van der Laar and Fermont (Van der Laar and Fermont, 1989) and trends in the subaerial-facies percentage and coal percentage. Overlapping wells HGV-1 and JOP-1 required a thickness reduction to 95% and 85% for the match with KPK-1. Thickness of the non-overlapping well RLO-1 was reduced to 90% (average of JOP-1/HGV-1). Stippled lines indicate marine bands. **b)** Original cyclothem sequence for Kentucky (top left) and Kentucky datasets stretched to 280% to match the Dutch sequence based on marine band correlation.

Duckmantian and Bolsovian as anchor points for correlation (Riley and Turner 1995). For each cyclothem we calculated the subaqueous-facies ratio and the percentage of coal in its subaerial part.

Results

Results for the Dutch wells are presented in Figure 4a. Note that the subaqueous-facies ratio is plotted in mirror image, i.e. as a subaerial ratio, giving a better visual representation. The original correlation by Van der Laar and Fermont (1989) is confirmed by our data and needed little adjustment. Wells HGV-1 and JOP-1 overlap with KPK-1 and after a thickness adjustments to 85% (JOP-1) and 95% (HGV-1) to correct for differential subsidence, a good match was achieved, in particular for the coal percentage. We applied a thickness adjustment to 90% (average of HGV-1/JOP-1) to well RLO-1 to correct for the slightly higher subsidence rate compared to the more southerly well KPK-1. From RLO-1 and KPK-1 we then constructed an Upper Langsettian to Upper Bolsovian composite of 145 cyclothems and matched it with the Kentucky sequence (Fig. 4b).

Correlation with the Kentucky sequence is based on correlative marine bands at the base and top of the Duckmantian (Riley and Turner 1995). This required a 2.8 stretching factor. The overlapping Duckmantian interval, which consists of 62 cycles in the Netherlands, is represented by only 16 cycles in Kentucky. The subaerial-facies ratio data in the two areas match well and coal-percentage peaks line up, although less pronounced (Fig. 4b), which further supports the validity of the interbasinal correlation proposed by Riley and Turner (1995).

Cyclothem thickness in the Dutch interval varies strongly, with cycles distributed evenly between 5 and 20 metres, and occasional cycles between 20-36 m. The average cycle is 12.5 m thick. The Kentucky cycles are evenly distributed between 3-27 m with occasional cycles up to 44 m, and an average of 17.3 m. We attribute the greater mean thickness of the Kentucky cycles to less compaction due to a much higher sandstone percentage, and to the undetected merger of some of the cycles due to fluvial incision during lowstand (Aitken and Flint 1995).

Cyclicity interpretation

Figure 5 shows our cyclicity interpretation of the Dutch sequence. The subaqueous-facies ratio shows cycles on two scales. The large-scale cycle has a period of ~255 m, illustrated by the sine-wave overlay. The small-scale cycles line up with a sine wave overlay with a period of 22.5% of the large-scale period, which equals a wave length of ~60 m (Fig. 5b).

The coal-percentage data match to a certain degree with the reverse of the major sine wave (Fig. 5a), although there are a number of obvious peak mismatches. In the Langsettian to Lower Bolsovian interval, the short-term fluctuations in the coal-percentage data correlate well with the ~22.5% sine wave (Fig. 4b).

Absolute cycle periods were determined using recent U/Pb age determinations of volcanic-ash layers in the Duckmantian Fire Clay coal (314.6 Ma) and in the Langsettian Upper Banner coal (316.1 Ma)(Lyons et al. 2006). The position of the Fire Clay coal is known (Fig. 5c) and the approximate position of the Upper Banner coal bed was extrapolated from a nearby gas well (Rice et al. 1987) to slightly below the base of the Dutch composite. The ~1.5 My long interval defined by the two ash-fall deposits contains ~3.8 large-scale cycles, giving a cycle period of ~395 ky, which is close to the 413-ky period of the long-eccentricity cycle. The (~22.5%) short-term cycle period then equals ~93 ky, pointing at 95-ky short eccentricity.

The 145 individual cyclothems in the Dutch sequence have a highly variable thickness, all on a sub-eccentricity scale. The complete sequence is 1728 m long and it equals ~7 long-eccentricity or 31 short-eccentricity cycles, which amounts to ~2.9 My. Based on a linear depth-thickness relation, cyclothem duration ranges between 5-32 ky; cyclothem periods are evenly distributed and there is no dominant period. Some cyclothems have higher estimated durations up to ~60 ky. The average cyclothem measures 12.5 m, which equals 21 ky.

The highly variable thickness of individual cyclothems suggests no specific control by precession or obliquity, but points at cycle interference. The average duration of the cyclothems (21 ky) is close to the main precession period, which equalled 17 ky during the Pennsylvanian, and

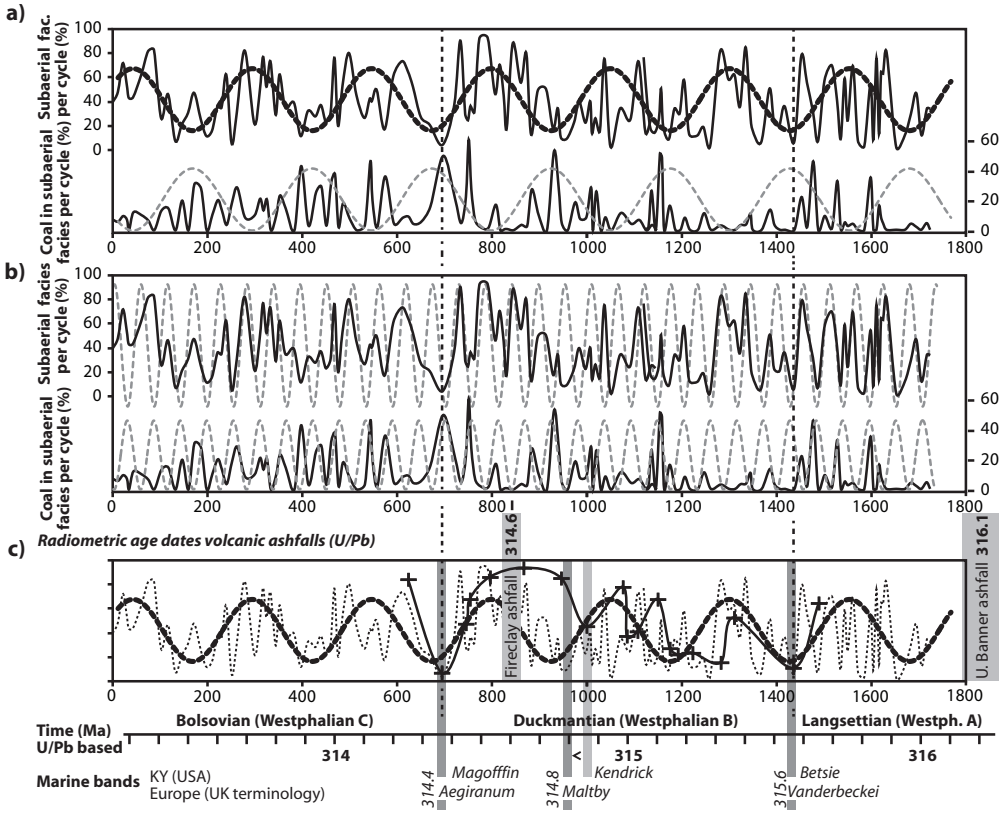

Figure 5 a) Subaerial-facies ratio and coal percentage for the Dutch composite section. Sine-wave overlay with 255 m wavelength matches the large-scale trend in the subaerial ratio. The large-scale trend is less well defined in the coal-percentage data (coal in subaerial facies per cycle; wave reversed). **b)** Sine-wave overlay with a period of ~22.5% of the large-scale sine wave. Also peaks in the coal-percentage data line up relatively well (wave reversed). c) Absolute-time interpretation based on Middle Pennsylvanian radiometric age dates (U/Pb) from the USA.

the maximum duration for the bulk of the cyclothems (32 ky) is close to the main obliquity period (34 ky). This suggests that the amplitude of precession-driven sea-level fluctuations was sufficiently high to prevent that obliquity and short eccentricity cycles were recorded as discrete cyclothems.

The observation that 63 cycles in the Dutch section are represented by only 17 cycles in Kentucky, indicates that only one out of four cyclothems (on average) was preserved in the Kentucky succession. Absence of part of the cycles is in line with the observation that regionally extensive erosion surfaces mark the base of cycles in the Appalachian Basin (Aitken and Flint 1995). Chesnut (1997) noted that areas of low subsidence in the Appalachian Basin preferentially show 400 ky cycles, whereas in higher subsidence areas 100 ky cycles have been preserved. Comparison with the Dutch succession suggests that this trend of increasing preservation of shorter cycles with increasing subsidence continues into areas of even higher subsidence, where sub-eccentricity cycles may be preserved.

The comparable thickness of cyclothems in the two study areas indicates that cyclothem thickness was probably not controlled by subsidence rate, but instead by glacio-eustatic sea-level fluctuations. Because these were global, and of higher magnitude than typical subsidence rates

(Rygel et al. 2008), different areas experienced the formation of accommodation space at relatively comparable rates during periods of long-term sea-level rise. This likely resulted in the formation of cyclothems of relatively comparable thickness in different areas on the globe. During subsequent periods of overall sea-level fall, non-deposition and/or erosion occurred. In areas of low subsidence these periods of non-deposition lasted longer than in areas where subsidence rates where high, resulting in less complete successions.

Implications for Pennsylvanian chronology

Chronological interpretations of Pennsylvanian stratigraphy are based on integrating radiometric ages (Burger et al. 1997, Davydov et al. 2004, Davydov et al. 2010) with cyclostratigraphic interpretations (Heckel 2008, Falcon-Lang et al. 2011), which over the years has resulted in a progressive refinement of the Upper Carboniferous time scale. Because radiometric ages were determined using different methods (Ar/Ar vs. U/Pb) results cannot easily be compared and integrated (Davydov et al. 2004, Villeneuve 2004). Most of the available radiometric ages are from the Ar/Ar isotope system (Fig. 6). They are internally consistent, also between basins (Lyons 1992, Lyons et al. 2006). Recent radiometric ages are based on the U/Pb isotope system (Lyons et al. 2006, Eros et al. 2012a). These are more accurate, but due to a different standard they yield systematically older ages (Davydov et al. 2004).

To integrate ages from both isotope systems, Ar/Ar age determinations were shifted to match the U/Pb time scale, based on the Fire Clay reference bed from the Appalachian Basin. For the Fire Clay coal bed both an Ar/Ar age (310.9 Ma) and an U/Pb age (314.6 Ma) are available (Lyons et al. 2006), which indicates that 3.7 My must be added to Ar/Ar dates to fit the U/Pb scale. Note that the Fire Clay level (Late Duckmantian) is an interesting calibration point, because its U/Pb age of 314.6 Ma is very close to the U/Pb age of 314.4 Ma determined for the base Moscovian in Eastern Europe (Eros et al. 2012a) and it could serve as tie point for North American, Western European and Eastern European stratigraphy

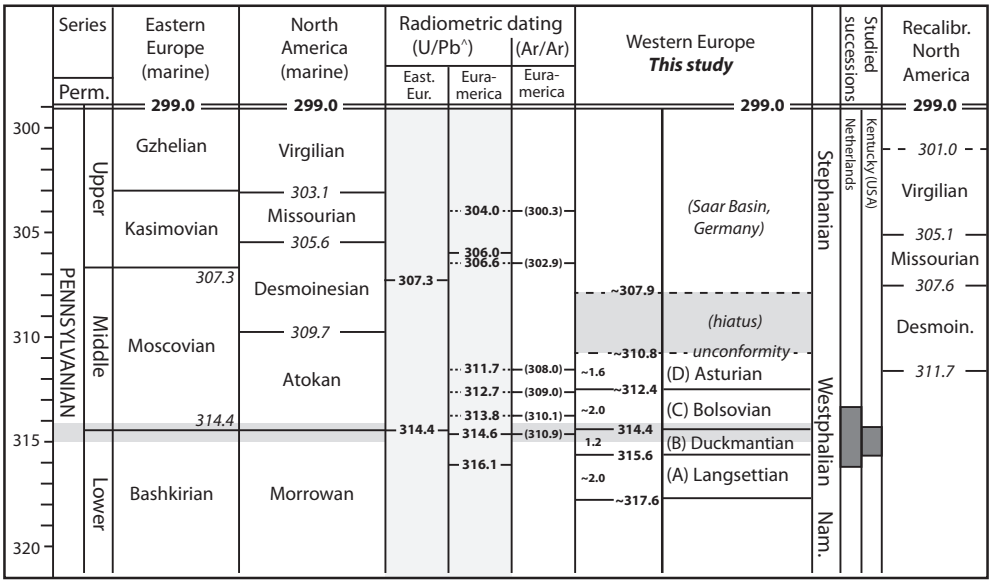

Figure 6 Chronostratigraphic interpretation of the European Westphalian stage and substages based on radiometric U/Pb age datings from the Appalachian Basin and Eastern Europe. Grey horizontal bar indicates 314.4 U/Pb tie point between Eastern Europe, Western Europe and North America. Recalibrated stratigraphy for midcontinent North America is based on the new 307.3 Ma age for the top of the Moscovian. See text for further explanation.

(Fig. 6).

Our cyclothem analysis has shown that the Duckmantian substage (Westphalian B) measures 3 long and 13 short-eccentricity cycles, which amounts to 1.2 My (Figs. 5, 6). If the Fire Clay coal bed is taken as a reference level (314.6 Ma), the marine band at the base of the Duckmantian has an age of ~315.6 Ma and the marine band at the base of the Bolsovian has an age of ~314.4 Ma. The intra-Duckmantian marine band (Kendrick/Maltby) then lines up at approximately ~314.8 Ma (Fig. 5).

The Bolsovian substage (Westphalian C) in the Dutch succession represents at least 3 long-eccentricity cycles, which equals 1.2 My. However, the Dutch sequence has been erosionally truncated and the duration of the Bolsovian substage thus must be longer. Numerous Ar/Ar age datings of volcanic ash-fall layers are available from the Bolsovian of central Europe (Hess and Lippolt 1986, Burger et al. 1997, Gradstein et al. 2004) and based on these the total duration of the Bolsovian is estimated at ~2.0 My (Fig. 6). This places the base of the Asturian at approximately 312.4 Ma. Extrapolation of radiometric ages based on Burger et al. (1997) places the youngest Asturian rocks, which are truncated by a major unconformity, at ~310.8 Ma. Downward extrapolation from Stephanian radiometric age data gives a base Stephanian age of ~307.9 and indicates that the duration of the Westphalian-Stephanian hiatus in the German Saar Basin equals some three million years (Burger et al. 1997).

Only a small part of the Langsettian (Westphalian A) substage is covered by our cores and radiometric ages are not available below the Late Langsettian Upper Banner coal bed. Therefore an accurate estimate of the duration of the Langsettian is not possible. However, when we extrapolate the Langsettian thickness of 1200-1350 m (Drozdzewski 1993) from the nearby Ruhr Basin (Fig. 2), and assume constant subsidence, the Langsettian substage has an estimated duration of ~ 2.0 My. This gives an estimated age for the base Langsettian of ~317.6 Ma (Fig. 6).

Based on our analysis the total duration of the Westphalian stage equals ~7 My, which is considerably less than an earlier estimate of 11.5 My by Menning et al. (2000). The shortening is primarily due to the newly available age datum for the Late Langsettian Upper Banner coal bed. In addition, Menning et al. (2000) did not incorporate the notion that there is a significant unconformity between the Westphalian and Stephanian successions throughout Europe representing at least a few million years (Ziegler 1990, Lyons and Wagner 1995), which pushes up the top of the Asturian in their time scale.

Our ~7 My is close to the 6.5 My assigned to the Westphalian stage in the Geological Time Scale 2004 of Gradstein (2004), but based on recent U/Pb age datings from the Appalachian Basin (Lyons et al. 2006) and Eastern Europe (Davydov et al. 2010, Eros et al. 2012a), the entire stage is interpreted to be a few million years older, ~311-318 Ma (Fig. 6) instead of 307-314 (Fig. 2). Furthermore, our interpretation of substage boundaries is different with a longer estimated duration of the Langsettian, and a shorter duration of the Bolsovian substage.

The Desmoinesian stage in the Midcontinent USA and the Upper Moscovian stage in Eastern Europe are interpreted to partly overlap with the (Upper) Westphalian in Western Europe (Greb et al. 2008, Heckel 2008, Falcon-Lang et al. 2011, Eros et al. 2012a). However, our age determinations place the entire Westphalian stage below the base Desmoinesian (309.7 Ma) of Heckel (2008). The base Desmoinesian as defined by Heckel is based on counting long-eccentricity cycle bundles (413 ky) downwards from the base Permian, which is dated at 299.0 Ma (U/Pb), and calibrated to an alleged 305.4 U/Pb date for the top Moscovian. The latter age determination was based on personal communication between Heckel and M. Davydov in 2005 (Heckel 2008). However, in a recent publication by Eros et al. (2012b) this top Moscovian sample (or equivalent) appears to be ~2 million years older. When the midcontinent sequence of North America is recalibrated considering this older top Moscovian age, the new ages for the base Desmoinesian, Missourian and Virgilian are 311.7, 307.6 and 305.1 Ma, which makes the two successions overlap and yields a more consistent chronostratigraphic framework for the Pennsylvanian of Euramerica (Fig. 6).

Coal accumulation rates

The Duckmantian and Bolsovian stages are the most prolific coal intervals in the Pennsylvanian

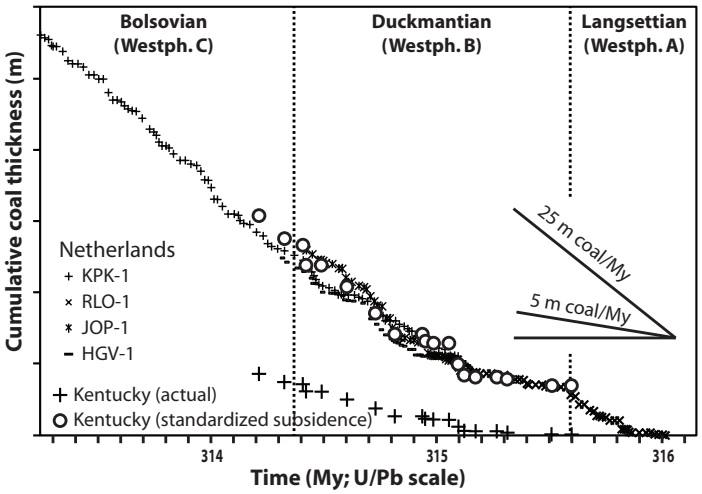

Figure 7 Cumulative coal accumulation through time for the Dutch and Kentucky intervals. Open circles dataset Kentucky data standardized to Dutch subsidence rates.

and represent a large percentage of the terrestrial carbon buried during the Late Palaeozoic ice house period (Berner, 2003). The accurately dated sedimentary record from the Netherlands allows a precise determination of the long-term burial of coal in one of the largest and fastest subsiding Pennsylvanian basins (Fig. 7). The coal-accumulation patterns are correlatable between wells and show low accumulation rates (5-10 m coal/My) until ~315.1 Ma (U/Pb) after which accumulation accelerated to ~25 m coal/My.

Cumulative coal accumulation in Kentucky, although being much slower, shows a similar acceleration at 315.1 Ma. The cumulative coal accumulation patterns are almost identical, when the Kentucky coal-accumulation rates are multiplied by the stratigraphic stretching factor of 2.8 that was required to line up the marine bands in the high-subsidence Dutch succession and the low-subsidence Kentucky succession (Fig. 7). This suggests that overall coal accumulation was externally controlled by climate or sea level, and comparable between the areas, the amounts of buried coal depending on subsidence which also controlled the percentage of cycles deposited and preserved. From outcrops it is known that coal thickness may show rapid lateral changes, but our results show that this did not significantly affect the overall long-term coal-accumulation patterns.

Discussion and conclusion

The cyclicity in Euramerican coal basins has since long been related to sea-level changes associated with Late Palaeozoic glaciations (Wanless and Shepard 1936). Although it seems more than a coincidence that cyclothem formation was widespread and coeval with Late Palaeozoic glaciation, there was as yet no evidence that unambiguously demonstrated Milankovitch control. We attribute this to the fact that previous analyses were based on cyclothem thickness, which is unlikely to reflect the sea-level fluctuations that shaped them, because –depending on the ratio between sea-level change, subsidence and sediment accumulation– cyclothem boundaries may be formed almost anywhere during a sea-level cycle. Furthermore, previous studies were carried out in areas where the Pennsylvanian sequence is relatively thin and incomplete, and cycle duration is typically estimated by dividing sequence duration by the number of observed cycles. When many cyclothems are missing, cycle duration is grossly overestimated. This means that estimated cycle periods may be too long although still falling in the Milankovitch range (Algeo and Wilkinson 1988).

We showed that sea-level fluctuations can be

revealed by quantitatively analysing variations in cyclothem composition through time, such as the subaerial-facies ratio and the coal percentage per cycle when applied to high-subsidence areas where stratigraphic successions are most complete. In combination with radiometric ages the data show a strong short and long-eccentricity control, which is in agreement with current ideas (Eros et al. 2012a, Waters and Condon 2012). However, our data also show that the 100 ky estimate is too high for individual cyclothems and includes missed beats and/or eroded stratigraphy. Individual cyclothems have a sub-eccentricity duration, which is probably the result of high-amplitude precession interfering with obliquity and eccentricity. The interpreted dominance of precession cycles is remarkable when compared with $\delta^{18}O$ records from the Quaternary which point at a dominance of obliquity (before 0.7 Ma) and short eccentricity (after 0.7 Ma). The influence of precession-controlled climate fluctuations is particularly strong at low latitudes (De Boer and Smith 1994), and it is therefore not expected to play an important role during ice house periods. However, Late Palaeozoic ice sheets extended into low-latitude areas (Frakes et al. 1992, Poulsen et al. 2007), maybe even down to 30° S during the Westphalian, when glaciation was at its peak. At such low latitudes precession-driven climate fluctuations may have been equally or more important than obliquity in controlling or modulating the waxing and waning of ice caps.

Integration of our cycle interpretation with recent U/Pb radiometric age datings from the Appalachian Basin allowed chronostratigraphic dating of the main marine bands at the base, in the middle and at top of the Duckmantian substage at 315.6, 314.8 and 314.4 Ma. This makes a robust chronostratigraphic framework for the Late Langsettian to Early Bolsovian interval that links the coal basins from Europe and North America. Based on Ar/Ar radiometric age datings from Europe (recalculated to U/Pb) we estimate that the entire Westphalian stage lasted approximately 7 My, and overlaps slightly with the midcontinent Upper Pennsylvanian reference section of Heckel (2008). The bases of the Westphalian substages are estimated at 317.6 (Langsettian), 315.6 (Duckmantian), 314.4 (Bolsovian) and 312.4 Ma (Asturian).

The observation that the pattern of coal accumulation through time can be correlated between the Dutch wells, and even between basins after correction for subsidence and missing cycles, is intriguing. It requires further study to establish if the recorded patterns are indeed global rather than the result of local sedimentary conditions. If indeed correlatable over larger distances, coal patterns may be an interesting correlation tool and a possible proxy of palaeoclimate and sea level.

The methodology we applied here has the advantage that it is quantitative and therefore leaves less room for speculation when it comes to the interpretation of cycle periods. However, it requires thick, continuous stratigraphic successions in high-subsidence areas with a 'complete' sedimentary record. Based on a few good-quality sections, such as the Langsettian 'Joggins' section of Nova Scotia, it might be possible to extend the Duckmantian-Bolsovian chronology presented here to the base of the Langsettian and into the Asturian thus covering the entire Westphalian coal interval, giving a high-resolution time framework for the peak period of the Late Palaeozoic glaciation.

Chapter 3

FLUVIAL SANDSTONE DISTRIBUTION CONTROLLED BY FAULT BLOCK TILTING; A QUANTITATIVE EXAMPLE FROM A LOWER PENNSYLVANIAN (CARBONIFEROUS) COAL-BEARING SUCCESSION, POLAND

F.J.G. van den Belt, P.L. de Boer and F. van Bergen

Conceptual models of the evolution of axial fluvial systems in half-grabens, or tilted fault blocks in other settings, assume rotational subsidence exactly perpendicular to a fault, and predict that the fluvial-sandstone proportion increases towards that fault. However, tilting may have a basin-axis-parallel component, which could lead to a different facies architecture. Such a case is presented from the Upper Silesian Coal Basin in Poland.

The studied interval is a Lower Pennsylvanian cyclothemic alternation of fluvial sandstone, coal and floodplain mudstone with a thickness ranging from 165 to 245 metres, controlled by syndepositional fault-block tilting. The sequence consists of three wedge-shaped units, each containing approximately 45 m floodplain mudstone and coal, while a variable amount of sandstone completes the units. This indicates that they represent deposition of mud and peat on a floodplain equally long, regardless of differential subsidence. Tilting events resulted in bypass of mud, due to a downstream tilting component, until fluvial sands had infilled the faulted topography. The predictable distribution of sandstone implies that fluvial sandstones in the study area are not incised valleys but aggradational systems whose thickness was controlled by differential subsidence. This scenario is different from standard models, which predict floodplain deposition during tilting and an up-dip increasing mudstone proportion.

Introduction

Pennsylvanian (Upper Carboniferous) sedimentary successions in Euramerican basins are characterized by repetitive fluvio-deltaic cycles that formed in response to glacio-eustatic sea-level fluctuations (Davies 2008, Greb et al. 2008, Rygel et al. 2008). These cycles, also known as 'cyclothems' (Weller 1930), are a few metres to tens of metres thick and commonly comprise deltaic or marine shales overlain by alternations of fluvial sandstone, floodplain deposits and coastal-plain coal beds (Fielding 1984b, Guion et al. 1995). The fluvial sandstones are mostly extensive, erosively based bodies with a thickness up to 15-20 m, and their width is estimated to be anywhere between a few and tens of kilometres (Fielding 1986, Aitken and Flint 1995, Guion and Rippon 1995, Rippon 1996, Jones and Glover 2005, Rygel et al. 2008). These sandstone bodies are potential hydrocarbon reservoirs, e.g. in the Southern North Sea area, and reservoirs for carbon dioxide storage. Understanding the dimensions and distribution of these bodies is therefore of economic importance.

Synsedimentary tectonics may have influenced the distribution and (stacked) thickness of the fluvial sandstones. In the Pennine Basin (UK) major fluvial sandstone bodies appear stacked on hangingwall blocks (Fielding 1984b, Fielding 1986, Fielding and Johnson 1987, Guion and Fielding 1988, Rippon 1996). This is attributed to the tendency of fluvial channels to seek low-lying areas after avulsion events (Alexander and Leeder 1987). Collinson et al. (1993) described comparable sandstone stacking in the Pennsylvanian below the adjacent Southern North Sea. The 'diagonal stacking' of channel bodies observed by Fielding (1984b) was considered evidence of progressive down-slope channel migration.

In various subbasins of the Appalachian foreland basin (USA) similar observations were made. For the Warrior Basin (Alabama) Weisen-

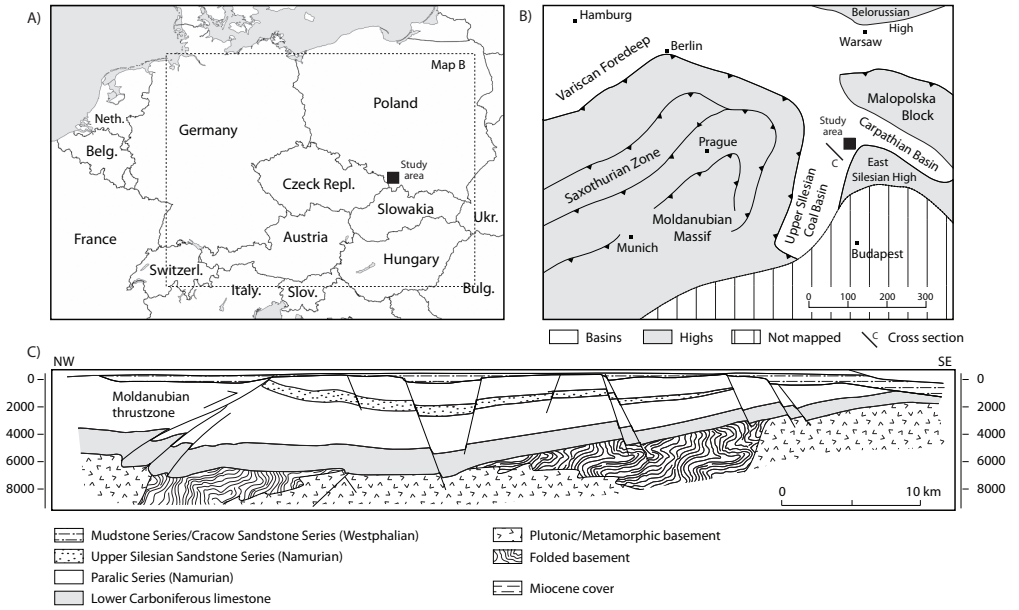

Figure 1 a) Map of Central Europe showing location of the study area, **b)** Structural organisation of north-central Europe during the Namurian (after Ziegler 1990), **c)** NW-SE cross section through the northern part of the Upper Silesian Coal Basin close to the study area (after Kotas 1994).

fluh and Ferm (Weisenfluh and Ferm 1984) and Ferm and Weisenfluh (1989) described how a number of ~1 km wide fluvial channels flowed parallel to a major fault on the hangingwall block over a distance of 10-15 km, where they stacked into a 30 m thick compound sandstone unit. Horne (1978) and Allen (1993) observed similar channel-stacking patterns in the Pennsylvanian of eastern Kentucky and West Virginia. Also in those cases clustering of fluvial-channel sandstone bodies was attributed to the tendency of channels to migrate to low-lying areas at the downthrown side of synsedimentary active faults (Ferm and Weisenfluh 1989).

The mechanism by which fluvial-channel deposits are stacked in areas of maximum subsidence (Alexander and Leeder 1987, Leeder and Gawthorpe 1987) has been subject of studies carried out since the late 70s, mainly by theoretical analysis and computer modelling (Bridge and Leeder 1979, Bridge and Mackey 1993, Mackey and Bridge 1995), and it is supported by semi-quantitative field observations (Mack and James 1993, Leeder et al. 1996). The so-called LAB-models (Bryant et al. 1995) based on these studies predict how tilting of a floodplain forces a channel system to the area of highest subsidence with only occasional deposition of channel sands on more elevated parts of the floodplain. The latter happens only when sedimentation outpaces subsidence while at the same time a level floodplain is maintained (Bridge and Mackey 1993). We note that the conceptual LAB models are based on situations in which a floodplain on top of a fault block is tilted at an angle of exactly 90 degrees towards the block-margin fault. In practice tilting may have a component parallel to the fault, possibly resulting in a different facies architecture.

In this paper, results are presented of a detailed quantitative analysis of the control of subsidence on the distribution of fluvial sandstones in a rotational fault-block setting with tilting axes at variable angles to the controlling normal faults. We analysed a three-dimensional borehole data set from a Lower Pennsylvanian coal-bearing sequence in a coal-mining concession area in the Upper Silesian Coal Basin in Poland (Van Bergen 2006, 2009).

The boreholes are from a mining site and

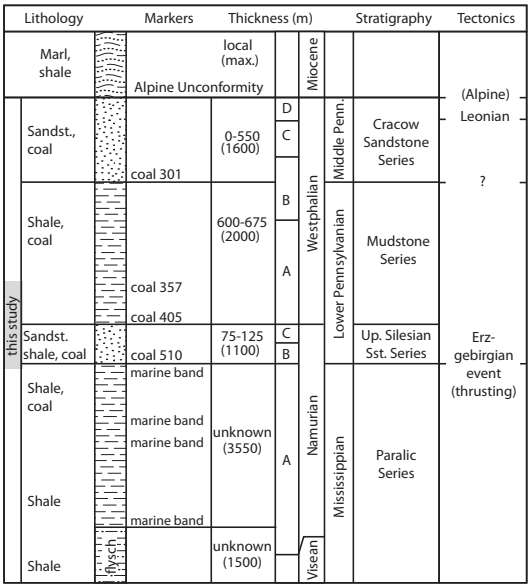

Figure 2 Stratigraphic column for the Upper Silesian Coal Basin with major coal beds/zones and marine bands indicated (after Kotas 1994); thickness values indicated are for the study area, maximum thickness in the basin between brackets. Studied interval indicated in the left-hand column.

sedimentary logs are not very detailed, therefore hampering an accurate interpretation of facies. However, a high borehole density in an area of considerable differential subsidence and a well-established coal-bed framework makes this an interesting data set to quantitatively test how differential subsidence controls the distribution of sand-rich facies.

Geological background

The Upper Silesian Coal Basin (USCB) is a narrow, north-south aligned foreland basin (Fig. 1) in Poland and the Czech Republic (Ziegler 1990, Zdanowski and Zakowa 1995). It is bordered by the Moldanubian thrust zone in the west and the East Silesian High in the east, and it is strongly asymmetrical. The basement consists of strongly folded metamorphic and plutonic Precambrian and Cambrian rocks. In many parts of the basin, including the study area, the basement is block-faulted, and normal faulting and fault-block rotation associated with this fault system influenced sedimentation during the Devonian (Ziegler 1990) and Carboniferous (Jureczka and Kotas 1995). Ziegler (1990) attributes subsidence to tectonic loading of foreland crust, but notes that a major dextral shear component is required to explain crustal shortening in the Rhenohercynian Basin.

During the Mississippian (Early Carboniferous) the basin was characterized by carbonate-platform deposition throughout, and at the onset of the Namurian deep-water clastics accumulated in the narrow foredeep east of the Moldanubian thrust zone, indicating the onset of regional compression and accelerated subsidence (Zdanowski and Zakowa 1995). Thrusting started in the Namurian and resulted in a Namurian-Westphalian clastic sediment wedge that thickens westward (Fig. 1c) and is more than 8 km thick locally (Kotas 1994, Zdanowski and Zakowa 1995). Alternations of fluvio-deltaic sandstone, mudstone and coal characterize the Namurian-Westphalian succession. Fluvial systems were sourced from the Moldanubian thrust zone and drained to the north-northeast (Kotas 1994).

The Carboniferous stratigraphy of the basin is illustrated in Figure 2. The studied interval spans the Upper Silesian Sandstone Series (Namurian C) and the lower part of the Mudstone

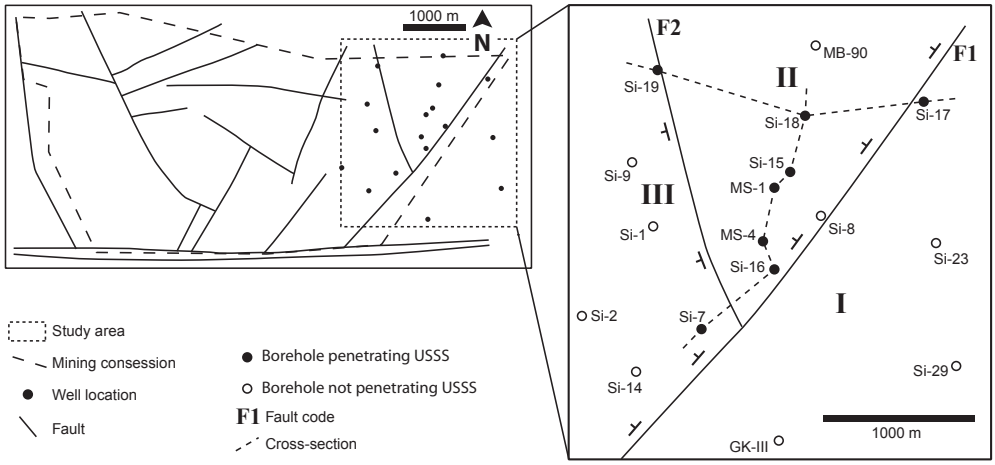

Figure 3 Map of the Silesia mining concession (left) showing major faults (F1, F2) and borehole locations for the study area (right). The study area covers 3 fault blocks (numbered I to III) with densely-spaced boreholes. Map after Van Bergen (2006). Wells not incorporated in the cross-sections do not penetrate the studied interval or only partly and were therefore not included in the quantitative analysis (open circles).

Series (Westphalian A-B). The Upper Silesian Sandstone Series (USSS) is a sandstone-rich unit with a thickness of up to 1.1 km close to the thrust zone, and thinning rapidly eastward (Kotas 1994). In the study area it is only between 125 and 200 m thick. It unconformably overlies mudstone-dominated sediments from the Namurian A and across most of the basin its base is marked by regional coal bed 510. The USSS contains nearly 10% coal and many of the coal beds are between 4 and 8 m thick (Kotas 1994). The abundance of sandstones is associated with the 'Erzgebirgian' thrusting event occurring at the western basin margin during the Late Namurian (Kotas 1994, Zdanowski and Zakowa 1995). Sandy sediment sourced from the upthrusted area was transported north-eastward by basin-parallel fluvial systems close to axis of maximum subsidence (Kotas 1994). In the eastern parts of the basin subsidence rates were low, shielding the area from sediment input, thus promoting the formation of thick peat bodies. For instance, the thickness of coal bed 510, which constitutes the base of the USSS, increases from 6 m in the study area to 24 m in the east. The top of the USSS is a goniatite-bearing 'marine band' that marks the Namurian-Westphalian boundary (Kotas 1994).

The overlying Mudstone Series is dominated by meandering channel deposits (Gradzinski et al. 1995). It is unconformably overlain by the Cracow Sandstone Series (Westphalian C-D), a unit dominated by sandy and conglomeratic braided-fluvial-channel deposits (Gradzinski et al. 1995, Doktor 2007). To the east the Cracow Sandstone Series is unconformably overlain by red and variegated sediments without intercalated coal beds that are probably of Stephanian age (Zdanowski and Zakowa 1995). The Pennsylvanian section is truncated by an Alpine unconformity, overlain by Miocene deposits, the depth of truncation increasing westward (Fig. 1).

The Study Area

This study is based on sedimentary records of 8 boreholes and on fault maps from a 5 km^2 area within the Silesia coal mining concession about 40 km south of Katowice in southern Poland (Fig. 3). The youngest Pennsylvanian deposits in the area are Westphalian C sandstones of the Cracow Sandstone Series; these are buried below a ~250 m Miocene cover (Van Bergen et al. 2006). The stratigraphic interval under investigation comprises the USSS and the basal section of the Mudstone Series. In the study area this interval is present at depths between 950 and 1250 m.

The concession area is dissected by two sets

of steep faults that strike NE-SW and NW-SE (Fig. 3). The faults intersect at ~60° angles and the NW-SE striking faults abut against the NE-SW striking faults. Offset of coal beds indicates normal displacement. Both the steepness of the faults and the 60-70° intersection angles of the two sets point at normal reactivation of an original strike-slip fault system, possibly related to Late Devonian dextral shear (Ziegler 1990). The E-W trending fault that defines the southern margin of the coal-mining concession area is of Alpine origin (Van Bergen et al. 2006).

The study area is located at the eastern end of the coal-mining concession area (Fig. 3). It is characterized by a major NE-SW trending normal fault (F1) that separates a footwall block in the SW (fault block I) and a composite hanging-wall block in the NW. This hanging-wall block consists of two higher-order fault blocks (II and III) that are separated by fault F2. Note that fault block II is part of the hangingwall block of fault block I, but it also serves as a (higher-order) footwall block to fault block III.

Sedimentary framework

The sedimentary framework is based on core descriptions, wireline logs and coal-bed depth/thickness maps. The available core descriptions were drafted for coal-exploration purposes, with a lithology record but lacking descriptions of sedimentary structures. From regional work it is known that the USSS generally comprises an alternation of floodplain mud-stones, coal beds and braided fluvial sandstones; marginal marine shales are restricted to the interval below coal bed 405 (Kotas 1994, Zdanowski and Zakowa 1995). The rudimentary character of the sediment descriptions did not permit the recognition of possible lacustrine intercalations within floodplain shales, nor the distinction between small fluvial-channel deposits (e.g. pointbars) and possible mouthbar or crevasse sandstones. Some of the interpretations may therefore be slightly simplified.

Figure 4 shows N-S and an E-W correlation panels based on coal bed interpretations of the mining company and following the regional coal-bed terminology. The studied interval, comprising the USSS and the lower 50 m of the Westphalian 'Mudstone Series' is characterized by four relatively thick, correlatable coal beds (510, 405, 401, 354). These main coal beds define three sedimentary units (Unit 1-3) with an average thickness that decreases upward from 115 m to 50 m. Units 1 and 2 have a distinct wedge shape and thicken to the northwest. Unit 3 has a more tabular shape. Internally each unit is composed of ~3-4 sedimentary cycles, which are typical 'cyclothemic' alternations of sandstone, mudstone and coal. Units 1 and 2 are dominated by thick, laterally extensive sandstone bodies. Sandstone bodies in Unit 3 are thinner and more isolated.

Thick sandstone bodies are abundant in Units 1 and 2, where they alternate with mudstone and coal beds. Their abundance decreases upward from Unit 1 (average sandstone content ~55%) to Unit 2 (~30%). In Unit 3 thick sandstone bodies have not been encountered in any of the boreholes. The thick sandstone bodies are between 10 and 20 m thick and most of them appear laterally extensive. Occasionally, sandstone bodies in the vicinity of faults wedge out toward adjacent boreholes (e.g. borehole Silesia-18/19). Close to faults sandstone bodies are more numerous, often stacked, and their cumulative thickness is greater than further away from those faults.

Thin, isolated sandstone bodies are observed in all three units. They are most pronounced in Unit 3, where they make up ~10% of the succession. These sandstone bodies are usually only a few metres thick and cannot be traced to neighbouring boreholes. In contrast to the fluvial sandstones that dominate Units 1 and 2, these channel sands are encased in floodplain fines.

Coal beds are present throughout the sequence and occur in distinct bundles. Two types of coal bed characterize the study area. The first type comprises thick coal beds (1-6 m) that are present across the entire study area (Fig. 4). The other type comprises non-continuous thin coals (< 1m); these wedge out laterally or are possibly truncated by fluvial sandstone bodies. Coal beds show pronounced thickness variation across the study area. For example, the thickness of coal bed 510 ranges from 0.6 m (Silesia-17) to 6 m (Silesia-19) over a distance of ~3 km.

The thick, laterally extensive sandstone bodies that dominate Units 1 and 2 have dimensions in the range of major fluvial sandstone bodies in the Pennsylvanian of Europe and Northern

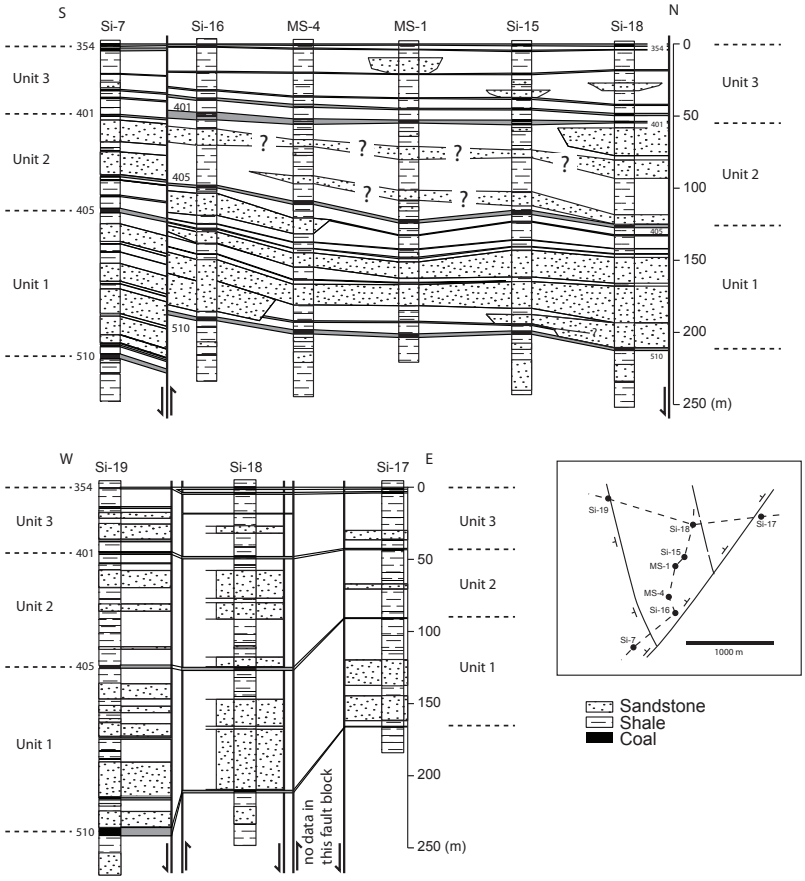

Figure 4 Correlation panels showing north-south (left) and east-west transects (right) through the study area. Correlations based on coal-bed stratigraphy. Sandstone bodies seem well correlatable in the lower part of the studied interval; correlations in the middle part are more tentative. Numbers 510, 405, 401 and 354 indicate major coal beds.

America (Fielding 1984b, Aitken and Flint 1995, Jones and Glover 2005, Greb et al. 2008, Rygel et al. 2008). In general Pennsylvanian fluvial systems are interpreted as either sheet-like fluvial braidplain deposits with basal erosion surfaces (Haszeldine and Anderton 1980, Jones and Hartley 1993, Jones and Glover 2005) or as incised valley deposits (Aitken and Flint 1995, Hampson et al. 1999). Based on their sheet character and the regular alternations with mudstone and coal, the majority of the major sandstones in the study area are interpreted as the deposits of fluvial braidplain systems. Some of the sandstone bodies in the vicinity of faults wedge out rapidly which suggests that these bodies are incised fluvial systems. The thin, isolated sandstone bodies encased in floodplain muds are interpreted as the deposits of small channels meandering across the floodplain. Other types of floodplain sandstones such as crevasse splays may be represented as well, but could not be identified due to the rudimentary nature of the dataset.

Thick upper Carboniferous coal beds are commonly interpreted as coastal-plain and floodplain peat accumulations (Fielding 1984a, McCabe 1984), and based on the associated facies the coals in the study area are probably floodplain coals. The great thickness and lateral extent of some of the coals indicate that peat swamps were extensive and built up considerable peat

accumulations. The thin, non-continuous coal beds probably formed in local depressions, such as lakes and abandoned channels (Greb and Chesnut 1992). The change of coal thickness over short distances may be related to synsedimentary faulting and differential subsidence (Guion and Fielding 1988, Greb et al. 2002, Greb et al. 2005) or to infilling of inherited topography (Greb and Chesnut 1992, Greb et al. 1999).

Reconstruction of fault-block movements

Regional subsidence variations were approximated by measuring the thickness of the studied interval (coal bed interval 354-510) and the thickness of the three units at the borehole locations (Table 1). This is a reasonable approximation because the occurrence of coal beds throughout the sequence indicates deposition near base level (Bohacs and Suter 1997) and shows that sedimentation kept up with subsidence continuously. The studied interval contains relatively equal amounts of mudstone at the various borehole locations (Table 1), so that the thickness variations cannot be due to differential compaction of mud. Since coal is more abundant in the thicker sequences, the thickness variations of the studied interval can neither be attributed to preferential compaction of peat (Table 1). Also note that Nadon (1998) showed that the deep burial compaction of peat, long considered to be around 10:1, is not higher than ~2.5:1 which equals the compaction of mud. This is because most compaction occurs in the plant-to-peat rather than the peat-to-coal stage (van Asselen et al. 2010).

Thickness maps

In Figure 5 thickness maps are shown for the studied interval as well as for the individual Units 1-3. Map a shows the variation of the thickness of the entire sediment column (between coals 510-354); it ranges from 166 m (Silesia-17) on fault block I to 242 m on fault block III (Silesia-19). With a mean thickness of 205 m these extremes reflect a differential subsidence range between -19% and +18% (Table 1). The data further show that the thickness increases northward across fault blocks II and III.

Figure 5b shows the variation of interval thickness for Unit 1. The unit has a maximum thickness of 119 m in borehole Silesia-19 and a minimum thickness of 76 m in borehole Silesia-17. With an average thickness of 94 m differential subsidence ranges between -18% and +28 %. The thickness of Unit 1 on fault block II shows a slight *southward* increase from 88 to 94 m. However on block II the unit thickness increases *northward* from 105 to 119 m.

In Figure 5c the thickness variation for Unit 2 is shown. In borehole Silesia-19 the unit has a maximum thickness of 72 m; it has a minimum thickness of 48 m in borehole Silesia-17. The mean thickness is 62 m, giving a differential-subsidence range from -23% to +16%. On fault block II the thickness increases northward from 51 to 72 m and on fault block III the thickness increases northward as well, from 65 to 79 m.

Figure 5d shows the thickness variation for Unit 3. It is characterized by a fairly constant thickness of 48-54 m across most of the study area, indicating limited differential subsidence, ranging between 5% and +8%. Borehole Si-17 on fault block I shows a more reduced thickness of 42 m (-17%).

Subsidence history

The maps of Figure 5 indicate that the thickness variations are not random, but follow directional trends. The data indicate that much of the thickness differences can be attributed to relative movements between fault blocks, but thickness changes on individual fault blocks indicate that rotation of fault blocks contributed considerably.

Subsidence rates were lowest in the southeast and increased overall to the northwest. Reduced thickness for all units in borehole Silesia-17 indicates that fault block I served as a footwall block to fault blocks II and III. Fault block III experienced the highest subsidence rates; during the deposition of Units 1 and 2 it subsided more rapidly than the fault blocks to the east and southeast. The rather constant thickness of Unit 3 north of fault F1 indicates that differential subsidence between fault blocks II and III came to a halt after deposition of Unit 2, and that they continued to subside as a compound block, only slightly faster than fault block I.

The thickness differences indicate that differential subsidence was greatest during and shortly after deposition of coal bed 510 and had ceased mostly after deposition of Unit 2, the top of which

Borehole	Sediment column thickness	Lithology (cum. thickness)				Lithology (percentage)				Deviation from mean				
		Sand-stone	Coal	Mud-stone	Mud-stone + coal	Sand-stone	Coal	Mud-stone	Mud-stone + coal	Sediment column	Sand-stone	Coal	Mud-stone	Mud-stone + coal
	(m)	(m)	(m)	(m)	(m)	(%)	(%)	(%)	(%)	(%)	(%)	(%)	(%)	(%)
Silesia-07	219	94	1	107	124	43.1	7.8	49.1	56.9	6.2	13.9	37.8	-3.2	-3.9
Silesia-15	202	69	15	118	133	34.2	7.4	58.4	65.8	-1.6	-16.4	21.6	6.8	3.1
Silesia-16	193	70	11	111	122	36.5	5.7	57.8	63.5	-6.5	-15.2	-10.8	0.5	-5.5
Silesia-17	166	44.5	4.5	117	121.5	26.8	2.7	70.5	73.2	-19.2	-46.1	-63.5	5.9	-5.9
Silesia-18	213	104	12.5	96	108.5	48.9	5.9	45.2	51.1	3.5	26.1	1.4	-13.1	-15.9
Silesia-19	242	114	14	114	128	47	5.8	47.2	53	17.6	37.6	13.5	3.2	-0.8
MS-1	204	62.5	13.5	128	141.5	30.6	6.6	62.7	69.4	-0.6	-24.2	9.5	15.8	9.6
MS-4	201	47	10.5	143.5	154	23.4	5.2	71.4	76.6	-2.1	-43.0	-14.9	29.9	19.3
Mean:	205	83	12	111	129	39	6	55	55					
Correlation coefficient with sediment-column thickness:		0.84	0.78	-0.2	0									

Table 1 Thickness and lithological data for the studied interval between coal beds 510-354

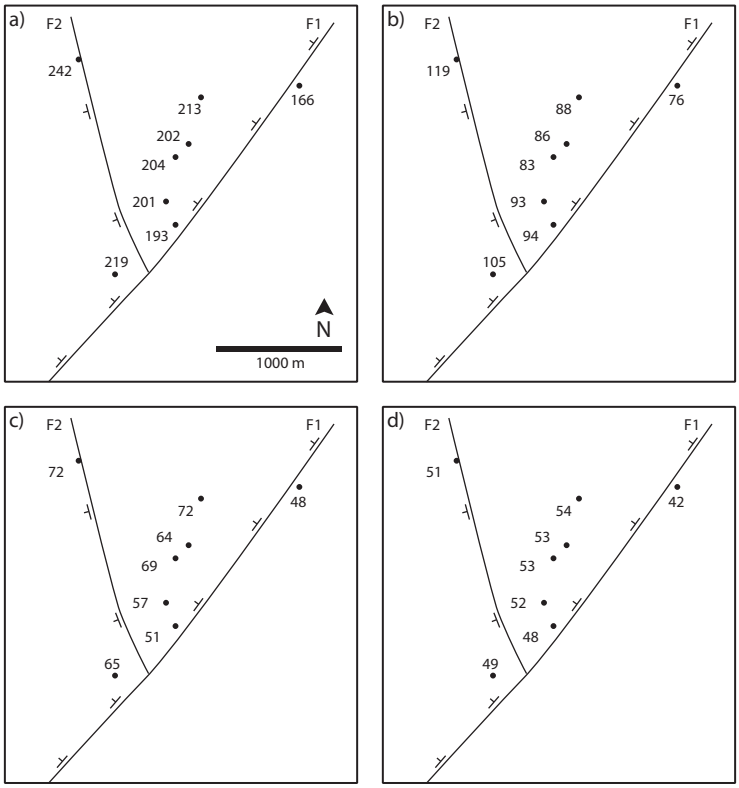

Figure 5 Thickness maps for the complete studied interval (a), Unit 1 (b), Unit 2 (c) and Unit 3 (d).

marks the Namurian-Westphalian boundary. This coincides with the end-Namurian termination of the 'Erzgebirgian' thrusting event (Kotas 1994), possibly indicating that thrusting events caused immediate loading-induced subsidence, which was accommodated by normal displacement of the block-faulted basement. Then, when thrusting came to a halt subsidence was dominated again by background subsidence.

Thickness variations on individual fault blocks point at superimposed rotation. This was consistently northward for fault block III, whereas fault block II rotated southward during deposition of Unit 1 and northward during deposition of Unit 2. For fault block I the rotation history could not be reconstructed due to limited borehole control.

Quantitative analysis of sediment distribution

To assess the mechanism that controlled sediment distribution in the study area a quantitative analysis of the influence of subsidence on the distribution of sandstone, mudstone and coal was carried out for the entire studied interval (between coal beds 510 and 354) and for the three units separately.

Cumulative thicknesses and the proportions of the different lithologies (Table 1) show a strongly positive correlation between the thickness of the studied interval and the cumulative amount of sandstone (correlation coefficient: 0.84). Also the percentage of sandstone increases with increasing thickness of the studied interval. A similar relation is observed for coal, with higher values for cumulative coal thickness and coal percentage where the thickness of the studied interval is greater (correlation coefficient: 0.78). Conversely, the cumulative mudstone content shows a slightly negative relation with interval thickness (correlation coefficient: -0.20). Note, however,

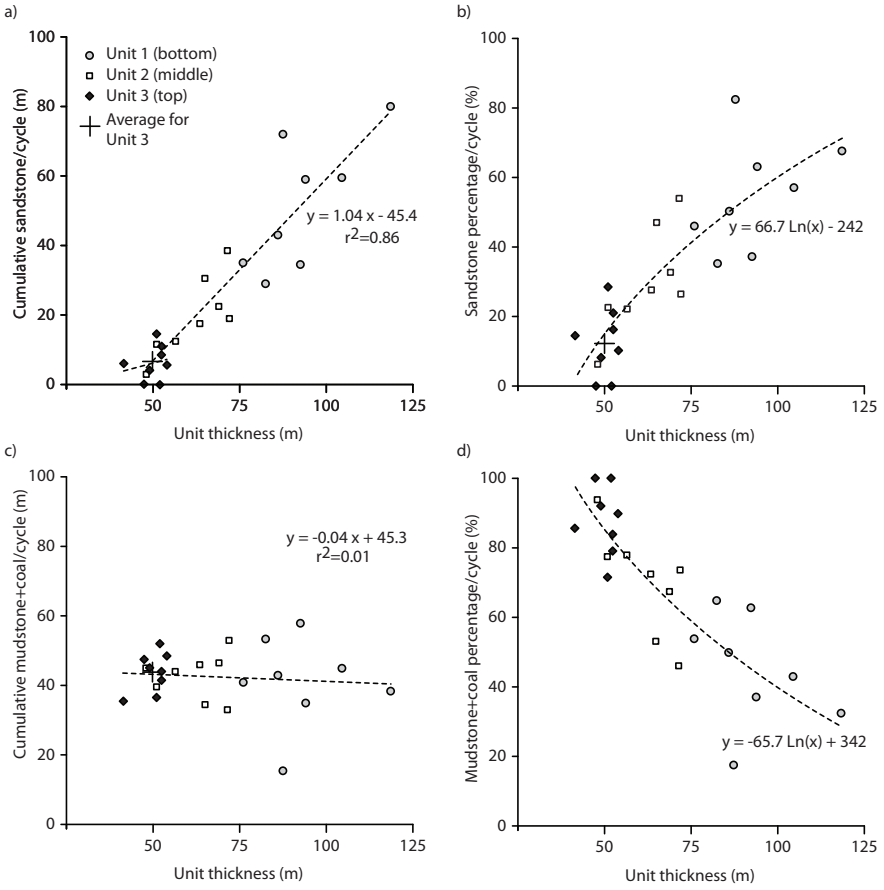

Figure 6 Cross-plots for cumulative sandstone thickness (a), sandstone percentage (b), cumulative mudstone/coal thickness (c) and mudstone/coal percentage (d).

that the cumulative thickness of mudstone and coal (those lithologies added up) shows a correlation coefficient of 0.00 with unit thickness.

The plots in figure 6 show that the strong positive correlation between interval thickness and cumulative sandstone thickness is maintained at the scale of individual units. Note that the cumulative-sandstone-thickness data for each unit constitutes a well defined data cluster in the cross-plot, and that only the data for Units 1 and 2 overlap slightly. The plots for the cumulative mudstone/coal thickness and the mudstone/coal percentage (Fig. 6c) show that the three units contain approximately equal amounts of mudstone/coal (~45 m), and that no relation exists between unit thickness and mudstone content.

Interpretation

The observed relations between unit thickness and sediment distribution indicate that areas of higher subsidence contain disproportionally high amounts of sandstone, and that mudstone is present in more or less equal amounts throughout the area, regardless of subsidence. Subsidence may have slightly influenced the distribution of coal, with somewhat more peat accumulating in areas of higher subsidence, but this was entirely at the expense of mudstone.

That sandstone amounts increase with subsidence while equal amounts of mudstone-coal are present at each borehole location indicates that fault-block tilting was discontinuous, and that mud and peat were deposited on the flat depo-

sitional surface in between tilting events. Larger amounts of sandstone in high-subsidence areas indicate that fault-block rotation resulted in an overall change from accumulation of mud and peat to bypassing of mud and accumulation of sand, and that more rapidly subsiding areas accommodated more sand. Hence, differential subsidence by means of fault-block rotation controlled the distribution and thickness of the major sand bodies, rather than faulting. Supply of the required large quantities of sand could be controlled by thrusting as well, causing downstream shedding of sand volumes stored in upstream locations.

That differential subsidence was the controlling mechanism is well illustrated by differences in sediment distribution between the wedge-shaped Units 1 and 2 and the tabular Unit 3. Figure 6a shows that a single regression line fits the sandstone values for all three units, and this line originates from the (mean of) the data cluster for Unit 3. This suggests that Unit 3 can be considered as a baseline unit for the study area, i.e. any unit deposited in the study area (of the same duration) would at least be ~50 m thick and contain the (average) cumulative amounts of ~5 m of (minor channel) sandstone and ~45 m of mudstone/coal, supplemented by an additional amount of sandstone if fault-block tilting occurred during unit formation.

The calculated regression-line equations confirm that differential subsidence was the driving mechanism. The regression line for mudstone/coal ($y=0.04x+45.3$) with a slope of 'zero' confirms that the cumulative mudstone/coal thickness in the units is independent of differential subsidence. It equals 45 m on average for both tabular and wedge-shaped units. The regression line for sandstone ($y = 1.04x - 45.4$) with a slope of 'one' on the other hand shows that all accommodation space, minus the 45 m for mudstone and coal, comprises sandstone.

Syntectonic depositional model

The alternation of tabular mudstone/coal deposits (with encased small-scale sandstone bodies) and wedge-shaped braidplain deposits reflects that continuous, regionally constant subsidence was at times overprinted by pulses of fault-block rotation and sand supply, in this case controlled by thrusting. It is envisaged that thrusting-induced loading was accommodated by reactivation of the block-faulted basement.

In Figure 7 a depositional model is depicted that shows how periodic fault-block tilting superimposed on regional subsidence explains the sediment distribution in the study area. A level depositional plain existed when regionally constant subsidence prevailed. The absence of a depositional gradient permitted standing water, thus promoting the settling of fine-grained sediment and the accumulation of peat (Fig. 6a). Channels flowed across the floodplain and experienced regular avulsions, resulting in a more or less random sandstone distribution. The random distribution of fluvial sands is considered the direct result of constant subsidence rates throughout the area, i.e. there were no low-lying areas that preferentially attracted channel systems (Alexander and Leeder 1987).

Periodic thrusting events resulted in the rotation of basement fault blocks and tilting of the depositional plain in various directions, but with a downstream-tilting component; this led to the interruption of floodplain conditions because the newly created depositional gradient secured fast run-off and prevented ponding of water and subsequent deposition of overbank mud. Instead, sand supply increased and accumulated in the low-lying areas, probably in braidplain systems, adapting to the new base-level profile (Fig. 6b). The braidplain systems thus filled up the newly available accommodation space, the fine-grained sediment fraction being transported to low-gradient areas further downstream (Fig. 6c). Once thrust and fault activity stopped, and the faulted topography had been levelled, a horizontal floodplain depositional system was re-established (Fig. 6d).

Coal beds are slightly thicker in areas of higher subsidence, even though they are part of the tabular floodplain layers. This may be because peat swamps were formed where the groundwater level was highest during the transition from braidplain to floodplain, i.e. when the area was not completely level yet. That floodplain arrangement, with swamps preferentially on the hangingwall blocks, may have been maintained during the subsequent floodplain phase.

Repeated alternations of floodplain and braid-

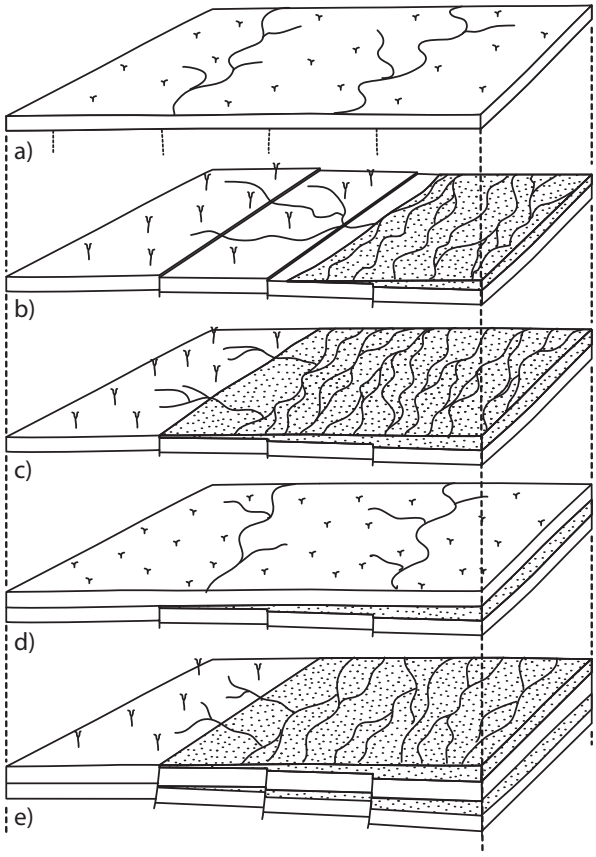

Figure 7 Depositional model for fluvial deposition on top of faulted topography where tilting has a downstream component. a) Under conditions of regionally constant subsidence a level floodplain exists. Floodplain deposition is dominated by overbank mudstone, with small channels, contained within stable vegetated levees, distributed randomly. Dashed vertical lines below the floodplain indicate hidden, temporarily inactive faults; b) When faulting takes place, additional accommodation space is created which becomes occupied by a high-energy braidplain system, eventually filling up the faulted topography (c); note that laterally the floodplain is a surface of non-deposition. The existence of a gradient in the downstream direction results in bypassing of the mud fraction, and allowing deposition of sand only. d) Once faults become inactive and the available accommodation space has been filled by the braidplain system, a level depositional plain is re-established, and floodplain deposition takes over again. e) Alternating periods of floodplain deposition and braidplain deposition result in the stacking of 1) tabular units consisting of mudstone, coal and rare isolated sandstone bodies and 2) wedge-shaped sandstone bodies.

plain conditions resulted in the architecture depicted in Figure 6e, with wedge-shape sandstone layers alternating with more tabular, mudstone-dominated layers. The thickness of these layers is variable, depending on the frequency and intensity of thrusting and fault-block rotation events. Note that the model presented here applies to low base-level situations only, otherwise faulting events would have resulted in the formation of lake bodies on top of the faulted topography (Blair and Bilodeau 1988).

Lateral extent of fluvial sandstone bodies

Within the study area there is no evidence of uplift of fault blocks during rotation, as the wedge-shaped units are thicker than the 50 m of the baseline unit at all locations. The major sandstone bodies are extensive and mostly run from fault to fault, their thickness gradually increasing towards areas of higher subsidence. Their regular, predictable distribution implies that the sandstone bodies are largely aggradational in nature and are not or hardly incised into the substrate, although minor erosion is bound to be associated with their basal scour surfaces.

The model predicts that the major sandstone bodies are continuous throughout the study area. Local deviations can partly be ascribed to general noise, such as the random distribution of small channels and differential compaction, but in a few boreholes the sandstone content deviates strongly. For instance, borehole Silesia-16 contains thick sandstone bodies at the base of Unit 1 that wedge out over a few 100s of metres (Fig. 4). This borehole was drilled immediately at the downthrown side of a synsedimentary fault, i.e. where the subsidence rate was maximal. Such locations must have attracted most of the run-off and likely were more sensitive to erosion, resulting in local incision, either as isolated bodies or as localized deeper basal incisions at the bases of aggradational sandstone sheets (Fig. 7).

Controls on cyclothem formation

The above analysis indicates that the accumulation of the major sandstones took place after thrusting and faulting events. Hence, the apparent 'cyclothemic' alternation of fluvial sandstone, floodplain mudstone and coal beds in the study area is of tectonic origin, rather than being controlled by glacio-eustasy. This is in line with interpretations by others (Klein and Willard 1989, Klein and Kupperman 1992, Jones and Glover 2005, Greb et al. 2008) for sandstone-rich Pennsylvanian successions that cyclothemic arrangement has a strong tectonic overprint. On a large scale, however, the three coal-bounded units that constitute the main sedimentary framework are likely to be eustatically controlled, because the equal amounts of mudstone/coal in the units, deposited under conditions of regionally constant subsidence, point to a equal duration of each of the three units.

Discussion and conclusions

This study demonstrates how differential subsidence may control the lateral and vertical distribution of sandstone, mudstone and coal under conditions of fault-block tilting in a foreland-basin setting. It shows that sandstone content increases more than proportional toward areas of higher subsidence. This is close to LAB-model predictions (Bridge and Leeder 1979, Bridge and Mackey 1993, Mackey and Bridge 1995), but the lateral distribution of mudstone shows that the controlling mechanism is intrinsically different. The LAB-models predict an increase of sand towards areas of higher subsidence, and at the same time a decrease of mudstone. In the case described here the amount of mudstone/coal is independent of differential subsidence.

In the LAB models fluvial sands and floodplain deposits are deposited synchronously, whereas the area discussed here experienced alternating phases of sand-dominated and mudstone-dominated deposition. This alternation resulted from thrust-controlled punctuated, differential subsidence events superimposed on continuous, regionally constant subsidence. This is a different scenario to the constant gradual rotation of fault blocks in the LAB models. Indeed the LAB models apply to situations where fault-blocks rotate around an axis parallel to the strike of the controlling normal fault. Rotation then does not result in gradient changes in the downstream direction as was the case in the study area. This downstream tilting made that fine-grained sediment was washed away downstream.

The study area is small and it is far-fetched to attribute local fault-related sandstone-stacking

in other Pennsylvanian sequences to the mechanism described here, but the straightforward relation with differential subsidence implies that the mechanism could well be applicable elsewhere. This can be tested by calculating linear regression equations for cumulative sandstone thickness versus thickness of the studied interval. The mechanism described here results in a slope of ~1.0 (Fig. 6a), whereas the slope predicted by LAB-models is between 0.7 and 0.9 (calculated after Bridge and Leeder 1979, Bridge and Mackey 1993 and Mackey and Bridge 1995).

Both mechanisms result in high sandstone percentages in areas of high subsidence, but sandstone-body width and interconnectedness are likely to be different. The LAB-models predict numerous sandstone bodies of limited lateral extent, which are likely to be vertically connected. The model described here predicts laterally extensive sandstone bodies that in most cases are vertically disconnected by intervening floodplain mudstones. In addition to the above-described local variations in sandstone proportion such architectural differences should be taken into account when these models are used as predictive tool in hydrocarbon exploration and production studies.

Acknowledgments

This study originated from the RECOPOL field experiment for underground storage of carbon dioxide in coal beds in southern Poland, a project funded by the 5th framework of the European Commission. The work presented here was carried out separately at TNO/Geological Survey of the Netherlands and the University of Utrecht. Henk Pagnier, Kees Geel (TNO/Geological Survey of the Netherlands) and an anonymous reviewer are thanked for comments on an earlier version of this chapter. The Central Mining Institute of Poland is thanked for providing access to the data in the scope of the RECOPOL project.

Chapter 4

SEDIMENTARY ARCHITECTURE AND PALAEOGEOGRAPHY OF LOWER SLOCHTEREN AEOLIAN CYCLES FROM THE ROTLIEGEND DESERT-LAKE MARGIN (PERMIAN), THE MARKHAM AREA, SOUTHERN NORTH SEA*

F.J.G. van den Belt and F.F.N. van Hulten

The Rotliegend gas play in the Southern Permian Basin has yielded over 200 gas fields in the Netherlands; they are found in an E–W fairway along the southern flank of the basin. Sandstones generally pinch out basinward, but localized, isolated sands are present north of the main fairway. The Rotliegend of the Markham gas field and a number of smaller fields in its vicinity (Markham area) provides a good example of such an isolated sand occurrence, and it may serve as a model for exploration in the "feather edge" of the Rotliegend desert lake.

The reservoir interval (Lower Slochteren Member) is a diachronous sequence, 20–50 m thick, from aeolian-dune sandstones to desert-lake mudstones. Periodic fluctuations of lake level, probably controlled by short-period Milankovitch rhythms (precession or obliquity) resulted in the formation of desert-lake mudstone drapes that compartmentalize the reservoir over kilometres. The Lower Slochteren interval consists of four aeolian cycles, 5–15 m thick, which are retrogradational from sharp-based aeolian sandstone, via sandflat and mudflat deposits to desert-lake mudstone. Toward the south the clay-bearing facies pinch out and aeolian sandstones merge into a compound aeolian sandstone body 20 m thick. The aeolian cycles accumulated in an eastward-dipping, 10-km-wide palaeovalley in the Base Permian Unconformity. The cycles onlapped onto the valley margins until the entire valley was filled and a depositional plain came into place. The plain was flooded by the Rotliegend desert lake, followed by the formation of progradational cycles about 5 m thick, each consisting of a basal desert-lake mudstone grading upward into mudflat and sandflat deposits.

The change from retrogradational (fining-upward) cycles to progradational (coarsening-upward) cycles seems controlled by the rate of formation of accommodation space during lake-level rise. Initially palaeotopography restricted the creation of accommodation space, thus allowing sediment supply to keep up with rising lake level and forcing dune sands to stack up against rising palaeogeography, resulting in aggradational to retrogradational sequences. However, lake-level rise across the depositional plain caused regional flooding and rapid and far retreat of the lake-margin depositional system, causing accommodation space to be filled after the flooding and resulting in progradational sequences.

The Markham case shows that the presence of isolated Rotliegend sandstones is related to palaeotopography and that their internal architecture is controlled by periodic expansion and contraction of the desert lake. It emphasizes the importance of accurate seismic definition of the Base Permian Unconformity and detailed, sedimentology-driven correlation for future exploration at the fringes of the Rotliegend-play fairway.

Introduction

The Markham gas field, discovered in 1984, is the main field in a cluster of Rotliegend (Late Permian) gas fields in what is here referred to as the 'Markham area'. It is situated approximately 150 km north-west of the Dutch coast line in the

**Published 2011: SEPM Special Publication 98, The Permian Rotliegend of the Netherlands, p. 161-176*

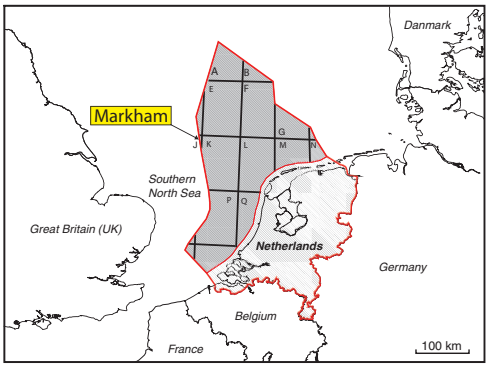

Figure 1 Location of the Markham field on the median line dividing the Dutch and UK continental shelf, Southern North Sea.

Southern North Sea on the median line that divides the Dutch and United Kingdom (UK) continental shelf (Fig. 1). The gas-producing sandstones in the Markham area are from the (Lower) Slochteren Formation, which is equivalent to the Leman Sandstone Formation in the UK, and were deposited in aeolian-dune and sandflat (sabkha) environments (Myres et al. 1995). The sandstones alternate with and pinch out northward into sandy mudflat and clay-playa (desert lake) mudstones. The abundance of mudstone interbeds in the Markham area is directly related to its relatively northerly location, at the southern margin of the Rotliegend desert lake.

After its discovery, several other Rotliegend gas accumulations were found nearby, such as Windermere (Bailey and Clever 2003) in the UK and J3-C and K1 A in the Netherlands (Fig. 2). There are numerous Rotliegend gas fields to the southwest in license blocks K5 and K6 that are characterized by a comparable stratigraphic and sedimentological setting (NLOG), but they lie in the main Rotliegend-play fairway. The Markham area is separated from the main fairway by an area where Rotliegend sandstones are absent and where gas is produced from Upper Carboniferous fluvial sandstone bodies (Fig. 2).

The Markham field is covered by offshore licenses J6 and J3b in the Netherlands and 49/10b and 49/5a in the UK. The field has been studied extensively by various partners participating in

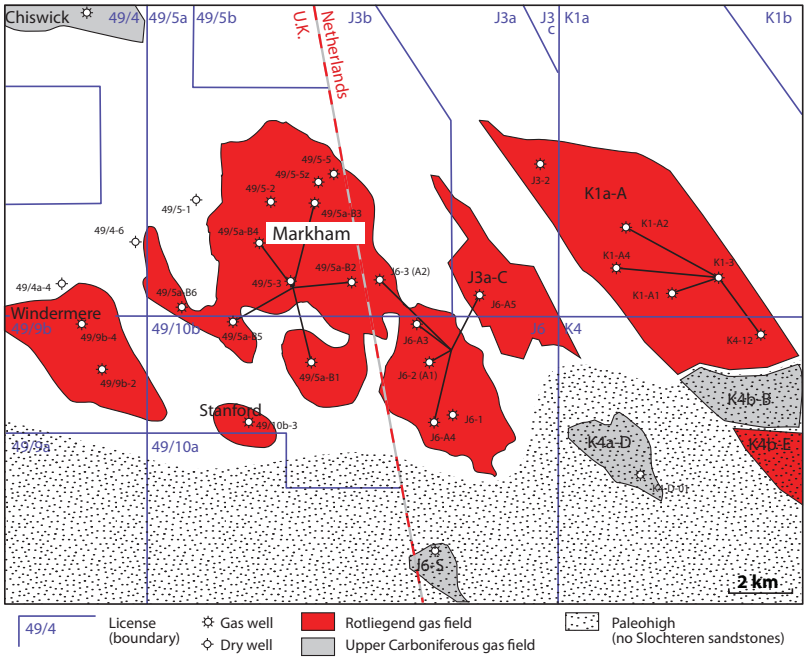

Figure 2 Rotliegend and Carboniferous gas fields and well locations in the Markham area.

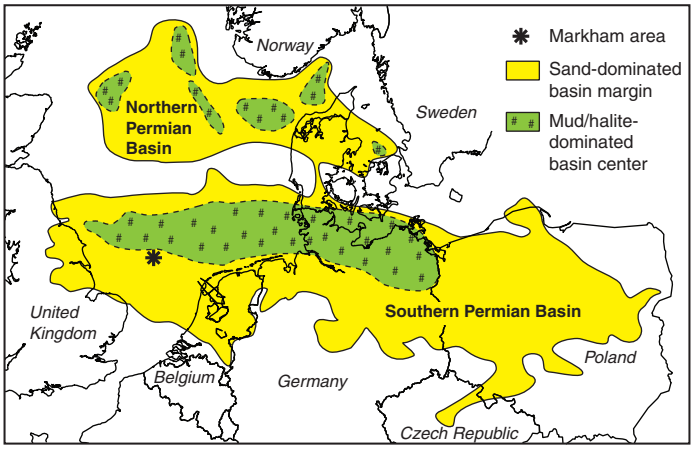

Figure 3 General map of the Northern and Southern Permian Basin.

the Markham field development (Myres et al. 1995). Its location in two states and several offshore licenses required equity determinations and an international treaty (Sharples et al. 1994). With many wells and more than 500 m of cored section, the Markham case is a well documented example of the Lower Slochteren depositional system at the southern margin of the Rotliegend desert lake.

This paper deals with the sedimentary architecture of the marginal dune field in the Markham area and the effects and causes of repeated transgressions by the Rotliegend desert lake. In addition, the influence of palaeotopography on the distribution and stacking of aeolian sandstones is discussed. The Rotliegend play is highly mature and most exploration wells are drilled in the vicinity of existing fields. At the same time, higher risk exploration has shifted to the 'feather-edge' margin of the Rotliegend desert lake and the data presented here may support such exploration efforts and provide quantitative input for reservoir-modelling studies.

Geological background

Rotliegend deposition took place in the E-W aligned Southern Permian Basin, an arid intracontinental depression between the Variscan thrust belt in the south and the Caledonian Highlands and Baltic Shield in the north (Fig. 3). It was located at a palaeolatitude of approximately 10°N with very low precipitation because the Variscan highlands created a rain shadow for humid Tethyan trade winds (Glennie 1998). It was an elongate basin that by the end of the Permian was some 1500 km wide and extended from the UK to Poland (Ziegler 1990, Verdier 1996, Gast et al. 2010). The main depocentre was located in Germany, where an up to 2.5 km thick Rotliegend succession accumulated (Bachmann and Hoffmann, 1997; Gast et al., 2010).

After an initial phase of volcanic deposition centred in Germany (Lower Rotliegend) and long lasting erosion with localized sedimentation (Upper Rotliegend 1), the basin was filled with desert-lake mudstones and evaporites in the centre and with aeolian-dune and fluvial-fan sandstones along its margins (Hedemann et al. 1984, George and Berry 1993, Verdier 1996, Glennie 1998) belonging to the Upper Rotliegend 2 (Glennie 1997, Gast et al. 2010). The progressive widening of the basin resulted in an overall onlapping succession, with sandstone-dominated deposits at the base that are overlain by mudstone and evaporite-dominated deposits. The central-basin lake is thought to have been well below global sea level, maybe up to some 300 m (Glennie 1997). The basal sands are diachronous and are particularly thick at the margins of the basin (Glennie 1998, Bailey and Lloyd 2001). Areas of aeolian and fluvial deposition were geographically separated, with large fan-shaped fluvial systems being linked to the tectonically controlled sediment-supply routes and aeolian dune

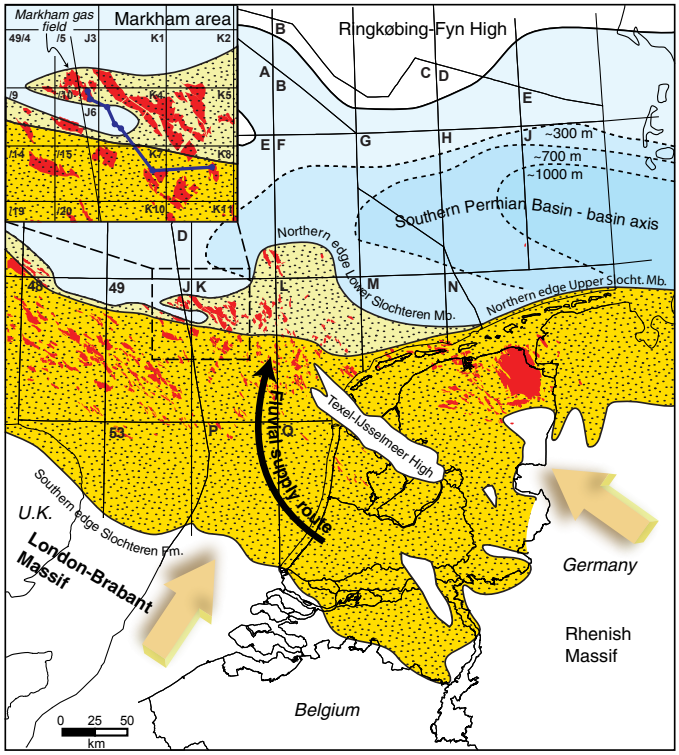

Figure 4 Outcrop belt of the Lower and Upper Slochteren members at the southern margin of the Southern Permian Basin in northwest Europe. Rotliegend gas fields in red. Inset shows the Markham area; note the ridge that separates Markham from the main Rotliegend-play fairway. In blue: correlation panel of Figure 5. Black arrow: major fluvial sediment-supply system (after George and Berry, 1997), possibly the source of Markham sands.

fields developing in areas downwind of these fan systems (Verdier 1996, George and Berry 1997, Mijnlieff and Geluk 2011).

Rotliegend of the Netherlands

In the Netherlands the Upper Rotliegend Group is generally 200-400 m thick with more than 700 m of mudstone and evaporites near the basin axis in the northeast (Fig. 4; Van Adrichem Boogaert and Kouwe 1993, Geluk 2007). All sandstone facies of the Upper Rotliegend Group in the Netherlands are part of the Slochteren Formation, which is found on the southern flanks of the basin along an E-W trend that parallels the present-day barrier islands along the northern Dutch coastline (Fig. 4). The sandstones of the Slochteren Formation are overlain by mudstone and evaporites of the Silverpit Formation (Fig. 5). Markham is one of the more northerly-located Slochteren gas fields and is isolated from the main Rotliegend fairway by a narrow ridge; in the nearby license blocks E18 and F16 Lower Slochteren sandstones are located even more northerly (Figs. 4, 5).

Along the margins of the Rotliegend desert lake the Slochteren Formation consists of the Lower and Upper Slochteren members, which are separated by desert-lake mudstones and mudflat deposits of the Ameland Member (Fig. 5). The latter pinches out toward the south, where the Lower and Upper Slochteren members merge into a compound sandstone unit. At the northerly location of the Markham area only sandstones of the Lower Slochteren Member are

present (Fig. 4); Upper Slochteren sandstones pinch out into desert-lake mudstones a few kilometres south of Markham (Fig. 5).

Palaeogeographic maps prepared by George and Berry (1993, 1997) for the Southern North Sea show that a major fluvial supply system was located east of the Markham area, originating from the southeast (Fig. 4) and supplying sediment to the Rotliegend desert lake. This fan system may have been the source for the aeolian sands in the Markham area, being transported by easterly winds.

Palaeotopography of the Base Permian Unconformity

The culmination of the Variscan orogeny during the Late Carboniferous resulted in uplift of the Variscan foreland, causing severe erosion of the Carboniferous sequence over a period of 10-20 My and resulting in an angular unconformity (*Base Permian Unconformity*; Gast et al. 2010) between Permian sediments and mildly folded and faulted Carboniferous-age strata (Ziegler 1990, Glennie 1998, Maynard and Gibson 2001, Geluk 2007). This resulted in an accentuated terrain at the level of the top Carboniferous, which influenced deposition during the Rotliegend. For instance, the total thickness of the Rotliegend was controlled by palaeotopography, with thicker sequences overlying palaeotopographic lows (George and Berry 1993, Bailey and Lloyd 2001). Crugnola et al. (1996) showed for the central Dutch offshore that palaeoscarps, with a 045°-225° strike and perpendicular to the main palaeowind direction (toward 280°-310°), influenced the distribution of aeolian sands, with aeolian-dune deposits being preserved at their lee sides. Also Maynard and Gibson (2001) concluded that aeolian sandstones are preferentially preserved in topographic depressions. For the Dutch offshore Geluk and Mijnlieff (2001) related palaeotopographic highs and lows to the lithology of the subcropping formations and their structural dip, with inclined sandstone formations forming 'cuestas'.

For the Markham area the influence of palaeotopography is demonstrated in a NW-SE correlation panel (Fig. 5), which shows that Lower Slochteren sandstones are present in the lows to the north and south of a topographic ridge. Note also that the Upper Slochteren depositional system did not prograde beyond this ridge.

The Markham Field

The Markham field is an excellent example of an isolated Rotliegend sand accumulation. It is made up of a basal, 20-50 m thick sandstone-mudstone alternation (Lower Slochteren Member) at a depth of about 3500 m, overlain by some 200 m of fine-grained deposits of the Silverpit formation (Fig. 5). The overburden comprises an Upper Permian-Lower Triassic sequence of carbonates, evaporites and red beds and a Cretaceous-Tertiary sequence dominated by carbonates and marine siliciclastics; these sequences are separated by an unconformity caused by Jurassic rifting (Fig. 6).

The field is a structural trap with dip closure, sealed by mudstones of the Silverpit Formation and Zechstein (Permian) evaporites. The gas was sourced from underlying Carboniferous coals and shales, although lateral migration played a role in the Markham area (Van Hulten 2007).

Myres et al. (1995) described the sand-rich Lower Slochteren interval as the deposits of a sand sea (aeolian dune) that graded northward into sabkha (sandflat, mudflat) and playa (desert lake) environments. The Lower Slochteren thins to the south, which they attribute to onlap against an easterly extension of the Cleaver Bank/Inde High (or Inde pediment) located to the south(west) of the Markham field (George and Berry 1997, Bailey and Lloyd 2001, Maynard and Gibson 2001).

The aeolian-dune sandstones from the Markham field are characterized by fairly good porosity (15-25%) and permeability (10-1000 mD; Myers et al., 1995). Sandflat to mudflat deposits in the northern part of the Markham Field have moderate to poor reservoir quality due to detrital clay and diagenetic overprint, as a result of proximity to the desert lake. With a Q50 (productivity under 50 bar drawdown) of over $1 \bullet 10^6$ m^3/day in the southern part of the field (Myres et al. 1995) the productivity of the field is much higher than for comparable lake-margin sandstones from the Upper Slochteren Member of the Ameland gas field ($0.03 \bullet 10^6$ m^3/day); this is related to pervasive clay-mineral diagenesis (Crouch et al. 1996).

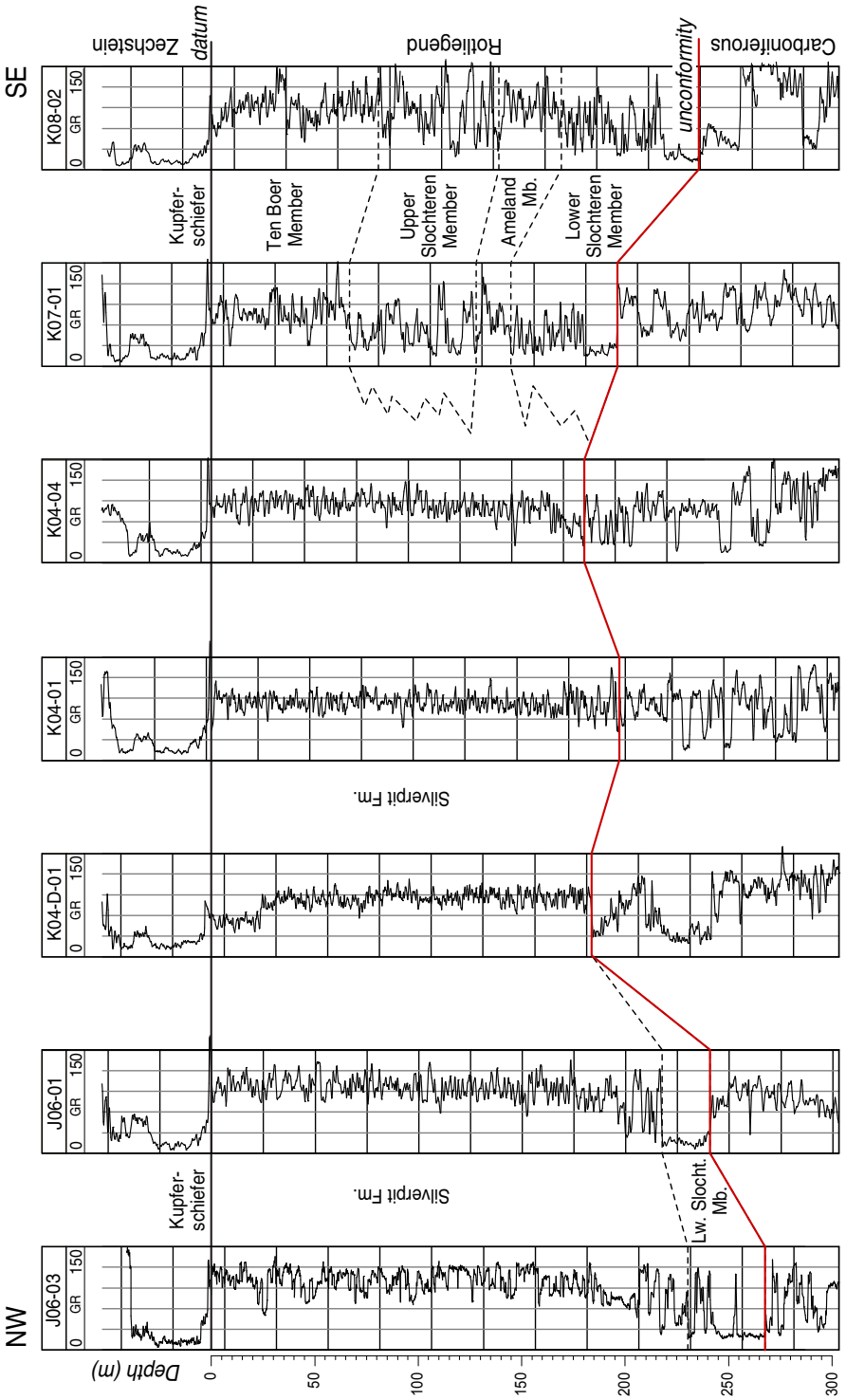

Figure 5 Regional cross section from the Markham area (NW) to the SE (see Fig. 4 for location), flattened on the base-Zechstein Kupferschiefer. The panel shows a palaeotopographic ridge in the Base Permian Unconformity (red). Note that both Lower and Upper Slochteren sandstone units have not prograded beyond this ridge and that Lower Slochteren sandstones to the north and south of the ridge are diachronous.

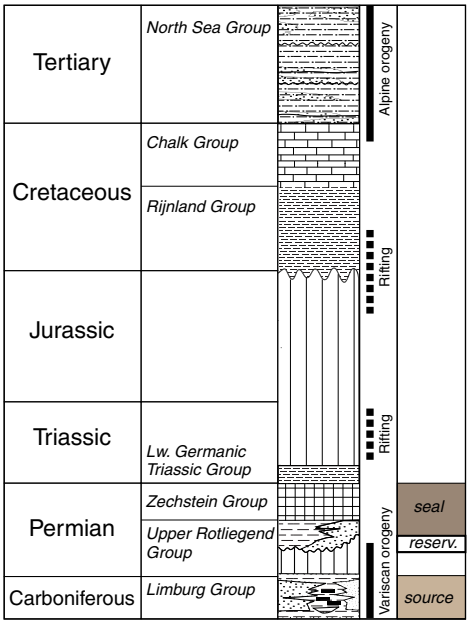

Figure 6 Stratigraphy, tectonism and elements of the Rotliegend gas-play for the Markham area.

Sandstones in the Markham area are mostly mature arenites; the dominant grain-size is fine to very fine. The petrological composition of Markham sandstones is typically 50% mono-crystalline quartz and 10% polycrystalline quartz. The sandstones contain less feldspar than the typical 2.5% for Rotliegend sandstones (Almon 1981), which is attributed to dissolution of feldspar grains (Myres et al. 1995). The abundance of lithic fragments (4%) is similar to the average value for Rotliegend sandstones in wells from quadrants K8 and K11. Sandflat sandstones and siltstones are characterized by substantially higher rock-fragment abundance and slightly higher feldspar abundance (2-3%). Authigenic minerals in aeolian sandstones comprise quartz-overgrowth cement and kaolinite clays, which do not severely reduce primary porosity. Sandflat facies are characterized by ferroan dolomite and anhydrite cements due to proximity to basin-centre evaporites, leading to reduced reservoir quality with permeabilities of 0.1-10 mD (Myres et al. 1995).

Sedimentary analysis

Sedimentary facies from a wide range of depositional environments have been recorded in the Rotliegend of the Southern Permian Basin, including aeolian dune, fluvial fan, wadi, sandflat and mudflat (sabkha) and desert-lake (playa) deposits (George and Berry 1993, Glennie 1998). The sedimentary evolution of the Lower Slochteren depositional system was studied based on the integration of core observations and wireline-log patterns (gamma-ray) from a total of 19 wells in the wider Markham area. The interpretations of sedimentary facies are based on core descriptions by Intergeos/TNO (1995) complemented by new core observations (Fig. 6). Subsequently sedimentary facies were assigned to the uncored intervals based on the typical gamma-ray patterns in the cored intervals.

Sedimentary facies observed in core

Rotliegend core descriptions are presented for the wells J06 01, J06 02, J06 03, J06 A3, 49/5 2, 49/5 3, 49/5 5 and 49/5 5z (Fig. 8). The following main facies were observed: aeolian dune, aeolian sandsheet, sandflat, mudflat and desert lake. The facies are described below; core photographs are shown in Figure 7.

Aeolian-dune facies - This facies is observed in all cored sections, but is most abundant in wells from the southern and central parts of the Markham field; it is dominated by cross-laminated sandstones (Fig. 7, photograph 1). The sand is moderately to well sorted and is mostly fine to medium grained, with localized, thin coarse-grained intervals. Beds of cross-laminated sandstone are stacked into 5-20 m thick compound units. Cross-sets are commonly 1-2 m thick, but are up to 5 m thick in places. Cross-sets display tangential cross-lamination with sub-horizontal basal lamination and cross-lamina dips increasing upward to around 25°. Strings of pebbly sandstone in places characterize the base of cross-sets and are indicative of deflation by wind. The coarseness of the pebbles indicates fluvial activity, which is attributed to occasional (low-quantity) fluvial input from the exposed Carboniferous ridge just south of the Markham area (Bailey and Lloyd 2001). Locally, cross-sets alternate with thin intervals of horizontally laminated, wind-rippled deposits of interdune origin. Limited cross-set thickness and interdune facies

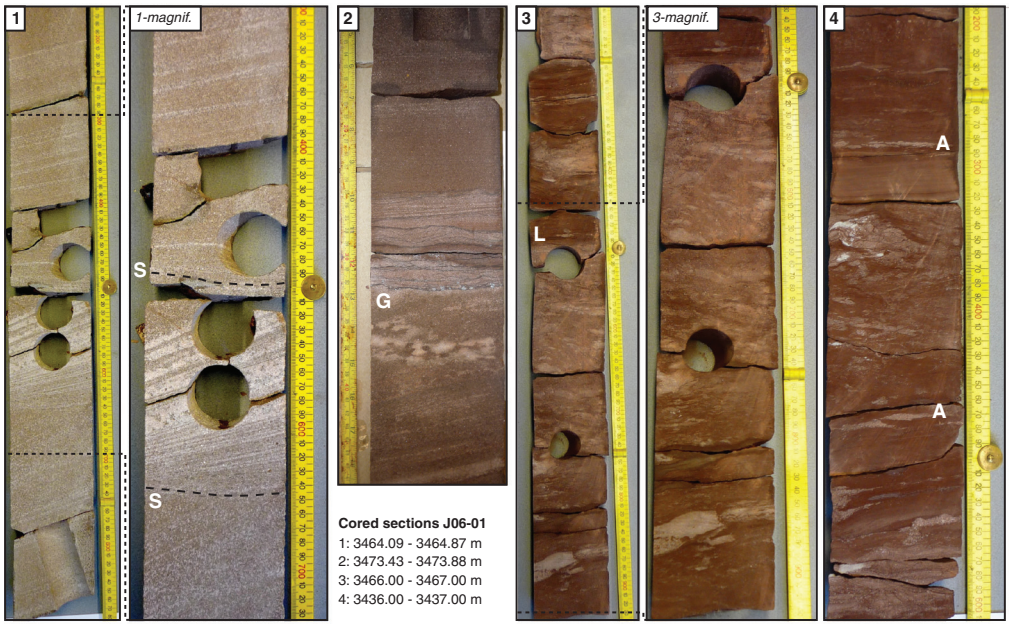

Figure 7 Cored sections from Well J06-01: examples of selected facies. 1) Dm-scale cross sets of low and high-angle aeolian-dune sandstones showing undulatory set boundaries (S) and tangential cross laminae. 2) Cross-laminated aeolian-dune sandstone and horizontally laminated aeolian sandsheet deposit separated by thin heterolithic interval with granule lag (G) and silt drapes indicative of fluvial reworking. 3) Mudflat deposits showing disrupted lamination due to mudcracking, adhesion rippling and salt-mineral growth and dissolution. Note localized preserved laminations of desert-lake origin (L) indicating periodically high water tables. 4) Alternation of well-laminated desert-lake mudstones and wavy-laminated mudflat heterolithics. Note sandy adhesion ripples (A) encased in clay matrix.

point at stacking of small to moderately sized dunes. Aeolian-dune intervals in places grade upward into aeolian sandsheet deposits; the facies sharply overlies the Base Permian Unconformity and mudflat and sandflat deposits higher up in the sequence.

Aeolian-sandsheet facies - This facies comprises moderately to well-sorted sandstones of fine to medium grain size. It consists mainly of horizontally to low-angle cross-laminated sandstones, with bimodal lamination in places (Fig. 7, photograph 2). Laminae occasionally contain thin wind-ripple trains. The deposits are present as beds or layers no more than a few metres thick and commonly overlie aeolian-dune facies, grading upward into sandflat deposits. The facies is interpreted as the deposits of sandsheets with poorly developed incipient dunes.

Sandflat facies - This facies consists of poorly to moderately sorted argillaceous and silty sandstones with a clay percentage up to 25%; the sediments are poorly to bimodally sorted. The deposits have a wavy-laminated to structureless or chaotic texture, resulting from adhesion rippling and disruptive processes such as salt precipitation/dissolution and sand injection. The facies is present as m-scale units and alternates on a m-scale with aeolian facies and mudflat facies. Thin sandflat intervals, typically no more than a few decimetres, may be present between successive aeolian-dune build-ups. Sandflat deposits accumulated in the transitional area between dune fields and the desert lake where ground water reached the sediment surface occasionally result-

ing in capturing of wind-blown clay.

Mudflat facies - The mudflat facies is the mud-rich equivalent of sandflat deposits and contains more than 25% clay. It is particularly common in cored sections from the north of the study area and from cores taken in the Silverpit Formation. The facies comprises red-coloured, muddy sandstones and sandy mudstones with a horizontally laminated to wavy laminated texture, reflecting alternating subaqueous and subaerial deposition. Mud cracks and adhesion ripples are common (Fig. 7, photographs 3 and 4). In places, bedding is disrupted due to sand injection and desiccation. The facies alternates on a m-scale with sandflat and desert-lake facies. It was deposited along the flanks of the desert lake, where the high water table resulted in accumulation of clays. Sand that was blown across the mudflat was preserved as adhesion ripples.

Desert-lake facies - This facies is dominated by massive, red-coloured mudstones, which alternate on a dm to m-scale with laminated silty mudstones and intervals of sandy mudstone with disrupted lamination (Fig. 7, photographs 3 and 4). In the sandy intervals adhesion ripples and mud cracks are present. This facies alternates on a m-scale with mudflat facies. The desert-lake facies is abundant in the northernmost part of the Markham field, especially toward the top of the studied interval. The mudstones accumulated in shallow, marginal parts of the Rotliegend desert lake, under semi-permanent high-water-table conditions. Mud cracks and adhesion ripples indicate that these shallow lacustrine areas dried out occasionally, pointing at contraction of the Rotliegend desert lake.

Sedimentary facies in uncored intervals

Sedimentary facies were assigned to uncored intervals using wireline logs (Fig. 8). Bailey and Lloyd (2001) demonstrated for the Rotliegend in the Markham area that the gamma ray (GR) log is a crude proxy for lithology and that it can be used for basic facies break-down. Due to higher GR values for clay-rich facies there is a general trend toward higher GR values from aeolian sandstones, via sandflat and mudflat to desert-lake deposits. Because clay content is low in both aeolian-dune and aeolian sandsheet facies those facies cannot be distinguished based on GR values. They were grouped under the log-facies name 'aeolian dune', although not necessarily cross-laminated. The facies was assigned to log intervals that are characterized by continuously low (minimal) GR values and a low-amplitude pattern. Typical GR values for pure sandstone vary by well: they are mostly 20-25 API, but may be as high as 40-50 API.

At the other end of the spectrum intervals characterized by continuously high (maximum) GR values represent pure mudstones of desert-lake origin. Because these mudstones are commonly thin they are characterized by distinct GR peaks, but where desert-lake mudstone intervals are thicker GR values are relatively constant (in most wells between 125-150 API). Because of the limited vertical resolution of the GR tool thin peaks are characterized by subdued values.

Sandflat and mudflat deposits, with their highly variable mud content, are characterized by intermediate values and by GR patterns that are more variable, displaying trends and higher-amplitude patterns. The cut-off value between sandflat and mudflat deposits was defined at 25% between the GR minimum and maximum, typically 50-60 API (reflecting a mudstone percentage of about 25%).

Well correlation

Wireline-log correlations of Rotliegend lake-margin deposits are often based on flooding surfaces (or 'flood' surfaces, cf. Langford and Chan 1988), i.e. mud-rich layers that are characterized by distinctive high-gamma-ray peaks (Martin and Evans 1988, Crouch et al. 1996). Flooding surfaces in lake-margin areas break up aeolian-dune and sandflat dominated sequences into m-scale intervals (Crouch et al. 1996). Crugnola et al. (1996) used multiple flooding surfaces to correlate wells from the Rotliegend in the central Dutch offshore, which allowed them to demonstrate that Lower Slochteren sands infill a base-Permian palaeotopography.

Correlation and datum levels

The organic-rich Kupferschiefer (Copper Shale) at the base of the Zechstein (Upper Permian) evaporite sequence, represented in GR

logs by a narrow peak (Fig. 5), defines a datum from which successive correlations in the Silverpit Formation can be hung in a top-down manner (Bailey and Lloyd 2001); this allows the identification of time lines within the diachronous Lower Slochteren Formation.

In the study area wireline-log correlations in and above the Lower Slochteren interval are based on two datum levels. The upper datum is present in the lower part of the Silverpit Formation and constitutes a narrow, high GR peak, which is sharply overlain by a 20 m thick retrogradational (fining-upward) sequence from moderate to high GR values (Fig. 8: Silverpit datum). The second datum is near the top of the Lower Slochteren Member and it constitutes the sharp base of a m-scale aeolian-dune unit that is sharply overlain by a progradational (coarsening-upward) mudflat sequence (Fig. 8: Lower Slochteren datum). This dune-mudflat sequence is a 10 m thick unit that is distinctive almost throughout the entire study area; only in the southernmost, sandstone-dominated wells the unit consists of aeolian-dune sandstone entirely and loses its distinctive pattern.

Within this basic correlation framework additional flooding surfaces were defined and correlated throughout the study area (Fig. 8). In the Lower Slochteren interval three major flooding surfaces were correlated (Slochteren flooding 1-3), of which the lower one is localized. In the Silverpit interval four major flooding surfaces were defined (Silverpit flooding 1-4). The lower three surfaces extend throughout the study area; the fourth, uppermost flooding surface is present in the northern wells only. The flooding surfaces could be traced from well to well throughout most of the study area, but flooding surfaces in Lower Slochteren Formation lose their high-GR expression toward the aeolian-dune dominated southern part of study area.

Thickness and facies trends

Lateral thickness variations

Thickness maps were drawn for (1) the interval between the base Lower Slochteren and the Lower Slochteren datum (Lower Slochteren interval) and for (2) the interval between the Lower Slochteren datum and the Silverpit datum (Silverpit interval); these maps are shown in Figure 9. The map for the Lower Slochteren interval displays strong lateral thickness variations. Assuming that the Lower Slochteren datum represents a flat palaeo-depositional surface (which is suggested by the constant thickness and the regionally consistent facies arrangement of the sedimentary cycle overlying this datum), the thickness pattern of the Lower Slochteren interval reflects the palaeotopography of the Base Permian Unconformity. This palaeotopography comprises a 10 km wide, eastward to north-eastward dipping valley that is bordered to the west, north and south by gentle flanks. Along its axis this palaeovalley deepens eastward to a (post-compaction) depth of some 35 m.

The thickness pattern of the overlying Silverpit interval is different, displaying a gradual thickness increase from 18 m in the south to 24 m in the north, and then suddenly to 29 m. This map shows that the base-Permian palaeotopography had been levelled completely after deposition of the Lower Slochteren Member and that the depositional gradient had changed from eastward to northward. This northward gradient is in line with the overall E-W elongation of the basin and reflects increasing rates of subsidence toward the basin axis. That the Silverpit interval is about 5 m thicker in the northern part of the study area, with no indication of a gradual thickness increase, suggests that an E-W aligned fault may have been active between the southern and northern areas, resulting in increased accommo-

Figure 8 (*next 2 pages*) Wireline correlation panels based on gamma ray logs. Correlation lines include flooding surfaces (green) and dune-base surfaces (red). Depth scale in true vertical depth (TVD (m)); facies columns include core facies (CF) and log facies (LF). Text labels on the right give names of correlation lines, labels on the left names of sedimentary cycles. All panels flattened on the Lower Slochteren datum. Due to flattening on an intra-Slochteren datum the possible post-Slochteren fault (red stippled) in panel 1 extends upward instead of downward.

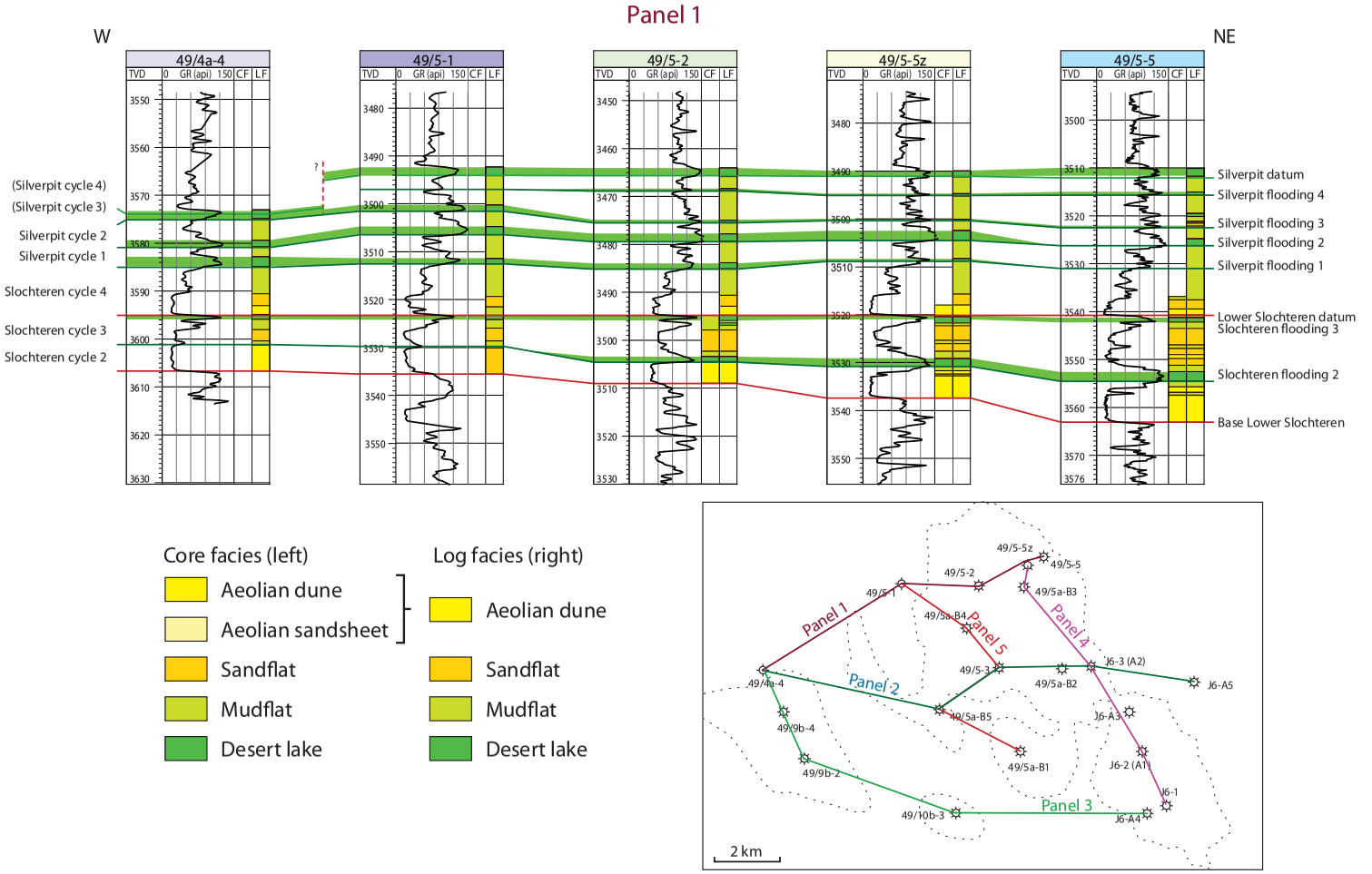
Panel 1
W
NE
49/4a-4
49/5-1
49/5-2
49/5-5z
49/5-5
TVD
GR (api)
CF
LF
(Silverpit cycle 4)
(Silverpit cycle 3)
Silverpit cycle 2
Silverpit cycle 1
Slochteren cycle 4
Slochteren cycle 3
Slochteren cycle 2
Silverpit datum
Silverpit flooding 4
Silverpit flooding 3
Silverpit flooding 2
Silverpit flooding 1
Lower Slochteren datum
Slochteren flooding 3
Slochteren flooding 2
Base Lower Slochteren
Core facies (left)
Aeolian dune
Aeolian sandsheet
Sandflat
Mudflat
Desert lake
Log facies (right)
Aeolian dune
Sandflat
Mudflat
Desert lake
49/5-5z
49/5-5
49/5-2
49/5-1
49/5a-B3
49/5a-B4
Panel 1
Panel 5
Panel 4
49/5-3
J6-3 (A2)
J6-A5
49/4a-4
Panel 2
49/5a-B2
49/5a-B5
J6-A3
49/9b-4
49/5a-B1
J6-2 (A1)
49/9b-2
J6-1
Panel 3
49/10b-3
J6-A4
2 km

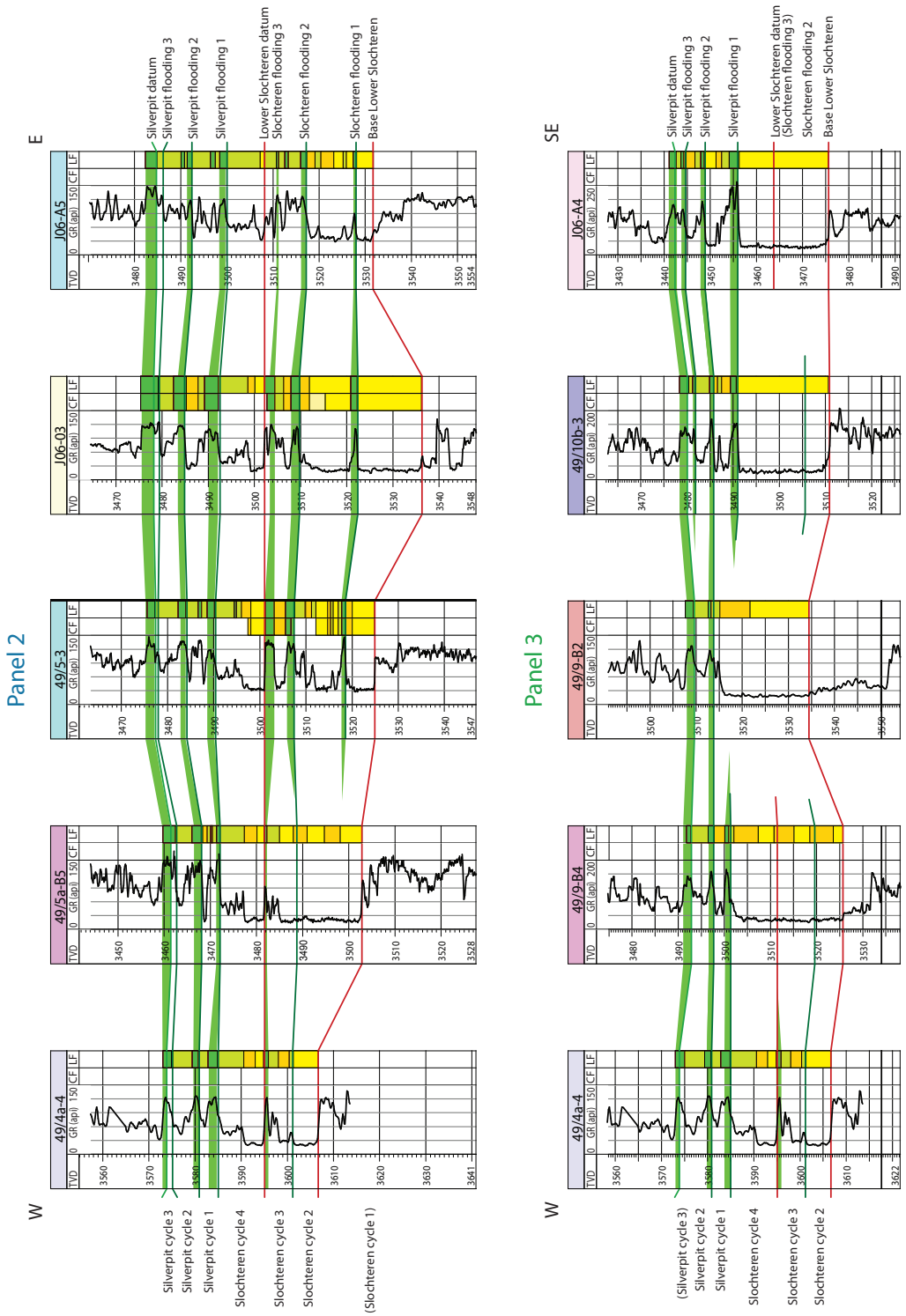
Panel 2
W
E
49/4a-4
49/5a-B5
49/5-3
J06-03
J06-A5
Silverpit cycle 3
Silverpit cycle 2
Silverpit cycle 1
Slochteren cycle 4
Slochteren cycle 3
Slochteren cycle 2
(Slochteren cycle 1)
Silverpit datum
Silverpit flooding 3
Silverpit flooding 2
Silverpit flooding 1
Lower Slochteren datum
Slochteren flooding 3
Slochteren flooding 2
Slochteren flooding 1
Base Lower Slochteren
Panel 3
W
SE
49/4a-4
49/9-B4
49/9-B2
49/10b-3
J06-A4
(Silverpit cycle 3)
Silverpit cycle 2
Silverpit cycle 1
Slochteren cycle 4
Slochteren cycle 3
Slochteren cycle 2
Silverpit datum
Silverpit flooding 3
Silverpit flooding 2
Silverpit flooding 1
Lower Slochteren datum
(Slochteren flooding 3)
Slochteren flooding 2
Base Lower Slochteren

dation space in the north.

Vertical facies trends and sedimentary cycles

The studied interval is an overall retrogradational sequence from aeolian-dune and sandflat deposits to mudflat and desert-lake deposits. At its base aeolian-dune sandstones unconformably overlie the level of the Base Permian Unconformity (Fig. 8).

The Lower Slochteren Member is dominated by aeolian-dune sandstones and sandflat deposits, and comprises four 5-15 m thick, repetitive cycles. These cycles are retrogradational from aeolian-dune to mudflat and desert-lake facies (Slochteren cycles 1-4). The first cycle (Slochteren cycle 1) is localized, but Slochteren cycles 2, 3 and 4 are present throughout the study area. Because of the abundance of aeolian facies these cycles are referred to as 'aeolian cycles'. The aeolian-dune sandstone bodies at the base of each cycle sharply truncate underlying lithologies and are approximately 5 m thick in most parts of the study area. Note that the basal part of Slochteren cycle 3 (in the northern part of the study area) is different from that in other aeolian cycles, with its gradational base from desert-lake mudstone to sandflat.

The Silverpit interval (above Silverpit flooding 1) consists of four to five cycles, about 5-6 m thick, which coarsen upward from desert-lake mudstone to mudflat or sandflat deposits. These cycles are referred to as 'desert-lake cycles'. Toward the south some of these cycles show a transition toward sandier facies, such as sandflat and locally aeolian dune. Cycles 1-4 are present across the study area, the fifth cycle is present in the north only; this is the area where the Silverpit interval is some 5 m thicker, and it may be that movement along an E-W aligned fault resulted in the formation of an additional cycle in the north.

In the south the upward transition from the sandstone-dominated Lower Slochteren Formation to the mudstone-dominated Silverpit Formation is sharp. There aeolian sandstones have stacked into a 20 m thick compound sandstone unit, which is sharply overlain by a relatively thin interval of mudflat and desert-lake facies. This transition is more gradual in the north, where aeolian sandstones alternate with mudflat and desert-lake deposits.

Lateral facies trends in the Lower Slochteren Member

The study area extends approximately 8 km N-S and 10 km E-W. At this scale lateral facies transitions occur, especially in N-S transects, which are shown in the facies maps of Figure 10. For each of the Lower Slochteren cycles a map was drawn for (1) the dune phase (lower part of the cycle) and (2) the lake phase (upper part). In the following section the lateral and vertical facies distribution is described for each of the Lower Slochteren cycles.

Lower Slochteren cycle 1 - The first Lower Slochteren cycle is only present in the narrow E-W aligned palaeovalley in the centre of the study area (Fig. 10). During the dune phase it was characterized by aeolian-dune facies throughout with thicker accumulations in the deeper, eastern part. The map suggests that the northern flank

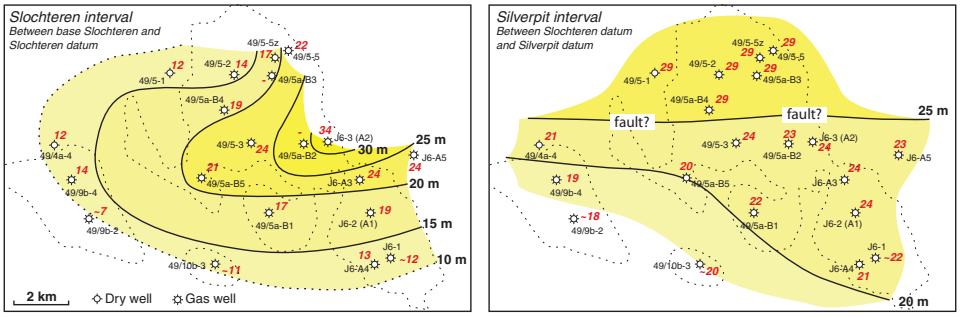

Figure 9 Hand-contoured thickness maps for the Slochteren interval (left) and the Silverpit interval (right). Thickness in red numbers. Field outlines as stippled lines. See text for explanation.

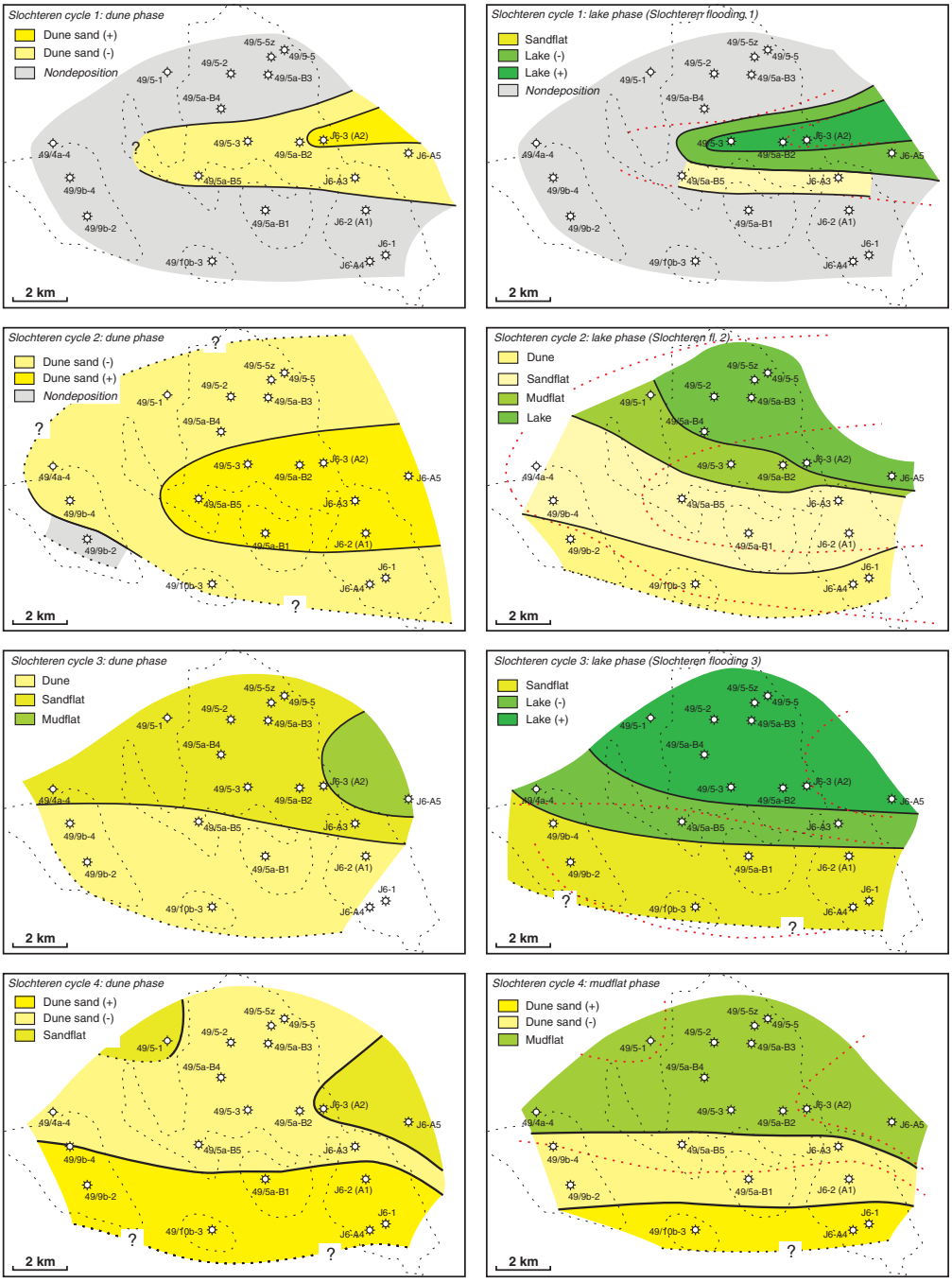

Figure 10 Facies maps for Slochteren cycles 1-4; *Left* dune phase for cycle 1-4, *Right* lake phase for cycles 1-3, mudflat phase for cycle 4. Dashed black lines: outlines of gas fields, dashed red lines: dune-phase facies boundaries. See text for explanation.

of the valley was steeper than the southern flank. Note that the northern flank of the palaeovalley coincides with the approximate location of the (assumed) fault that is responsible for the sudden northward thickness increase of the Silverpit interval (see Fig. 9), which suggests that the palaeovalley may have been fault-bounded in the north. Subsequent transgression resulted in deposition of desert-lake mudstones on top of the aeolian facies, with thicker mudstone packages along the axis of the valley. Only on the southern flank a narrow strip of sandflat deposits accumulated, which indicates that the northern flank of the valley was cut off from the south-eastern sediment source by the desert lake. Note that flooding of the area during the lake phase did not result in more widespread deposition than during the dune phase. This suggests that the basal, axial part of the palaeovalley may have been a prominent feature with relatively steep sides.

Lower Slochteren cycle 2 - During the dune phase of cycle 2 aeolian-dune facies accumulated across the entire study area, except in the immediate vicinity of well 49/9b-2, which suggest that regional subsidence had brought the entire area near or below base level. The thickest aeolian-dune accumulations again are found within the area of the palaeovalley, but the map for the lake phase indicates that the palaeovalley had become filled prior to flooding by the desert lake. The flooding resulted in deposition of desert-lake mudstones and mudflat deposits in the north of the area. Toward the south the desert-lake area was bordered by a sandflat and a narrow strip of aeolian dunes.

Lower Slochteren cycle 3 - The map for the dune phase of cycle 3 shows a 5 km wide, E-W aligned belt of aeolian dune deposits in the south, which grades northward into sandflat deposits. In the east the sandflat grades into a mudflat, which may indicate the presence of the desert lake more to the east. Subsequent lake-level rise resulted in transgression of the area by the desert lake some 6 km inland. This pushed the aeolian depositional system back to the south and resulted in a change from aeolian-dune to sandflat deposition at the southern edge of the study area. This cycle represents the moment of maximum transgression in the lower part of the studied interval.

Lower Slochteren cycle 4 - The dune phase of the final Lower Slochteren cycle is dominated by aeolian-dune sandstones, which are thickest in the south. Northward and upward through the cycle aeolian dune deposits grade into sandflat deposits (see Fig. 8). Note that for this cycle the facies distribution was mapped for the mudflat phase, which represents the minor flooding halfway up the cycle and not for the major flooding surface at the top (Fig. 8). In the north a 5 km wide belt of mudflat deposits is present, which grades southward into sandflat and then into aeolian-dune deposits. The facies belts for this cycle are completely E-W aligned and show fewer irregularities than those for the previous three cycles. This suggests that the palaeovalley in the Base Permian Unconformity, that initially influenced facies patterns had been filled completely by the time that the Lower Slochteren interval was flooded.

Depositional model

The observed sedimentary facies represent the range from an aeolian dune environment to a desert-lake environment (Fig. 11a)(Martin and Evans 1988, Myres et al. 1995). The mudflat and sandflat environments are transitional between areas of low groundwater and areas of high groundwater or slight inundation; the clay content is associated with the capacity of a wet sediment surface to capture wind-blown clay and silt. The preservation of aeolian-dune sands in the northerly and relatively remote Markham area was controlled by the presence of an eastward-dipping palaeovalley in the Base Permian Unconformity, which served as a trap for sand that blew into the area from an eastern source.

Its shape suggests that the palaeovalley may have originated as an erosional feature along the axis of an E-W aligned fold. The palaeovalley may have been a tributary to a large-scale valley system that drained the Base Permian Unconformity, possibly toward the basin axis in the north.

The overall retrogradational pattern of the Lower Slochteren is in agreement with regional observations and reflects onlap of the sedimentary system in response to the progressive expansion of the Southern Permian Basin and the as-

sociated, overall rise of lake level. The progressive change from sandstone domination to mudstone domination reflects marginward retreat of the sediment-supply system, but may be related to progressive drowning of the hinterland source areas as well (Bailey and Lloyd 2001).

Sediment by-passing and deposition

The correlatable, m-scale alternation of aeolian sands and desert-lake mudstones points at repetitive, small-scale expansion and contraction of the desert lake (Fig. 11b). That the aeolian cycles, which make up the Lower Slochteren Formation, are mostly sharp-based retrogradational cycles from aeolian sandstones to mudflat and desert-lake deposits (Figs. 8) is evidence of non-deposition and sediment by-passing during retreat of the desert lake. It seems likely that desert-lake lowering resulted in lowering of the ground-water level in lake-margin areas, thus preventing the preservation of mudflat or sandflat deposits that require a wet sediment surface. At the same time wind-blown sand seems to have been by-passed in a basinward direction where it was incorporated in progradational, lake-fill sequences at the margins of the shrinking desert lake. That this may have been the case is suggested by the coarsening-upward trend at the base of Slochteren cycle 3 in the north of the area (Fig. 8: e.g. well 49/5-5(z), 49/5-B3); it suggests that by-pass surfaces in proximal, aeolian sequences correlate with coarsening-upward sequences in the desert-lake area. During subsequent lake-level rise accommodation-space was created in lake margin areas allowing the accumulation of aeolian-dune deposits, in particular against rising palaeotopography. Ongoing base-level rise resulted in progressive retreat of the sedimentary system causing the formation of a retrogradational sequence from aeolian-dune sandstones to sandflat and mudflat deposits. Comparable retrogradational aeolian cycles, with basal 'sand-drift' surfaces and flooding surfaces at their top, have recently been described by Rodríguez-López et al. (2012) for the mid-Cretaceous of the Iberian Basin.

Influence of palaeotopography on cycle trends

As already noted in previous paragraphs, there is a marked difference in cycle character between the aeolian cycles from the Lower Slochteren interval and the desert-lake cycles of the Silverpit interval: the aeolian cycles are aggradational to retrogradational (fining upward), whereas the desert-lake cycle are progradational (coarsening upward, see Fig. 8). It has been shown that this change occurred at the stratigraphic level at which the base-Permian palaeotopographic lows had been completely sediment filled and it seems likely therefore that cycle trends were controlled by palaeotopography. It is thought that under the condition of existing palaeotopography a rise of lake level caused only limited retreat of the lake-margin sedimentary system, thus allowing sediment supply to keep up with lake-level rise and quickly fill newly available accommodation space, until the system was finally flooded. Thus, rising lake level forced sediments to stack up against palaeotopographic highs, in this case the flanks of the base-Permian palaeovalley, resulting in aggradational ('blocky') to fining-upward sequences. However, onwards from the moment that any existing palaeotopography became levelled and a flat sediment surface came into place, even a small rise of lake-level would result in far marginward retreat of the lake-margin system and in immediate and laterally extensive flooding of the area. The resulting accommodation space would then be filled after the flooding, resulting in progradational, coarsening-upward sequences.

Controls on sedimentary cyclicity

Lake-level fluctuations are commonly attributed to climate-controlled variations in aridity caused by shifting of climate belts (George and Berry 1993, Yang and Kouwe 1995, Howell and Mountney 1997), with periods of low precipitation and high evaporation resulting in contraction of the desert lake. That mechanism could well explain the sedimentary sequences observed in the Markham area. In any case, the presence of sediment by-pass surfaces between desert-lake/mudflat deposits and overlying sharp-based aeolian-dune sandstones indicates that desert-lake expansion and contraction was not controlled by climate-driven variations of sediment-supply, with increased outbuilding causing (apparent) lake retreat. Under such conditions progradational sequences from desert-lake, to mudflat, to

sandflat, to aeolian dune would have been preserved, and that is not observed here.

The sedimentary cyclicity in Rotliegend sequences is related to astronomical forcing by some (Yang and Kouwe 1995, Gast et al. 2010), but reliable determination of cycle periods is problematic due to absence of biomarkers, and time is therefore poorly constrained (Glennie 1997, Gast et al. 2010). For the Dutch offshore Yang and Kouwe (1995) proposed that the entire Rotliegend sequence comprises twelve 'third-order' cycles that are internally composed of

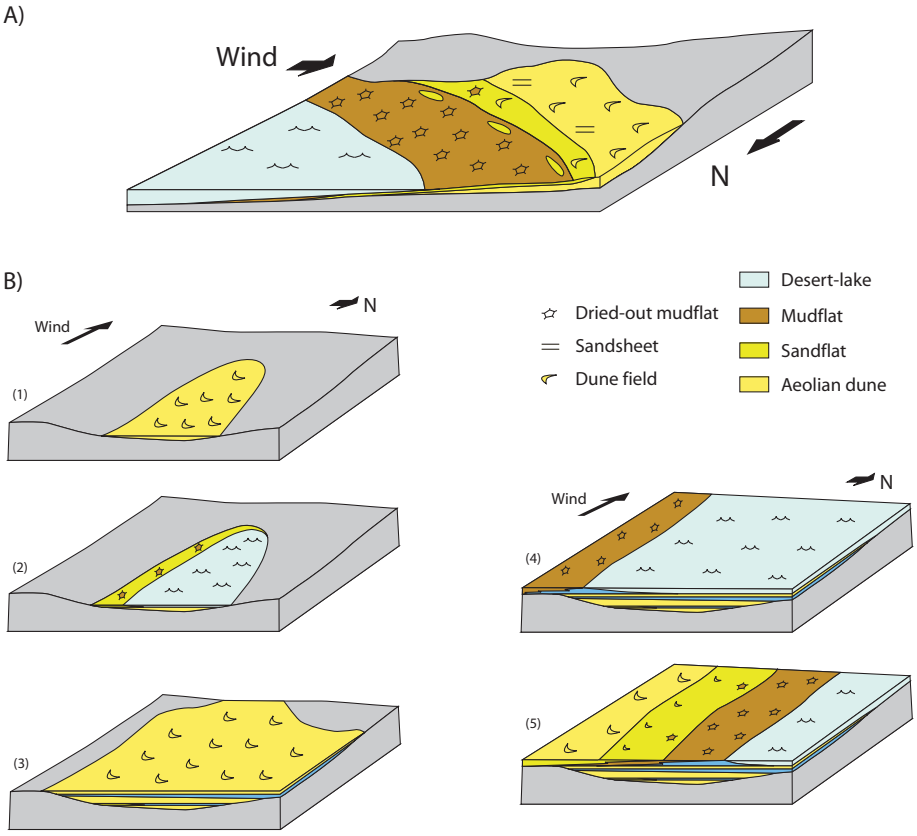

Figure 11 a) General depositional model for the Markham area: aeolian-dune field grading distally into desert-lake, via sandsheet and mudflat. Transgression by the lake results in retrogradational (fining-upward) cycles with a sharp-based aeolian package at the base and a thin desert-lake mudstone drape at the top. **b)** Summary of the depositional history of the Markham area: 1) aeolian sands infill palaeovalley incised into the Base Permian Unconformity; 2) Flooding of palaeovalley from the east by desert lake, resulting in mudstone drape over aeolian sands, note strip of sandflat deposits along southern shore. Northern lake margin is cut off from sediment source by the water body. Due to limited accommodation space within the palaeovalley sediment supply can initially keep up with lake-level rise, causing aggradation of aeolian sand and resulting in fining-upward cycles; 3) During a later cycle the complete infill of the palaeovalley by aeolian sands results in levelling of palaeotopography; 4) Flooding from the north results in far marginward retreat of the lake-margin depositional system and the formation of abundant accommodation space; 5) Accommodation space is filled by progradation of the mudflat/sandflat system, resulting in a coarsening-upward cycle. Dune fields may be present but preservation of dune sand is unlikely due to the absence of palaeotopography.

higher-order cycles with periodicities within the Milankovitch band. Also Howell and Mountney (1997) and Maynard and Gibson (2001) recognized 12 major cycles, but since thickness patterns for each of the 12-fold sequences are markedly different, the reliability of these subdivisions and their relevance in terms of time therefore seems low. Among others, Glennie and Provan (1990) and George and Berry (1993, 1997) subdivided the Upper Rotliegend in the UK and Dutch offshore into five large-scale units.

Large-scale subdivisions, other than the lithostratigraphic subdivision into the Lower Slochteren, Ameland, Upper Slochteren and Ten Boer members, are not particularly obvious in the Markham area. Large-scale coarsening-upward and fining-upward patterns can be observed, but patterns are not always consistent between wells (Fig. 5). On the other hand, small-scale cycles are quite prominent, as discussed above. Based on maximum flooding surfaces, sedimentary cycles are either 5-7 m thick or approximately twice that thickness (10-14 m). Note, however, that some of the thicker cycles are clearly composed of two sub-cycles. For instance, Lower Slochteren cycle 4 is characterized by a minor flooding surface halfway up the cycle. And particularly in the northern wells, where the influence of the desert-lake was strongest, a stacking of well-defined, 4-6 m thick cycles is evident (Fig. 8, panel 1). Based on the above it seems that the studied sequence is composed of stacked cycles, each approximately 5.5 m thick, which were occasionally merged together when lake-level rise did not extend far enough southward to deposit desert-lake muds entirely across the marginal dune field. Note that the aeolian cycles are slightly thicker than desert-lake cycles (Fig. 8), which is most likely related to differential compaction of sand and mud. The 5.5 m cycle well matches results of spectral analysis by Maynard and Gibson (2001), who detected a 16-20 ft (5-6 m) cyclicity, as well as a 51-60 ft (15-18 m) cyclicity, in wells from the UK desert-lake margin just west of Markham.

If the 5.5 m thick cycle indeed reflects a Milankovitch rhythm, then the 265 m thick Rotliegend sequence in the study area (maximum thickness in well J06-03, Fig. 5) represents the duration of about 48 such cycles. Cycle periodicity then depends on the duration of the Upper Rotliegend 2 interval (UR2), which however is poorly constrained (Glennie 1997, Gast et al. 2010). Recent work has suggested that the duration of UR2, originally estimated at some 10 My, may represent only 4-5 My in Germany, where the interval is most complete (Gebhardt et al. 1991, Glennie 1997). This means that the Rotliegend interval in the UK and Dutch offshore, where approximately a third of the UR2 interval is present (Glennie 1997) possibly represents no more than 1.3-2.7 My (George and Berry 1997).

If the 5.5 m cycles are obliquity controlled (35-44 ky; Berger and Loutre 1994) the Rotliegend sequence in the Markham area would be about 1.9 My long, which well matches the estimated duration of UR2. This gives a (post-compaction) subsidence rate of approximately 14 cm/ky, which is in agreement with expected rates of thermal subsidence for epicontinental basins (Gast et al. 2010). If controlled by precession (17-21 ky), however, the sequence would be about 0.9 My long, which is much shorter than the estimate of 1.3-2.7 My.

Precession is the more likely candidate to explain climate-driven variations of run-off and evaporation, and subsequent periodic contraction and expansion of the desert lake, because it primarily influences climate at low latitudes (De Boer and Smith 1994). This explains why precession is widely recognized in aeolian environments (Clemmenson et al. 1994), unlike obliquity that dominates at high latitudes (De Boer and Smith 1994). On the other hand, lake-level variations in the deep continental depression of the Southern Permian Basin may have been indirectly driven by (obliquity-controlled) glacio-eustasy (Glennie 1997), also considering that the Permian was characterized by south-pole glaciation (Crowley 1994). For instance at successive eustatic highstands sea water may have flowed into the basin (one-way), which would better explain the presence of marine foraminifer tests (Spirillina sp.) and glauconitic grains in thin sections from the Rotliegend of the UK West Sole gas field (Butler 1975, Gast et al. 2010), as well as the huge volumes of salt in the basin centre, although their low bromide content could indicate a non-marine source (Holster 1979).

Note that if the 5.5 m cycle indeed represents obliquity (35-44 ky), the 15-18 m cycle of May-

nard and Gibson (2001) would match eccentricity (95-123 ky). Although beyond the scope of this study it is finally noted that the pronounced high-frequency cyclicity in the GR pattern of the Silverpit Formation (Fig. 5, see well J06-01: 0-200 m), reflecting a m-scale alternation of anhydrite (low-value GR spikes) and mudstone beds (high-value GR spikes), could be precession controlled. A quick count shows that 200 m of Silverpit mudstones contain 80-90 anhydrite spikes; hence Silverpit anhydrite-mudstone cycles are on average 2.4 m thick, and based on the above time estimates represent 12-24 ky each.

Conclusions

The Lower Slochteren sandstones in the Markham area were deposited in a narrow dune field at the southern fringe of the Rotliegend desert lake. The presence of aeolian sand in this northern area is exceptional in the Dutch offshore and seems related to localized sand accumulation in a small palaeovalley incised within the Base Permian Unconformity. The studied interval is a retrogradational sequence from aeolian-dune sandstones at the base to mudflat and desert-lake deposits at the top.

Internally the sequence comprises stacked cycles that are between 5 and 15 m thick. The Lower Slochteren interval consists of four 'aeolian cycles', which are retrogradational from sharp-based, cross-laminated aeolian sandstones, via sandflat, to mudflat or desert-lake mudstones. The first two cycles fill an eastward-dipping palaeovalley within the base-Permian inconformity; during deposition of the next two cycles the base-Permian palaeotopography influenced deposition only slightly and was ultimately levelled by sediment. The drapes of mudflat or desert-lake facies at the top of each cycle (flooding surfaces) are traceable over distances of about 6 km and are evidence of periodic desert-lake expansion. The Silverpit interval consists of four to five approximately 5-m-thick progradational cycles that coarsen upward from desert-lake mudstone to sandflat deposits. The aeolian and desert–lake cycles are in the range of short-period Milankovitch rhythms (precession or obliquity).

Dune sands have stacked into a 20-m-thick, compound sandstone body in a narrow strip near at the southern edge of the Markham area, constituting good-quality, homogeneous sandstone reservoir. The area where dune sands are stacked is characterized by rapid southward thinning, which is the result of onlap onto the southern flank of the base- Permian palaeovalley. The reservoir quality decreases northward as aeolian-dune sandstones grade progressively into sandflat and mudflat deposits.

The observation that the sedimentary cycles are asymmetric, and are either retrogradational (aeolian cycles) or progradational (desert-lake cycles), indicates that periods of deposition and non-deposition alternated, but oppositely in dune and lake areas. This seems to be linked to progressive levelling of the base-Permian palaeotopography, with fining-upward cycles forming near palaeotopographic highs and coarsening-upward cycles forming on depositional plains.

It is clear from the Markham case that palaeotopographic lows in the Base Permian Unconformity at the fringe of the Rotliegend desert lake may be attractive sites for exploration, but this study also shows that good-quality aeolian sands may easily be compartmentalized vertically due to laterally extensive deposition of desert-lake mudstones, and that homogeneous, stacked sandstones may be laterally restricted in a narrow strip along the desert-lake margin. On the other hand, the good correlatability of the aeolian-sandstone units and intervening desert-lake mudstones shows that the reservoir architecture in similar settings may be relatively predictable.

Exploration for Markham-type aeolian reservoirs obviously requires a good understanding of palaeotopographic trends in the subcrop. Accurate seismic definition of the Base Permian Unconformity is therefore prerequisite, with state-of-the-art, long-streamer-surveying technology opening new possibilities. Palaeotopographic lows may enhance the preservation of aeolian sand, but their orientation, dip, and opening with respect to (north)easterly palaeowinds may be crucial for sand to have been preserved, which stresses the importance of regional sedimentological analysis.

Acknowledgments

This manuscript benefited from reviews by prof. dr. J. De Jager, prof. dr. R. Gaupp (University Jena) and one anonymous reviewer.

Chapter 5

A SHALLOW-BASIN MODEL FOR 'SALINE GIANTS' BASED ON ISOSTASY-DRIVEN SUBSIDENCE*

F.J.G. van den Belt and P.L. de Boer

The common assumption that saline giants must have formed in deep basins and that their thickness reflects initial basin depth ignores the principle of isostasy. Due to the high density of anhydrite and high precipitation rates for evaporite minerals, isostatic compensation is much more important in evaporite than in non-evaporite settings. The main implication is that evaporite precipitation drives subsidence instead of the opposite, and that thick evaporite deposits require an initial basin depth much less than their final thickness. Once initiated, evaporite precipitation and consequent isostatic subsidence is a self-sustaining process that can result in km-scale evaporite stratigraphy. Rapid isostatic compensation is facilitated by thin, fractured crust in extensional basins, which explains the typical occurrence of saline giants in such settings. We show that a shallow-basin origin in combination with rapid isostatic compensation can well explain the extreme thickness of saline giants as well as the commonly associated shallow-water sedimentary structures. Although there is no reason to exclude the possibility of a basin-wide dropdown of a few thousand metres as proposed for some saline giants, a desiccated deep basin is certainly not a requirement. An initially shallow basin which rapidly deepens by isostatic adjustment in response to the precipitation of evaporites, eliminates the need for deep-basin desiccation, gigantic waterfalls, and repeated opening and closure of a connection to the world ocean, and makes the extreme thickness of saline giants less enigmatic.

Introduction

A number of evaporite successions are characterized by extraordinary thickness and are therefore commonly referred to as saline giants. They are up to 4 km thick and are characterized by a number of stacked, thinning-upward evaporite cycles (Table 1). For example, the carbonate-evaporite succession from the Permian Zechstein reaches a thickness of 2 km (Taylor 1998); individual halite bodies are up to 600 m thick (Sannemann et al. 1978) and anhydrite bodies up to 280 m (Van der Baan 1990). The major Messinian evaporite series in the western Mediterranean was estimated to be 2-3 km thick (Hsü et al. 1973) and 2 km in the eastern Mediterranean (Tay et al. 2002). According to Krijgsman et al. (1999) the Mediterranean evaporite series was deposited in no more than 0.6 million years.

In the absence of recent analogues, developing models for saline giants has proven speculative. In the late 19th century (Ochsenius 1877) developed a depositional model based on evaporite precipitation in a restricted lagoonal environment. Hsü et al. (1973, 1977) felt it could not explain the new data from the Mediterranean, which they interpreted as deposits formed by precipitation from shallow-water salt lakes that occupied the deepest parts of kilometres deep, desiccated basins (Fig. 1). The model is known as the deep-basin shallow-water model and is often used in explaining thick halite deposits (Sonnenfeld 1984, Warren 2006, Warren 2010).

The formation of Zechstein halite bodies has also been attributed to deep-basin shallow-water deposition, although of different order (Tucker 1991). Here the estimate of maximum basin depth equals the thickness of the thickest halite body (approximately 600 m) (Tucker 1991, Warren 2006). Estimated basin depth before evaporite deposition was estimated in a similar way in,

Published 2007: IAS Special Publication 38, Sedimentary Processes, Environments and Basins, p. 241-252

Basin	Period	Setting	Underlying Facies	Cycles	Thickness (m)		
					Total	*Mean cycle*	*Halite*
Dead Sea *(Al-Zoubi et al., 2002; Neev and Emery, 1967)*	Pleistocene	Transtension	Lacustrine, alluvial	6	1500	250	375
W. Mediterranean Basin *(Blanc, 2000; Dercourt et al., 1986; Hsü et al., 1973)*	Miocene	Various	Various	-	2000	-	-
E. Mediterranean Basin *(Blanc, 2000; Tay et al., 2002)*	Miocene	Various	-	-	3500	-	-
Red Sea *(Sonnenfeld, 1984; Orszag-Sperber, F. et al., 1998)*	Miocene	Extension	-	-	3000-4000	-	-
Khorat Basin - *(Anderson et al., 1972; El Tabakh et al., 1999)*	Cretaceous	Extension	Red beds	3	1100	350	350
Cuanza Basin - *(Siesser, 1978)*	Cretaceous	Extension	Shallow marine	-	1500	-	-
Gulf of Mexico Basin - *(Reed, 1994)*	Jurassic	Extension	Red beds, volcanics	-	4000	-	-
S. Permian Basin (Zechstein) *(Sannemann et al., 1978; Van der Baan, 1990; Ziegler, 1990)*	Permian	Extension	Aeolian, shallow marine	4	2000	500	600
East European Basin *(Northrup and Snyder-Walter, 2000; Zharkov, 1984)*	Permian	Transtension	Aeolian, shallow marine	6	2500	420	500
Precaspian Basin *(Volozh et al., 2003)*	Permian	Thin crust	Deep marine?	-	4000	-	-
Delaware Basin *(Anderson et al., 1972)*	Permian	Transtension	Starved basin	2	1100	550	400
Paradox Basin *(Stevenson and Baars, 1986; Williams-Stroud, 1994; Zharkov, 1984)*	Carboniferous	Transtension	Shallow marine	5-7	2000	300	270
Michigan Basin *(Catacosimos et al., 1990; Cercone, 1988; Zharkov, 1984)*	Silurian	Extension	Shallow marine	5	1000	200	400
East Siberian Basin - *(Zharkov, 1984)*	Cambrian	Extension	Shallow marine	12	2500	210	-

Table 1 Summary of stratigraphic, facies and thickness data for various Palaeozoic to Cenozoic saline giants

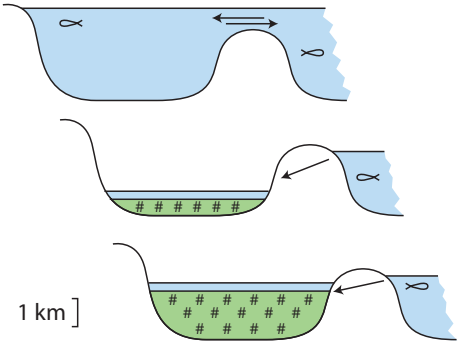

Figure 1 Deep-basin shallow-water model developed for saline giants (after Kendall 1992). The model does not take into account any syn-depositional isostatic compensation due to evaporite loading.

for example the Delaware Basin and the Paradox Basin (Anderson et al. 1972, Williams-Stroud 1994).

For the Zechstein (Southern Permian Basin) abundant drilling has shown that the thick evaporite succession consists of at least 4 major cycles, the thickest basal cycle being more than 600 m thick locally (Sannemann et al. 1978, Van der Baan 1990, Tucker 1991, Taylor 1998). These cycles are composed of a marginal carbonate wedge, an anhydrite platform and an onlapping halite body (Fig. 2). It is widely accepted that at the termination of each cycle, halite had filled the basin approximately to sea level, and that after continued tectonic subsidence the deposition of a subsequent evaporite cycle started (Van der Baan 1990, Tucker 1991, Taylor 1998, Warren 2006). Such an internal architecture, with anhydrite predating halite is common in evaporite basins (Sonnenfeld, 1984; Warren, 2000).

Despite the wide acceptance of a deep-basin origin of halite bodies, a number of aspects of their formation have not been adequately explained. Following Nesteroff (1973), Sonnenfeld (1985) argued against a deep-basin shallow-water origin for the Messinian evaporites, giving a long list of arguments among which was the unexpected occurrence of tidal sediments. Recently the deep-basin shallow-water origin of Messinian evaporites has been challenged (Hardie and Lowenstein 2004, Manzi et al. 2005).

Although a shallow-basin shallow-water model well explains the occurrence of mainly shallow-water depositional structures, the model is qualified as 'unlikely in most tectonic environments' by Kendall (1992) because it requires subsidence and deposition to be in equilibrium during the deposition of km-scale evaporite successions. In the discussion about the depth of such basins prior to the formation of saline giants, the role of isostasy on basin evolution and stratigraphic development is commonly not appraised. Here we focus on isostatic compensation as a mechanism that explains how thick evaporite sequences can form in shallow-water basins under long-term gradual subsidence.

Isostasy

Isostatic compensation is the response of the lithosphere to change of overburden by flexure or elastic rebound to achieve regional equilibrium (Watts 2001). Such corrections are accommodated by lateral displacement of more ductile, high-density asthenosphere beneath the flexing plate. That such corrections may be implemented rapidly is shown by the fast response to polar deglaciation, where unloading has been 90% compensated by glacial rebound during the 10 thousand years of the Holocene (Watts 2001).

It has been demonstrated that the deposition of a thick siliciclastic wedge at a basin edge causes a strong isostatic response (Watts 2001) and that should be more pronounced for an anhydrite wedge due to the higher density of anhydrite (Table 2). Hence, evaporite deposits such as from the Zechstein or the Miocene Mediterranean, which are 2 to 3 km thick and occupy basins many hundreds of kilometres across, must have created much of their own accommodation space by means of loading. It is therefore expected that the mechanism of isostatic subsidence during salt precipitation explains, at least partly, the great apparent basin depth of many evaporite basins (Fig. 3). A factor that is expected to facilitate isostatic correction during salt precipitation is the condition that the basement of many saline giants consists of thin, fragmented crust due to rifting or post-orogenic collapse (Table 1) (Burke 1975, Stanley 1986, Volozh et al. 2003).

Several authors have acknowledged the loading effect on the crust of thick salt deposits (Nor-

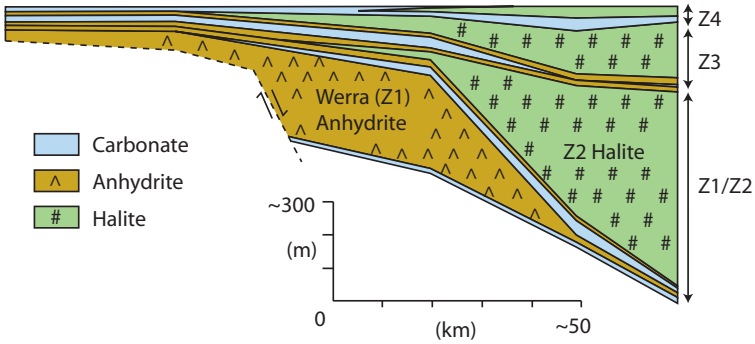

Figure 2 Stratigraphy and cyclical character of the Zechstein evaporites (after Visser 1956). The Zechstein 1 halite from the original figure is not represented here, as it did not precipitate in the main basin (Van der Baan 1990).

man and Chase 1986, Diegel et al. 1995, Van Wees et al. 2000), but do not consider this a syn-depositional phenomenon. An advanced analysis of isostatic compensation in relation to evaporite basin evolution was published by Norman and Chase (1986). They applied the 'Lake Bonneville' principle of Gilbert (1890), who showed that the Late Pleistocene desiccation of the present Great Salt Lake caused a 40 m uplift of the lake-shore deposits. Norman and Chase (1986) demonstrated that desiccation of the Mediterranean must have resulted in large-scale uplift of the basin floor as well as its margins. Besides that they argued that the Messinian Mediterranean was much shallower than now due to isostatic compensation in response to salt loading. Fabbri and Curzi (1979) invoked an isostasy model to calculate the depth of deposition for the lower Messinian evaporite in the Tyrrhenian Sea and concluded that it was deposited in a shallow instead of a deep basin. On the other hand, Ryan (1976) performed a quantitative reconstruction incorporating the effect of loading and he concluded that the Mediterranean Sea was locally more than 2.5 km deep (Balearic Basin).

Substance	Density
Quartz	2.65
Calcite	2.85
Sediment (30% water)	2.20
Halite	2.15
Gypsum	2.30
Anhydrite	2.95
Seawater	1.03
"Asthenosphere"	3.30

Table 2 Rock, mineral and brine densities relevant to this study (Valyashko, 1972; Schumann, 1987; Watts, 2001)

Halite

The deep-basin theory that was developed for saline giants requires that the unusually steep basin margins as they are observed now in the subsurface (Warren 2006) were already in place before the onset of evaporite precipitation (Fig. 1). If the basin margins were indeed as steep prior to halite deposition as after (Fig. 1), the marginal successions within such basins would be characterized by abundant clastic deposits. However, evaporite cycles are characterized by an absence of clastic interbeds except for anhydrite breccias, while such deposits may be common in underlying or overlying formations (Sonnenfeld 1984). We therefore assume the tectonic component of total subsidence in evaporite basins to be low.

We assessed the implications of isostatic compensation during the precipitation of evaporites by making simple calculations based on the Airy isostasy model (Fig. 4). It was not our intention to perform a state-of-the-art basin-scale modelling study. Instead we generally explored how the incorporation of isostatic compensation may help to develop an alternative model that explains the large-scale subsidence history of salt

basins as well as their sedimentary development.

Our calculations are based on two assumptions. First, we assume that isostatic adjustment of the lithosphere takes place during deposition. Note that the Late Permian, which was characterized by evaporite formation worldwide, lasted approximately 10 million years. Krijgsman et al. (1999) have demonstrated that the Messinian salinity crisis lasted only 600 thousand years: a short period for the precipitation of 2-3 km of evaporites. This should however be sufficient for isostatic compensation, as it occurs on an even smaller scale of 10 thousand years (Watts 2001). Secondly, we assume laterally extensive deposition in a large basin (e.g. 300 x 1500 km for the Southern Permian "Zechstein" Basin (Ziegler, 1990), such that the flexural wavelength of the lithosphere is significantly smaller than the scale of the basin. For these conditions we determined the maximum thickness of evaporite columns, if salt precipitation occurred under continuous isostatic compensation.

Rates of precipitation of halite are of the order of 10-150 mm per year (Schreiber and Hsü 1980, Sonnenfeld 1984 *and references therein*), which is up to 3 orders of magnitude greater than subsidence for extensional basins with average rates up to a few mm per year (Einsele 2000 *and references therein*). Precipitation rates for gypsum and anhydrite are of the order of 1-10 mm per year (Sonnenfeld 1984), thus of the same order as subsidence rates of extensional basins. We therefore conclude that the tectonic component of overall subsidence during halite precipitation can be ignored, whereas it is important during gypsum/anhydrite precipitation. Hence subsidence of a halite-accumulating basin is likely to be entirely controlled by loading due to halite precipitation.

Balancing the columns in Figure 4 for a case of a deep basin that dries out, yields that the amount of uplift due to desiccation is a function of the initial basin depth (D_{bas}):

$$Uplift = \left(1 - \left(\frac{\rho_{asthen.} - \rho_{wat})}{\rho_{asthen.}}\right)\right) * D_{bas} = 0.3 * D_{bas}$$

The density values used in the equations are presented in Table 2. As a density range applies to halite and anhydrite, we have used mean density. Hence the results vary slightly if lower or higher density values are used.

From the above equation it follows that the depth of a desiccated basin equates to 70% of the initial depth of a water-filled basin. For the desiccated deep-basin model of Hsü et al. (1973) it follows that a 2.0 km deep desiccated basin would be up to 2.9 km deep before drawdown, if isostasy were taken into account.

If that basin were filled with halite under continuous isostatic compensation, the thickness of the ultimate halite column (T_{hal}) is a function of the depth of the desiccated basin:

$$T_{hal} = \left(\frac{\rho_{asthen} - \rho_{air}}{\rho_{asthen.} - \rho_{hal}}\right) * D_{bas} = 2.9 * D_{bas}$$

This equation predicts that a 2.0 km deep desiccated basin is filled with a maximum of 5.8 km of halite if precipitation takes place under the condition of rapid isostatic adjustment. On the other hand a desiccated basin only 690 m deep would be sufficient to accommodate a 2.0 km thick halite sequence if halite precipitated under rapid isostatic compensation.

The deep-basin shallow-water model of Hsü et al. (1973) implies that the filling with halite of a 2 km deep desiccated basin, is followed by up to 2 km of subsidence to regain isostatic equilibrium. Note that a shallow-basin and a deep-basin both allow the formation of a 2 km thick evaporite succession (Fig. 5). However we feel that the

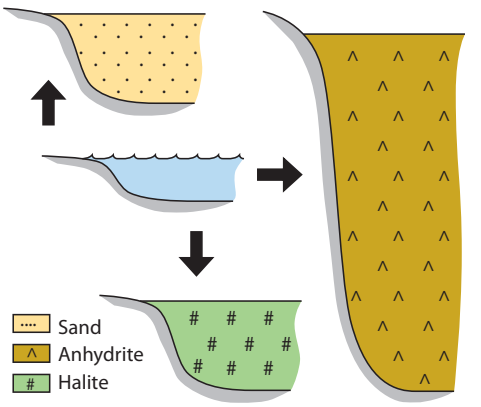

Figure 3 Due to a higher density, anhydrite precipitation causes a high degree of isostatic compensation, allowing the formation of thick successions in a shallow basin.

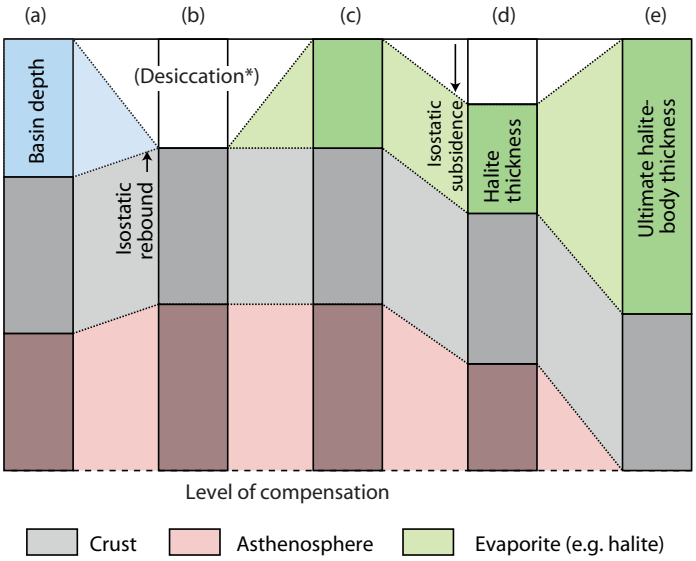

Figure 4 An Airy isostasy model for basin drawdown and evaporite precipitation. Stages: a) water-filled basin (isostatic equilibrium), b) uplift due to basin desiccation, c) halite precipitation, d) subsidence due to halite precipitation and e) maximum halite-accumulation potential for a 'stage a' basin (isostatic equilibrium). *According to the deep-basin, shallow-water model, the basin desiccates causing isostatic rebound. According to the shallow-basin shallow-water model, the basin remains water-filled.

shallow-basin model is more generally applicable and less restrictive where tectonic and geographical conditions are concerned. For example, it accounts for the occurrence of shallow-water sediments (early stage) as well as deeper-water sediments (late stage), without repetitive km-scale marine desiccation and re-filling.

Our calculations show that there is a simple alternative to the deep-basin shallow-water evaporite model, which well explains the thickness of saline giants as well as the occurrence of shallow-water sedimentary structures. The main implication of isostatic compensation in evaporite-basin evolution is that evaporite precipitation drives subsidence instead of the opposite, and that thick halite deposits as they are observed in the rock record require an initial basin depth much less than their eventual thickness.

A halite-deposition model, which explains the formation of saline giants under the condition of isostatic compensation, is shown in Figure 6. First the connection of a shallow water-filled basin with the open ocean becomes restricted such that much of the oceanic inflow evaporates and that little outflow of dense brines occurs. We attribute restricted outflow to a progressive narrowing of a straight, which for example may be controlled by anhydrite precipitation along the margins of a graben.

The precipitation of halite is a rapid process allowing halite to rapidly fill a shallow basin. The rapid deposition of halite causes disturbance of the isostasy balance, thereby forcing a subsidence reaction of nearly 50% of the thickness of the halite column (Fig. 4). This newly created accommodation space may consequently be filled with halite, again causing a subsidence reaction. As long as the basin receives ocean water, which is to be expected if not any tectonic events interfere, the process can continue until subsidence approaches zero. By that time a halite column of up to 3 times the desiccated basin depth or 2 times the water-filled-basin depth will have been accommodated. Note that our model requires a situation of continuous oceanic inflow and restricted outflow, whereas the deep-basin shallow-water model is based on repeated phases of complete isolation from the world's oceans (Fig. 1).

For a water-filled basin the ultimate halite thickness is a function of the initial water depth (D_{bas}):

$$T_{hal} = \left(\frac{\rho_{asthen.} - \rho_{wat}}{\rho_{asthen.} - \rho_{hal}} \right) * D_{bas} = 2.1 * D_{bas}$$

The above equation suggests that a halite body such as the thick Zechstein-2 halite (600 m) may form in a basin with an initial water depth of 285 m. A two km thick evaporite series representing a single precipitation event may be accommodated within a 950 m deep water-filled basin. In the case of two evaporite units separated by a period with tectonic subsidence, an average basin depth of 425 m is sufficient to accommodate 2 km of halite in two phases. Note that many saline giants consist of 4 or more anhydrite-halite cycles (Table 1). Hence, the average basin depth is then reduced to a few hundred metres or less.

Note that the derived depths are within the depth range of current desiccated continental depressions such as Death Valley, California (-85 m), the Dead Sea rift, Jordan (-411 m), the Qattara Depression, Egypt (-134 m) and the Danakil Depression in the Afar Triangle, Ethiopia (116 m). The flooded evaporite-precipitating Gulf of Karabokhaz, Turkmenistan is currently 35 m below global sea level. Hence, these depressions which are characterized by thinned and fractured crust may well host future saline giants if connected to the marine domain.

Anhydrite

Evaporation of marine-sourced brines causes calcium sulphate ($CaSO_4$) to precipitate well before the halite saturation point is reached (Hardie 1967). Consequently major halite bodies are found in association with $CaSO_4$ precipitates. Major anhydrite bodies have been shown to be basin-margin wedges and the bulk of these bodies precipitated in shallow coastal sabkha environments (Sonnenfeld 1984). Evaporation has the greatest net effect in shallow water and thus coastal platforms act as evaporite traps. Primary formation of anhydrite is inhibited by chemical boundary conditions, but primary gypsum may be directly converted into anhydrite under high temperature and/or high brine salinity, conditions commonly observed in coastal sabkha environments (Hardie 1967).

The stability of either of the two $CaSO_4$ minerals is important with respect to isostasy, since their density values are markedly different (Table 2). The density of anhydrite is much higher than that of porous sediment, thus a change from

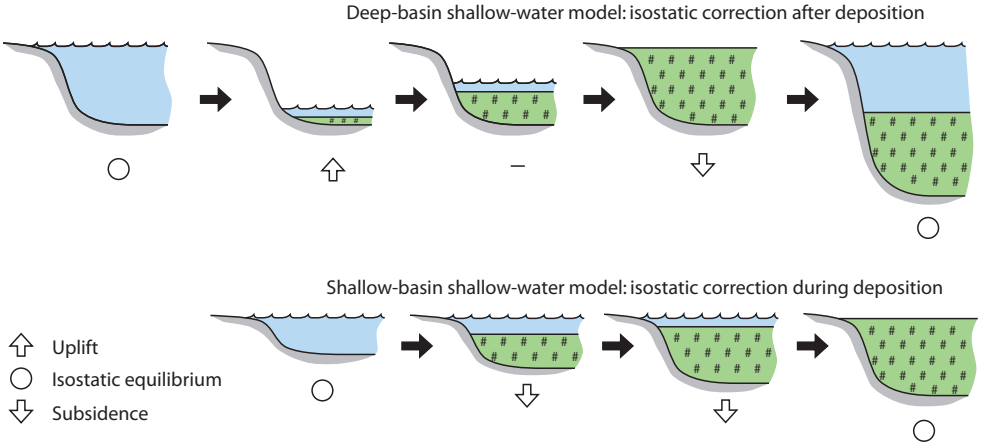

Figure 5 The deep-basin shallow-water model for saline giants is based on isostatic compensation after salt precipitation. The shallow-basin shallow-water model for saline giants is based on isostatic compensation during salt precipitation. Note that the latter model is characterized by an initially shallow basin whereas the former model is characterized by an initially deep basin, that after filling with halite is subjected to a phase of isostatic subsidence.

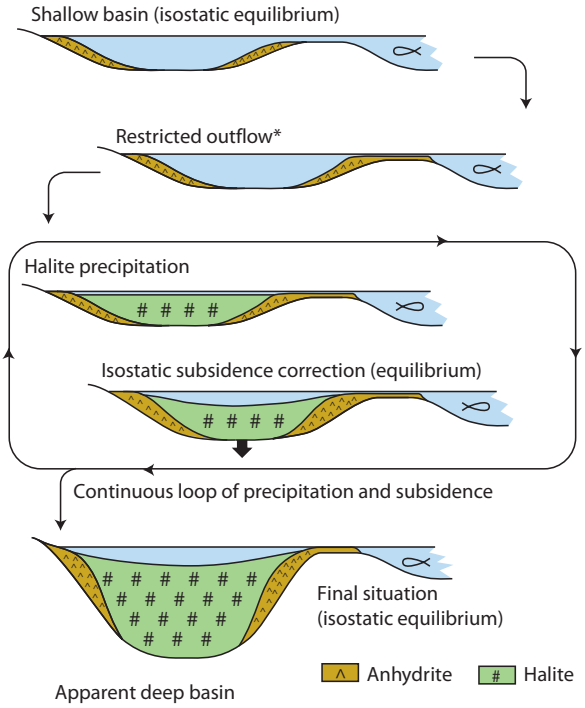

Figure 6 Model for halite precipitation under continuous isostatic compensation: rapid precipitation of halite in a shallow basin causes isostatic subsidence hereby resulting in an apparent deep-basin structure. *Restricted outflow may be controlled by anhydrite-platform progradation into a narrow strait (e.g. rift), connecting the evaporite basin with the world ocean.

non-evaporite to anhydrite deposition has a major effect on isostatic balance and subsidence. The density of gypsum is approximately equal to the density of porous sediment, so that both have a similar effect on the isostasy balance in terms of density. Gypsum precipitation also may result in accelerated isostatic subsidence because of the common high precipitation rate. Based on constraints of brine concentration and temperature, it is assumed that anhydrite generally precipitates on the platform (high net evaporation) while gypsum (selenite) precipitates on the platform slope (low net evaporation)(Tucker 1991, Warren 2006).

In an aggradational-platform situation where tectonic subsidence, sedimentation and isostatic subsidence are in equilibrium, a change from non-evaporite to anhydrite precipitation would approximately cause tripling of total subsidence according to the equation:

$$T_{anh} = \left(\frac{\rho_{asthen} - \rho_{sed}}{\rho_{asthen} - \rho_{anh}} \right) * T_{sed} = 3.1 * T_{sed}$$

The long-term laterally equivalent deposition of coastal-sabkha anhydrite and inland sabkha clay under continuous isostatic compensation therefore would result in a rapid basinward thickening rock column, where the anhydrite column is up to a factor 3 thicker (Fig. 7). Locally such differential subsidence may be facilitated by passive (non-tectonic) fault movement, as has been observed on seismic cross-sections for Zechstein anhydrite bodies (Van der Baan 1990).

The proposed model for anhydrite deposition is illustrated in Figure 7. As long as some tectonic subsidence occurs and fresh seawater is supplied, aggradational anhydrite precipitation along the basin margin can continue. Because the rate of anhydrite precipitation is expected to be higher on the platform than on the platform slope, a

progressive steepening of platform clinoforms is predicted. That may result in mass movement as observed in the Zechstein and other basins where slumped anhydrite and anhydrite turbidites occur (Van der Baan 1990, Tucker 1991, Warren 2006).

The thickest anhydrite body in the Zechstein is the up to 280 m thick Werra anhydrite (Van der Baan 1990). Most of its relief is filled with the 600 m of halite belonging to the Zechstein-2 cycle (Fig. 2). The precipitation of a thick anhydrite wedge results in the formation of an equally deep adjacent basin, which may be characterized by the precipitation of pelagic gypsum (varves) as observed in the Zechstein (Van der Baan 1990) or in the Delaware Basin, Texas (Sonnenfeld 1984, Van der Baan 1990), and is the later site of halite precipitation. Hence, the prolonged basin-margin precipitation of anhydrite initiated under shallow-water, lagoonal conditions may contribute to the formation of very thick halite bodies (Fig. 7).

Discussion

Isostatic compensation during evaporite deposition is expected to have a major influence on evaporite-basin evolution, due to the density values of the minerals involved and the high deposition rates of evaporite minerals. Saline giants typically formed in (post-orogenic) rifting-dominated areas (Table 1). Late-Carboniferous to Permian evaporites formed on thin, fragmented crust that developed during the collapse of Hercynian mountain chains (Stanley 1986, Volozh et al. 2003). Triassic to earliest Cretaceous evaporites formed in rift-basins that were transgressed by the sea during the break-up of Pangaea (Burke 1975).

A relatively weak and thin crust, dissected by faults thus seems to characterize sites of major evaporite formation. Such conditions will have allowed rapid isostatic adjustment allowing thick evaporite accumulations. The location of major evaporite bodies at the downthrown sides of major faults (Van der Baan 1990) suggests that reactivation of existing faults may have allowed a quick isostatic response locally.

The application of the isostasy principle predicts that kilometres deep continental depressions are not a prerequisite for the formation of saline giants, but that also relatively shallow depressions upon a weak crust such as the Dead Sea or the Danakil and Qattara depressions in the northernmost East African rift, offer favourable conditions. Brine and influx modelling by Tucker and Cann (1986) has shown that deep-brine basins are not required for the formation of thick evaporite series and that 'for most geological examples it is possible to postulate a shallow-basin origin in which the basin is continuously replenished by new influx', i.e., that many saline giants could have formed in basins of only a few hundred metres deep that were replenished by normal sea water. Their model requires that evaporite deposition is balanced by constant basin subsidence, which condition is met in a shallow-basin model by the isostatic effect of salt loading.

The shallow basin concept requires a shallow depth of deposition of sediments underlying saline giants. The evaporites from the Zechstein conformably overlie aeolian sands, playa shales and evaporites from the Rotliegend Group, the basal Zechstein Coppershale and a thin unit of basal Zechstein ramp carbonates (Taylor 1998). The Rotliegend itself developed on thin crust after orogenic decay. Similarly other saline giants appear associated with shallow marine deposits as well as arid terrestrial siliciclastics (Table 1).

Due to rapid precipitation during phases of strong evaporation, isostatic subsidence (loading) outpaced tectonic subsidence. Most evaporite successions are characterized by a number of anhydrite-halite cycles separated by relatively thin carbonate sequences. To allow such repetitive phases of evaporation, it is required that halite precipitation phases of short duration are followed by longer periods of carbonate or anhydrite deposition to allow the (tectonic) formation of accommodation space for a new phase of halite precipitation.

Considering the similarity in thickness and extent of the Mediterranean Messinian halite bodies and other saline giants (Table 1), the obvious question is if their genesis has been similar. A deep-basin model has been advocated for the Messinian evaporites based on assumed evidence of pre- and post-Messinian deep marine deposition (Hsü et al. 1973, Cita 2001) and on the assumption that the Mediterranean Sea was deep already before the Messinian period. Iso-

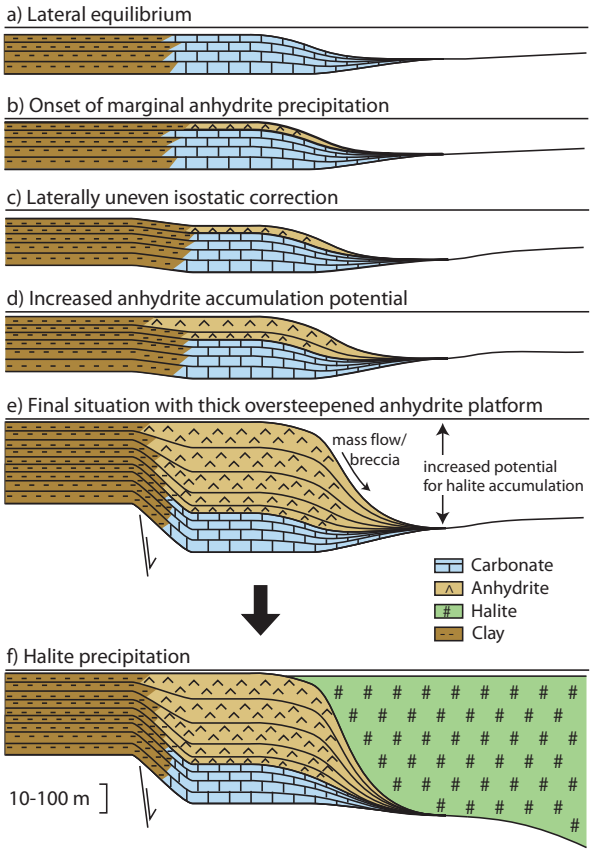

Figure 7 Anhydrite precipitation model: the high density of anhydrite causes accelerated isostatic subsidence, thus allowing the accommodation of a thick anhydrite platform at the site of an initially shallow basin. On the other hand anhydrite loading may result in the formation of a deep adjacent basin, which allows the consequent accumulation of a thick halite body.

static compensation of salt precipitating from continuously inflowing marine water in arid climate zones allows relatively shallow basins to develop into saline giants. Hence our model could provide a simple alternative for the deep-basin theory. Note that the model eliminates the need for repeated opening and closure of the oceanic connection, deep-basin desiccation and gigantic waterfalls.

Future saline giants may be formed in present-day arid-region continental depressions such as the Dead Sea and the Qattara and Danakil depressions of the East African rift. Once such tens to some few hundred metres deep depressions are connected to the world ocean by a relatively shallow strait, the formation of evaporites is expected to cause gradual isostatic subsidence and thus allow the deposition of evaporites much thicker than the present-day depth of these depressions. Note that the size of many of these areas is comparatively small, however continued rifting and subsequent flooding with seawater may result in a rapid increase of surface area. For example continued widening and collapse of the main East African rift, now only below sea level in the northernmost Afar Triangle may result in an evaporite basin as large as the Southern Permian Basin (Zechstein).

Acknowledgments

The manuscript has benefitted from reviews by G. Nichols and C.J. Ebinger (Royal Holloway University of London), and by A.B. Watts (University of Oxford).

Chapter 6

AN INTRA-BASINAL MECHANISM EXPLAINING MARINE-EVAPORITE CYCLICITY CONTROLLED BY SULPHATE PLATFORM PROGRADATION AND ISOSTATIC CORRECTION

F.J.G. van den Belt and P.L. de Boer

Marine evaporites such as the Zechstein consist of thinning-upward sulphate-halite-potash cycles, whose origin is still poorly understood. We investigated an intra-basinal mechanism that well explains their mineral composition and cycle build up. The mechanism involves the progressive obstruction of ocean connections by sulphate-platform progradation, causing a chain reaction of outflow reduction and subsequent accelerated sulphate precipitation. Numerical modelling shows this to be a self-accelerating process that ultimately triggers halite and potash precipitation. Isostatic compensation of the salt load explains the formation of accommodation space for subsequent cycles, each about half the thickness of the previous cycle.

Introduction

Giant marine evaporite bodies such as the Permian Zechstein have formed throughout the Phanerozoic (Zharkov 1981, Warren 2010). They commonly consist of a number of stacked sulphate-halite-potash cycles, each tens to hundreds of metres thick, with sulphate (gypsum/anhydrite) constituting basin-margin platforms and thin central-basin annual-varve sequences. The more soluble halite and potash salts fill the basin topography (Fig. 1). Despite many well studied examples (Sonnenfeld and Kendall 1989, Warren 2006) much is uncertain about the formation of giant marine evaporites and the mechanism driving cyclicity, also because there are no present-day analogues.

Evaporite models have been dominated by the idea that thick basin-evaporite bodies precipitated in deep desiccated basins, a concept developed for the Late Miocene Mediterranean (Hsü et al., 1973) and applied more generally since (Nurmi and Friedman 1977, Tucker 1991, Warren 2006). However, a persistent two-way ocean connection is more in line with the observation that marine evaporites are enriched in sulphate and depleted in higher-solubility salts relative to sea-water composition (Sonnenfeld 1985, Hardie and Lowenstein 2004). Hence, it is unlikely that much deposition took place during desiccation phases, and models are increasingly based on the filled-basin concept (Hardie and Lowenstein 2004, Manzi et al. 2005, Van den Belt and De Boer 2007, Krijgsman and Meijer 2008).

Existing models for evaporite-cycle formation are primarily focused on deep-basin desiccation and involve eustatic control (Tucker 1991) or tectonics (Krijgsman et al. 1999). However, if formed in basins with open connections to the ocean, the origin of evaporite cyclicity may need to be reassessed. Besides the general problem that the complete closure of an ocean connection imposes a salt influx problem, eustatic sea-level fluctuations have difficulty explaining that halite, in such cases interpreted as a lowstand deposit (Tucker 1991), overlies the tops of carbonate/sulphate platforms in places (e.g. Fig. 1e). Tectonic mechanisms, such as movement of a barrier (Benson 1972), are hard to reconcile with the cyclic character of evaporites because it requires a harmonica movement.

An alternative mechanism

Considering the abundance of marine evaporite bodies and the similarities between them, we investigated the potential of a more general mechanism, independent of external factors. With gypsum precipitation rates up to 10 m/ky (Schreiber and Hsü 1980, Sonnenfeld 1984), sulphate platforms are capable of rapidly prograding over 10s of kilometres (Cameron et al. 1992,

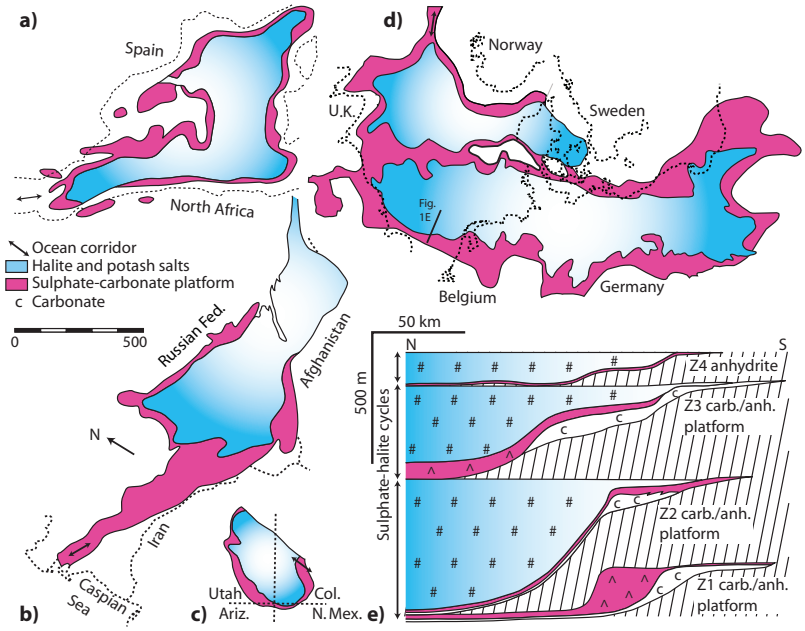

Figure 1 Palaeogeographic maps for various evaporite basins. Sulphate platforms occur along the basin margins and within ocean corridors, halite occupies the central basins; a) Miocene, Western Mediterranean (Hsü et al. 1973); b) Jurassic, Asia (Sonnenfeld 1984); c) Permian, Paradox Basin, USA (Peterson and Hite 1969); d) Permian, Zechstein Basin (Europe) (Ziegler 1990); e) Sulphate-halite cycles from the Zechstein of the UK with depositional geometry reconstructed (Cameron et al. 1992).

Kendall and Harwood 1996), which is reflected in the broad anhydrite rims that typically surround evaporite basins, also near their ocean corridors (Fig 1). This could lead to progressive obstruction of such corridors (Van den Belt and De Boer 2007), causing reduced brine outflow and raised salinities (Lucia 1972), followed by sulphate precipitation and accelerated platform progradation. If not interrupted externally, e.g. by sea-level rise or tectonics, this could lead to halite and potash-salt precipitation in the basin centre. The mechanism has the advantage that it progressively obstructs outflow while still allowing ocean-water inflow to continuously replenish evaporated basin water and thus maintain salt influx, e.g. by means of tidal spill-over. Lowering of sea level (or tectonic uplift of a barrier) also may obstruct outflow, but is likely to ultimately obstruct inflow as well unless the closing process accidentally stops at precisely the right time.

Model description

We developed a simple numerical model to test the validity of the mechanism, and verified if it results in realistic evaporite-cycle composition and operates on short-enough time scales to outpace tectonic and eustatic processes. The model simulates seawater/brine exchange, salinity evolution and precipitation in circular basins of constant depth, connected to the ocean by a narrow corridor (Fig. 2). The model is initiated at a steady state of incipient sulphate saturation, i.e. with basin water saturated for calcium sulphate but no precipitation taking place yet. Precipitation is then initiated by implementing a small reduction of the cross-sectional area of the ocean corridor, causing a chain reaction of 1) outflow reduction, 2) salinity rise, 3) sulphate precipitation on the basin floor and primarily along the basin margin. This results in a narrower ocean corridor and further outflow reduction.

We consider sulphate saturation as a state that is reached occasionally when marginal continental basins (in arid-climate belts) are invaded by the sea, e.g. in response to deglaciation. Of the many basins that are invaded, most will become fully marine, but if the cross section of their ocean corridors is small enough, basins may become saturated for sulphate, halite or potash. We only modelled sulphate saturated basins, but of course the middle and final modelling stages represent the evolution of halite and potash basins.

Main input values are surface area, evaporation rate and corridor width. Seawater composition and saturation concentrations are based on Sonnenfeld (1984). The model is initiated at steady state sulphate saturation, when $Salt_{in}=Salt_{out}$ and salinity (σ) equals 0.16 (Lucia 1972). Then $Volume_{in} \bullet \rho_{in} \bullet \sigma_{in} = Volume_{out} \bullet \rho_{out} \bullet 0.16$ (Lucia 1972); substitution of density and salinity values gives $Volume_{out}/Volume_{in} = 0.20$, where $Volume_{in} = Volume_{evap} + Volume_{out}$. We assumed a constant flow rate though the corridor and assumed that a reduction of the corridor width was at the expense of corridor outflow. Calcium sulphate precipitation is initiated by an instant 1% narrowing of the corridor, causing outflow reduction and a consequent salinity rise. Excess sulphate is precipitated as basin-margin platforms and central-basin varve successions according to an input platform-varve ratio (Fig. 2). Precipitation causes the platforms to build out tangentially across the mouth of the corridor causing further outflow reduction. After each time step (50-200 yrs) salinity and density are updated; complex volume/density effects of brine mixing etc. are approximated using a density-salinity function (Sonnenfeld, 1984). Halite is precipitated at a ('halite') concentration of ~300 g/L (Sonnenfeld, 1984). High solubility salts are approximated by an average 'potash' salt, which precipitates at a ('potash') concentration of ~230 g/L.

Calibration and modelled scenarios

We calibrated the model against the basal sulphate platform of the Permian Zechstein "Z1" evaporite (Fig. 1d-e), a much-studied sulphate platform that prograded over tens of kilometres without halite saturation being reached thus giving an indication of the lower limit of corridor closure needed for halite precipitation. The basin had a surface area of $1 \bullet 10^6$ km^2 and a corridor width of some 35 km (Ziegler 1990, Cameron et al. 1992). The dimensions of the Z1 platform vary by location, and we approximated it by a 200 m thick platform that extends basinward over ~30 km, where it grades into a ~20 m sequence of ~0.5-1.0 mm varves. The varve ratio, i.e. the proportion of total sulphate precipitated as varves in the central basin, is ~0.5 (Richter-Bernberg 1985, Cameron et al. 1992).

We first simulated a Z1 scenario for a closure/progradation ratio of 1, i.e. the case where 1 km of progradation perpendicular to the basin mar-

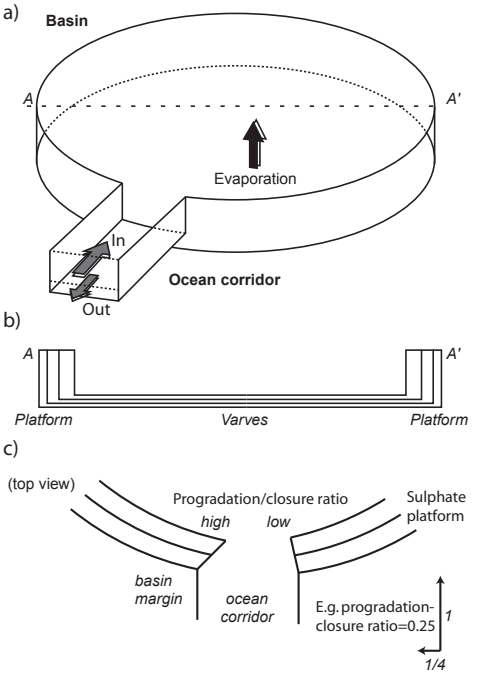

Figure 2 Model basin used in numerical modelling. **a)** Basin is circular and of constant depth and is connected to the ocean by a corridor of constant width/depth. Arrows indicate flow volumes and volume lost to evaporation. **b)** Cross section A-A' showing that sulphate is precipitated as thick platform beds along the basin margin and as thin varve laminae in the basin, the ratio being variable and based on observations in the rock record. **c)** Top view of the ocean corridor showing how the corridor is closed by platform progradation; range of applied closure/platform ratios based on model calibration with the Zechstein evaporite.

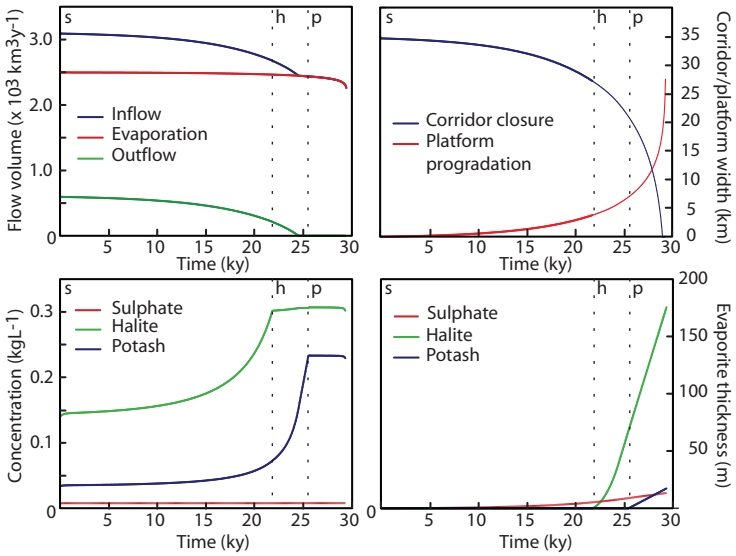

Figure 3 Model output for a fast-closure Zechstein-1 case, based on a 200 m deep basin, a surface area of $1 \bullet 10^6$ km^2, a varve ratio of 0.5 and a progradation/closure ratio of 1. **a)** Volumes of inflow, outflow and evaporation, 50 y time steps. **b)** Platform progradation and ocean corridor closure. **c)** Concentrations of sulphate, halite and potash salts. **d)** Cumulative thickness of precipitated evaporite minerals. Stippled lines *h* and *p* indicate initiation of halite and potash precipitation.

gin results in 1 km of closure at either side of the corridor mouth. This gives an indication of the minimal time required to reach basin-wide halite saturation. We then ran the model for lower closure/progradation ratios in order to find a match with actual Z1 dimensions and obtain realistic ratios for low closure rates. Using the thus-established range of closure/progradation ratios we modelled a suite of scenarios for basins between $2.5 \bullet 10^4$ (~Paradox Basin, Utah) to $2.5 \bullet 10^6$ km^2 (~present-day Mediterranean Sea) and for closure/progradation ratios between 0.1 and 1 to assess whether larger basins are indeed more prone to form evaporite cycles as the rock record indicates. Here we present the results for a basin depth of 100 m, a 25 km wide corridor, a net evaporation rate of 2.5 m/y and a varve ratio of 0.5. We modelled other situations as well (e.g. deeper basin, wider corridor, etc.), but results are proportional and give no further insight in the processes at work.

Discussion of model results

The first scenario (fast closure) shows that sulphate-platform progradation is indeed self-accelerating, and rapidly leads to halite precipitation after 21.7 ky (Fig. 3) by which time 3.8 km wide sulphate platforms have formed along the basin margin, and a 2.7 m thick varve column has developed at the basin floor with up to 0.4 mm thick varves. Halite initially precipitates at a rate of 4.7 m/ky, rising to 28 m/ky when the narrow corridor prohibits outflow at 24.4 ky. At 25.3 ky the precipitation of potash salt commences (4.9 m/ky), and after 29.2 ky the basin is filled entirely with 7% sulphate, 85% halite and 8% potash salts (by vol.). The calculated varve-column thickness and platform width amount to only 10% of their actual Z1 dimensions, indicating that corridor closure was slower in reality and sulphate precipitation more prolonged.

Variation of the closure/progradation ratios shows that a closure/platform ratio of 0.155 (155 m of corridor closure on either side of the ocean corridor for each km of platform progradation along the basin margin) matches well with Z1 dimensions, with 194 ky of platform progradation resulting in a 30 km wide sulphate platform and

a 21 m thick varve column in the basin centre, and individual varves of ~0.4 mm. In the Z1 case this was too slow to bring about the start of halite precipitation, and based on this value we set the lower limit in the experiment runs to 0.10. The results for a closure/progradation ratio of 1 (fast closure) show that reaching halite saturation takes only 5.1 ky for large basins to 44.5 ky for small basins (Table 1). For a closure/progradation ratio of 0.1 (slow closure) it takes from 44.8 ky for small to 390 ky for small basins. We verified the influence of changing corridor width, higher evaporation rates, etc., but these only affect the time required and not composition, and these effects are proportional, and we therefore do not discuss them separately.

Progradation rates in larger basins are higher because of a quadratic increase of surface area with basin circumference, hence more sulphate precipitates per unit shoreline. Corridors are therefore more rapidly closed. Due to faster closure, varve columns are thin in larger basins (Table 1) resulting in the typical steep slopes of evaporite platforms. Results further confirm that evaporite bodies in small basins are characterized by higher sulphate percentages (Zharkov 1981), particularly in case of slow closure, because prolonged sulphate precipitation leaves less space for subsequent halite and potash layers. As larger basins reach halite saturation quicker, ocean-corridor closure is less likely to be interrupted by subsidence events or sea-level rise.

Validation

An extensive set of dimensional and compositional data for 86 Palaeozoic evaporite basins collected by Zharkov (1981) confirms that halite bodies are indeed more common in larger evaporite basins, while the smaller basins mostly contain sulphate only (Fig. 4). The entire population of evaporite basins is lognormally distributed with a mode of ~$1 \bullet 10^6$ km^2. The sub-population of halite-bearing basins is lognormally distributed as well, and has a mode of ~$5 \bullet 10^6$ km^2, indicating that indeed a minimum surface area is required for halite saturation to occur. The data for basins containing only sulphate indicate that this minimum surface area equals ~$3 \bullet 10^6$ km^2.

The predicted trends of changing mineral-composition with surface area match the measured record well (Fig. 4d-f). A large percentage of the data falls within the range of our slow and fast-closure cases for a varve ratio of 0.5, and the majority of the data is covered when the varve ratio is varied between 0.2 and 0.8. The fact that there are no small sulphate-halite basins (Fig.

	Cycle duration			Platform	Basin		Evaporite ratio		
Basin surface area (km^2)	Sulphate phase (ky)	Halite phase (ky)	Entire cycle (ky)	Width (km)	Varves (mm)	Varve column (m)	Sulphate (%v)	Halite (%v)	Potash (%v)
Progradation-closure ratio: 1.0									
25,000	44.5	6.3	50.8	2.4	0.37	5.2	15	81	4.8
100,000	22.8	4.7	27.5	2.5	0.38	2.7	10	83	7.1
250,000	14.7	4.1	18.8	2.6	0.39	1.8	7	85	7.7
1,000,000	7.7	3.5	11.2	2.8	0.42	1.0	6	85	8.9
2,500,000	5.1	3.3	8.4	3.1	0.46	0.7	5	86	9.6
Progradation-closure ratio: 0.1									
25,000	390	14.1	404	22.9	0.36	40	62	38	0.0
100,000	208	12.2	220	22.9	0.36	23	43	57	0.0
250,000	135	10.3	145	23.0	0.36	15	32	67	0.4
1,000,000	69.4	7.7	77.1	23.3	0.36	7.9	20	77	2.4
2,500,000	44.8	6.4	51.2	23.7	0.37	5.2	15	81	4.4

Table 1 Model results for basins between 25,000 and 2,500,000 km^2

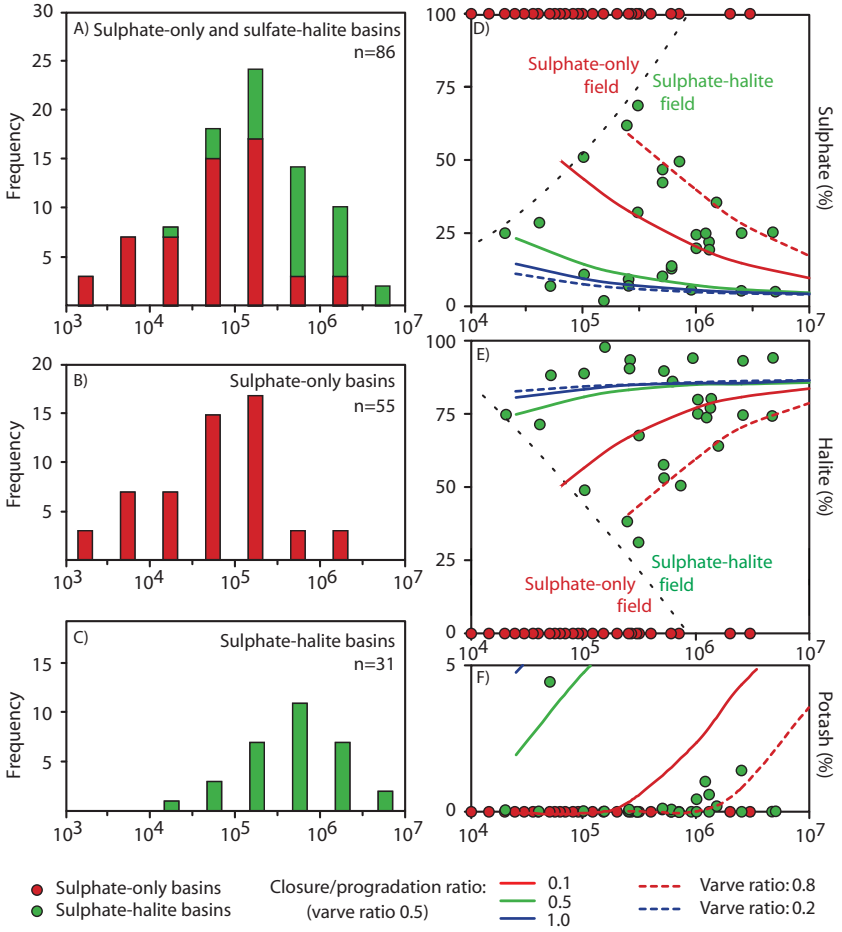

Figure 4 Model results compared with measured data for 86 Palaeozoic evaporite basins. Data collected by Zharkov (1981). Histograms (left) for the surface area of sulphate basins and sulphate-halite basins together (a), for sulphate basins only (b) and for sulphate-halite basins (c). Plots (right) show sulphate percentage (d), halite percentage (e) and potash-salt percentage (f) for sulphate-halite basins (n=27).

4d) is consistent with our model prediction that smaller basins require too much time to ever reach halite saturation, because the chance of interruption by e.g. extension events or sea-level rise is high.

The model correctly predicts that potash content increases with basin surface area, although absolute values are overestimated. This is at the expense of halite, which explains the slight underestimation in Figure 4e. We attribute this to our approximation of the highly complex process of potash precipitation (Harvey et al. 1980, Hardie 1991) by a single potash salt, and to the possibility that potash salts mixed with halite may not always be recognized as such.

Discussion

Sulphate-platform progradation is a rapid, self-accelerating process that can automatically trigger halite precipitation. Current depositional models depend on external control, whereas the mechanism proposed here is self-regulatory, which explains why giant marine evaporites are so common in the rock record. It is clear that

normal (tectonic) subsidence rates are not high enough to allow the rapid creation of sufficient accommodation for new cycles without somehow leaving the evaporite window. In many cases this can be attributed to isostatic subsidence following the deposition of salt. Loading may be (partly) compensated syn-sedimentary (Van den Belt and De Boer 2007), but rapid filling of basins with halite (~10 ky scale) likely causes isostatic compensation to mostly postdate halite precipitation. This allows rapid formation of new accommodation space, with an expected (maximum) depth of half the thickness of the halite body (Van den Belt and De Boer 2007). This explains the common upward thinning of evaporite cycles as for instance observed in the Zechstein sequence (Fig. 1e), the Mediterranean evaporite, or the Cretaceous Maha Sarakham evaporite from Thailand (El Tabakh et al. 1999).

In fact, observed thicknesses for Zechstein sulphate-halite cycles very well match with theoretical predictions of each subsequent cycle having 50% the thickness of its successor. The complete Zechstein sequence in the Netherlands consists of four sulphate-halite cycles and a fifth evaporitic-claystone cap. If the complete Zechstein sequence (which is up to ~2 km thick in places) is assigned a relative thickness of 1.0, then the thickness of the individual cycle equals approximately 0.53 (Z1/Z2 combined cycle), 0.27 (Z3), 0.09 (Z4), 0.05 (Z5), 0.06 (Z6 claystone cap)(Geluk 2007). The predicted cycle-thickness sequence, based on rapid basin filling followed by isostatic compensation, would be 0.50, 0.25, 0.125, 0,0625 and an infinite number of very small cycles with a combined thickness of 0.0625. This is very close and indicates that cycle thickness is indeed governed by isostatic compensation of the rapidly deposited salt load and that tectonic subsidence can be neglected. Periods between successive evaporite stages, when isostatic subsidence takes place, are typically characterized by carbonate sedimentation and may represent considerable amounts of time. For instance, the Z2 platform carbonate is estimated to represent ~0.3 My (Mawson and Tucker 2009). Note that tectonic subsidence will at most have contributed a few tens of metres of accommodation space during that time, which is little in relation to the km-scale thickness of the Zechstein sequence.

Of course, depositional conditions differ between basins, and our results are rough estimates and reflect probabilities rather than actual cases. For the modelled conditions, however, platform progradation explains evaporite cyclicity without invoking exceptional conditions. The model is in agreement with observed evaporite composition, the common absence of halite and potash salts in small marine basins, and thin varve columns and higher potash values in large basins. Of course, there are small basins that do contain halite and potash salts, such as for instance the Eocene-Oligocene Rhine Graben or the Cretaceous Bresse Basin (France), but for many such basins it is uncertain if they are marine or continental evaporites (Busson and Schreiber 1997).

Acknowledgments

We are grateful to Peter van Hoof and Frank Wildschut for discussions and suggestions concerning the modelling. This chapter has benefitted from reviews of a previous version by M.E. Tucker, B.H. Wilkinson and one anonymous reviewer.

Chapter 7

A PALAEOZOIC CLIMATE CHRONOLOGY BASED ON LONG-TERM SIZE VARIATIONS OF EVAPORITE BASINS

F.J.G. van den Belt

The Palaeozoic era is characterized by three major phases of widespread evaporite precipitation (Cambrian, Devonian and Permian), separated by phases of extensive glaciation and restricted evaporite precipitation. A quantitative analysis of the basin-surface area of halite basins during the Palaeozoic indicates that the width of subtropical arid-climate zones fluctuated following a ~120-My cycle in relation to changes in the organization of atmospheric-circulation cells. The results show that arid-climate zones during periods of extended aridity were approximately twice as wide (1500-3000 km) as during periods of restricted aridity (~850-1100 km). The transitions between periods of extended and restricted aridity are relatively abrupt and coincide with major Palaeozoic extinction events.

Introduction

Evaporite deposits are exceptional indicators of past arid and semi-arid climates, because prolonged evaporite precipitation only occurs when an area experiences long-term net evaporation (Gordon 1975, Hardie 1991, Kendall and Harwood 1996, Warren 2006). Such conditions may be local, e.g. when a mountain range creates a rain shadow (Kendall et al. 2003) and of relatively short duration, but the formation of giant marine evaporites requires that entire basins remain within a (semi-)arid-climate zone over long periods of time. Although more conditions must be met, such as a specific tectonic setting (e.g. rift basin, intracontinental depression) to allow a narrow connection with the ocean, the uneven distribution of giant marine evaporites over time is thought to reflect long-term climate variations (Frakes et al. 1992). Ziegler et al. (2003), Parrish et al. (1982) and others mapped the latitudinal distribution of evaporites and showed that subtropical arid-climate zones indeed have been more extensive during certain parts of the geological past than during other parts.

Marine evaporite deposition was widespread during e.g. the Cambrian, Permian and Jurassic, when many of the world's giant salt bodies were formed (Zharkov 1981). During other periods, such as the Ordovician and Carboniferous, marine evaporite precipitation was rare and of limited lateral extent. This alternation is commonly related to long-term greenhouse-icehouse alternations, with major marine evaporites having formed primarily during greenhouse phases (Frakes et al. 1992). According to Warren (2010) the higher frequency and amplitude of eustatic sea-level changes during icehouse phases prevented the precipitation of evaporites.

Palaeogeographic reconstructions indicate that arid-climate zones were subject to repeated long-term contraction and expansion. However, the time-averaging of these reconstructions makes that information on the exact timing of such climate-zone reorganizations, and the duration of transitions between subsequent climate states, is not well known. This hampers the comparison with other indicators of past climates, e.g. glacial indicators such as tillites and coal beds.

Below the long-term fluctuation of the overall width of arid-climate zones in continental areas during the Palaeozoic is reconstructed by analysing the size distribution of (halite-bearing) marine evaporite deposits over time. The results are compared with other climate indicators such as glacial deposits and palaeotemperature data to see if evaporite basin size is a reliable proxy of past atmospheric circulation. Results point at a large-scale circulation-driven climate cyclicity that is in harmony with cycles detected in biological extinction events (Rohde and Muller 2005).

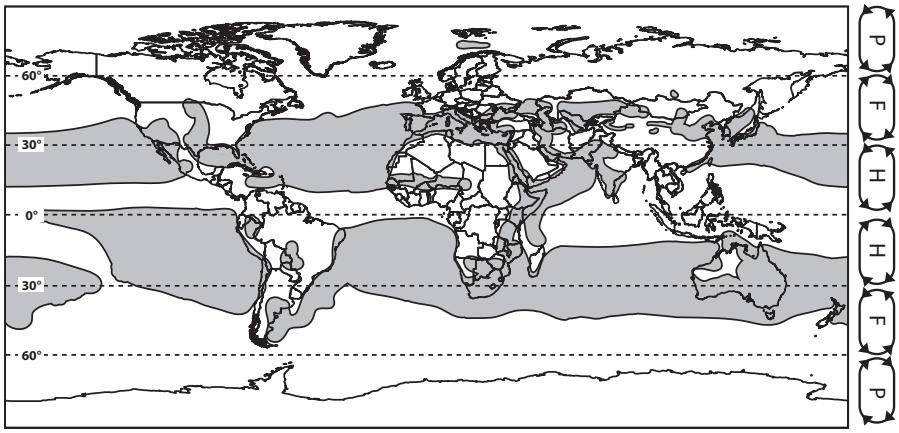

Figure 1 World map showing areas of net evaporiation in grey. H, F and P indicate Hadley, Ferrell and polar atmospheric circulation cells. After Kallberg et al. (2005).

Giant halite basins during the Palaeozoic

During the Quaternary, evaporite basins have been restricted to continental evaporite basins and small marine-fed basins, which may be related to the high amplitude and frequency of sea-level fluctuations during times of glaciation (Warren 2010; this thesis *chapter 6*). The youngest major marine evaporite body is the Late Miocene evaporite in the Mediterranean Sea (Hsü et al. 1973) and it covers a number of subbasins. Combined, they cover an area of some $1.5 \bullet 10^6$ km^2, which makes it one of the largest Phanerozoic marine evaporites (Zharkov 1981, Warren 2006).

Figure 1 shows the present-day extent of net evaporation across the globe, including the entire Mediterranean Sea. The map suggests that atmospheric circulation patterns have not changed much since the Late Miocene and it explains why such an extensive evaporite body could form in the area. Figure 1 suggests that there is little potential for future large evaporite basin in other continental areas, because most continental arid-climate zones are comparatively small, but it must be noted that evaporation in continental areas cannot be much higher than precipitation. Some dry areas, such as e.g. in North America (Death Valley and surroundings) and NE Africa (Afar Triangle), could host quite sizable future evaporite basins, if a narrow connection to the open ocean would develop.

The formation of giant marine evaporite bodies during e.g. the Cambrian and Permian seems related to expanded arid-climate zones, as is reflected in palaeogeographic reconstructions (Zharkov 1981, Scotese 2001). At times, major evaporite basins even covered the equator, e.g. during the Permian (Ziegler et al. 2003) and Cretaceous (Chaboureau et al. 2012) suggesting that the arid climate zones of the two hemispheres coalesced. Climate modelling by Poulsen et al. (2007) has shown that Late Palaeozoic (Permian) deglaciation under conditions of high pCO_2 may have been associated with cross-equatorial aridity extending from ~25° N to ~25° S.

During the Palaeozoic era at least a hundred sedimentary basins accumulated considerable amounts of evaporite minerals (Zharkov 1981). Hence, on average every ~3 My a basin experienced dry conditions to such extent that long-term net evaporation permitted the extensive precipitation of calcium sulphate (gypsum/anhydrite), halite and/or high-solubility potassium and magnesium salts. Many of these basins are dominated by sulphate minerals and contain little or no halite, and in many cases evaporite precipitation was restricted to (shallow-water) platforms at the basin margins where the effect of evaporation is highest. Such deposits are referred to as *platform evaporites* (Warren 2010).

Of these hundred basins some 35 are characterized by large volumes of basin-wide halite,

which equates to once every ~8 million years. These *basin-wide evaporites* (Warren 2010) typically occur in the larger evaporite basins. Whereas the halite-free platform-evaporite basins have surface areas of mostly between $1 \bullet 10^3$ km^2 and $3 \bullet 10^5$ km^2, those of halite-bearing basins are typically between $1 \bullet 10^6$ km^2 and $4 \bullet 10^6$ km^2 (Zharkov 1981, Table 1). Large basins may be more likely to accumulate halite because sulphate platforms along the margins of larger basins prograde basinward faster (basin circumference increases linearly with basin radius, and basin surface quadratically), and therefore more easily obstruct the ocean corridor thus hampering outflow of high-

	Halite Basin	Continent	Area (km^2)	Time (Ma)	Period
1	Iran-Pakistan	Asia	4000 x 10^3	542-503	Pre/E. Cambrian
2	East Siberian	Asia	3000 x 10^3	542-488	E.-L. Cambrian
3	Amadeus	Australia	150 x 10^3	526-510	E. Cambrian
4	MacKenzie	N. America	900 x 10^3	501-495	L. Cambrian
5	Canadian Arctic	N. America	700 x 10^3	466-461	M. Ordovician
6	Canning	Australia	500 x 10^3	458-444	M.-L. Ordovician
7	Williston (Ordovician)	N. America	300 x 10^3	447-444	L. Ordovician
8	Michigan (Silurian)	N. America	500 x 10^3	422-416	L. Silurian
9	Lena-Yeniseh	Asia	2000 x 10^3	419-416	L. Silurian
10	North Siberian	Asia	2500 x 10^3	407-367	E.-L. Devonian
11	Adavale	Australia	100 x 10^3	398-395	M.Devonian
12	Tuva	Asia	10 x 10^3	398-385	M. Devonian
13	West Canadian	N. America	1000 x 10^3	398-359	M.-L. Devonian
14	Morsovo	Europe	1500 x 10^3	395-392	M. Devonian
15	Hudson	N. America	300 x 10^3	395-392	M. Devonian
16	Michigan (Devonian)	N. America	250 x 10^3	395-392	M. Devonian
17	Russian Platform	Europe	1500 x 10^3	385-359	L. Devonian
18	Chu Sarysu (Carbon.)	Asia	300 x 10^3	367-352	L. Dev.-E.Carb.
19	Maritime	N. America	600 x 10^3	352-326	L. Carboniferous
20	Williston (Carbonif.)	N. America	500 x 10^3	345-336	L. Carboniferous
21	Mid-Tien Shan	Asia	40 x 10^3	345-326	L. Carboniferous
22	Sverdrup	N. America	600 x 10^3	318-315	M. Carboniferous
23	Paradox	N. America	50 x 10^3	312-309	M. Carboniferous
24	Eagle	N. America	20 x 10^3	312-309	M. Carboniferous
25	Amazon	S. America	1000 x 10^3	304-299	L. Carboniferous
26	Supai	N. America	250 x 10^3	290-276	E. Permian
27	East European	Europe	2500 x 10^3	297-254	E.-L. Permian
28	Midcontinent	N. America	1300 x 10^3	290-251	E.-L. Permian
29	Chu Sarysu (Permian)	Asia	250 x 10^3	285-276	E. Permian
30	North Mexican	N. America	500 x 10^3	276-271	E. Permian
31	Central European	Europe	1200 x 10^3	273-251	L. Permian
32	Peru-Bolivian	S. America	1250 x 10^3	273-271	E. Permian
33	Moesian	Europe	10 x 10^3	264-251	L. Permian
34	Alpine	Europe	100 x 10^3	261-254	L. Permian

Table 1 List of Palaeozoic halite basins inventoried by Zharkov (1981)

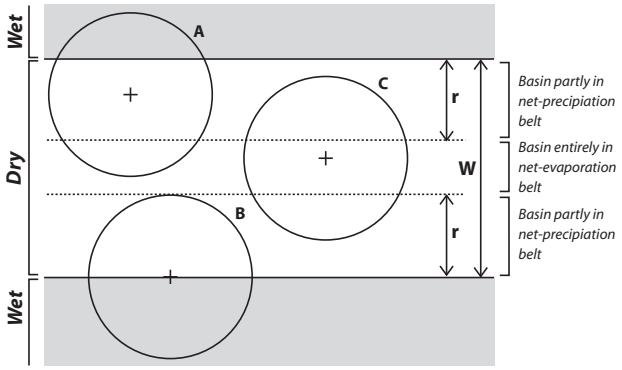

Figure 2 Illustration of the theoretical model used to estimate the width of the arid climate belt based on the radius of preserved evaporite basins. Model assumes that evaporite basins are circular. Basin A and B extend outside the net-evaporation belt, whereas basin C is located within it entirely.

salinity water (this thesis, *chapter 6*).

In this study only halite basins were considered, because calcium-sulphate precipitation may be localized and due to its relatively poor solubility is easily preserved (Warren 2006). Therefore it does not necessarily reflect basin-wide aridity. On the contrary, the preservation of halite, which is highly soluble and occupies the inner parts of evaporite basins, is indicative of basin-wide aridity because significant precipitation anywhere in the basin's catchment area would cause dilution and prevent halite accumulation.

Methods

The analysis is based on the work of Zharkov (1981), who collected information on basin size, composition and depositional history for some 86 Palaeozoic evaporite basins from around the globe, of which 34 contain significant amounts of halite (Table 1). These data were organized into a time series of evaporite-basin size, using the geological time scale of Gradstein et al. (2004).

The width of the continental arid-climate zones was quatified for periods of extensive marine-evaporite precipitation (Cambrian, Devonian and Permian) and for periods of rare or restricted marine-evaporite precipitation (Ordovician-Silurian, Carboniferous) based on basin surface area. Assuming that all basins had a circular shape allowed a simple mathematical approach. This ignores the fact that some evaporite basins are markedly elongate, but the long axes of such basins are not necessarily aligned parallel to the arid-climate zone, as in case of the Red Sea evaporite that precipitated during the Middle Miocene (Fig. 1), nor do arid-climate zones in continental areas preferentially strike E-W (Fig. 1). Hence, results are not precise and certainly not location specific, but they should give a reliable indication of the difference in scale of arid-climate zones between the two extremes.

Figure 2 shows the approach to estimating the width of arid-climate zones. A wet and a dry zone are distinguished and it is assumed that a basin needs to be within the dry zone entirely to precipitate basin-wide halite. Of course basins may extend considerably outside the dry zone and still have a negative precipitation budget, but we note that any basin is surrounded by catchment areas, either small or large, the surface area of which is not included in the basin surface area. Hence, in the model evaporite basins extend beyond the confines of the arid zone, but it was not attempted to quantify this and include in our calculations, because its effects depend strongly on the specific situation. For instance, major rivers may or may not drain into the basin, and the catchment area may or may not include extensive elevated terrain that generates significant run-off towards the basin.

The width of arid-climate zones was estimated using the formula W=2r/(1-p), where *W* equals the width of the arid-climate zone, *2r* equals the basin diameter and *p* equals the probability that a

basin, randomly placed in the arid-climate zone, fits entirely within that zone (Fig. 2). Note that based on these assumptions the maximum diameter for an evaporite basin equals the width of the arid-climate zone, but the probability that a basin of that size fits entirely within the arid zone equals zero. Hence, the diameter of evaporite basins must be significantly smaller than the width of the arid-climate zone in which they developed. The probability that a basin fits entirely within the arid zone equals p=(W-2r)/W and for a specific probability *p* the basin diameter equals 2r=(1-p)•W.

Because of great uncertainty with respect to the total number of continental basins that have been present in and around arid-climate zones, and -at same time- were located closely enough to the open sea and connected to the sea by a narrow corridor we performed calculations for a number of scenarios. Probabilities of 5%, 10% and 25% were used. The 5% case is considered as an indication of the minimal width of the arid climate zone relative to the basin radius; in that case the diameter of the basin equals 95% of the width of the arid-climate zone and only 1 out 20 basins would be located entirely within that zone. The 10% case is an intermediate case with a basin diameter of 90% of the width of the arid-climate zone and a 10% chance that a basin falls entirely within the arid zone. The 25% case (illustrated in Figure 2) is considered as an indication of the maximum width of the arid climate zone relative to the size of basins in which giant halite deposits may accumulate. For this case, 1 out of 4 basins fits entirely within the arid zone, and the basin diameter equals 75% of the width of the arid zone.

Results

Figure 3 shows the occurrence and basin-surface area of Palaeozoic halite basins plotted against time. Note that the vertical scale is logarithmic and that the size differences are extremely large. Basins roughly fall into three groups: large basins (10^6-10^7 km^2), medium-sized basin (10^5-10^6 km^2) and small basins (10^4-10^5 km^2). Large halite-bearing basins only developed during the Cambrian, Devonian and Permian, and for each period (intermittent) halite-precipitation occurred during almost the entire period, involving

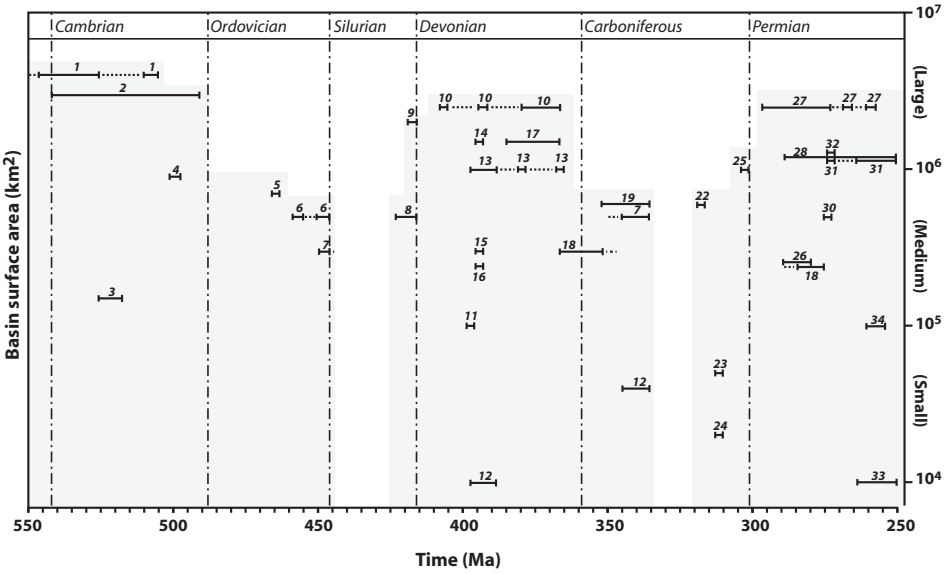

Figure 3 Basin-surface area of Palaeozoic halite basins through time based on Zharkov (1981) and geological time scale of Gradstein et al. (2004). Basin names, surface areas and time of deposition are tabulated in Table 1. Stippled lines indicate temporary interruption of salt precipitation in an evaporite basin.

2-5 basins. At the same time evaporite deposition in medium-sized and small basins occurred as well. Considering that halite precipitation can be extremely fast (this thesis, *chapter 6*; Krijgsman et al. 1999), and considering the relatively poor age datings for saline giants in the Palaeozoic, the ranges indicated in Figure 3 are likely too long or alternatively deposition of evaporites in individual basins may have been active only intermittently.

During the intervening Ordovician-Silurian and Carboniferous periods halite precipitation occurred in medium to small basins only, or not at all. Gaps occur in the Early to Middle Ordovician, Early to early Late Silurian and middle Carboniferous. Overall, halite precipitation seems to have been less frequent and of shorter duration during these latter periods, while relatively few halite basins are known for the Cambrian as well. The latter could well be related to age and a consequently smaller chance of preservation due to erosion and subduction.

Table 2 shows the predicted width of arid-climate zones for the probabilities of 5, 10 and 25 %, that a potential evaporite basin (i.e. a basin with its centre point in an arid-climate zone) falls entirely within that zone. A typical surface area of a large halite basin during periods of widespread aridity is $2 \bullet 10^6$ km^2 (Devonian, Permian) and even more during the Cambrian (Fig. 3). Results indicate that the continental arid-climate zone must be between ~$1.7 \bullet 10^3$ to ~$2.1 \bullet 10^3$ km wide to accommodate such basins, or up to $3.0 \bullet 10^3$ km for the Cambrian. For periods of restricted aridity (Ordovician-Silurian, Carboniferous) halite basins typically have a maximum surface area of $5 \bullet 10^5$ km^2. The calculations predict that the continental arid-climate zone was not wider than 0.85-$1.1 \bullet 10^3$ km during those periods.

Figure 4 shows the predicted width of the arid-climate zone for the 25% case for the entire Palaeozoic and it clearly shows that the arid-climate zone was roughly twice as wide during the Cambrian, Devonian and Permian as during intervening intervals. For the other scenarios (5%, 10%) the arid-climate belts are slightly smaller, but the relative size difference is similar. Also note that the transitions between periods of extended and restricted aridity are of relatively short duration.

Climate cycles

The size distribution of Palaeozoic halite basins over time shows a clear long-term cyclicity (Figs. 4, 5) representing alternating phases of evaporite precipitation in narrow arid-climate zones and in wide arid-climate zones. The Cambrian interval, characterized by extensive evaporite deposition, likely represents the upper part of an incomplete cycle that started in the Precambrian. The first complete cycle started at the Cambrian-Ordovician boundary and ended in the Late Devonian. The second cycle ended at the Permian-Triassic boundary. Triassic evaporite basins are not included in the dataset, but there is no record of large-scale Early Triassic halite accumulation and the first significant Mesozoic evaporite basins are from the Late Triassic (Warren 2006, 2010).

The Ordovician-Late Devonian cycle lasted

		5%		10%		25%	
Basin surface area (km^2)	Basin radius (km)	Width arid zone (km)	Latitudinal extent (degrees)	Width arid zone (km)	Latitudinal extent (degrees)	Width arid zone (km)	Latitudinal extent (degrees)
4,000,000	1128	2376	21	2508	23	3009	27
3,000,000	977	2057	19	2172	20	2606	23
2,000,000	798	1680	15	1773	16	2128	19
1,000,000	564	1188	11	1254	11	1505	14
500,000	399	840	8	887	8	1064	10
100,000	178	376	3	396	4	476	4

Table 2 Estimated width of the arid-climate zone based on basin surface area for three scenarios

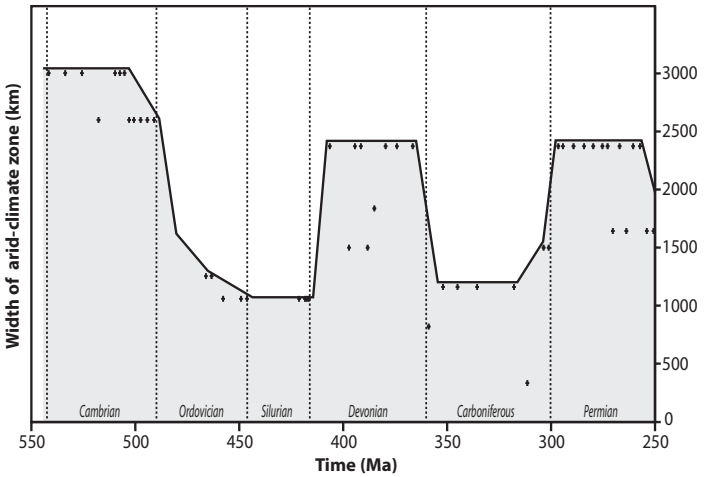

Figure 4 Fluctuation of the width of the arid-climate belt in continental areas during the Palaeozoic based on a 25% probability that a circular basin with its centre point anywhere in the arid-climate zone fits entirely within that zone. See text for explanation.

~125 My and the Late Devonian-Permian cycle ~115 My (Fig. 5). In both cases the first part of the cycle (narrow arid-climate zone) lasted ~65 My. The second part (wide arid-climate zone) lasted 60 My in the first cycle and 50 My in the second. Evaporite deposition in narrow arid-climate zones was occasionally interupted (e.g. most of the SIlurian) lasting 15-20 My.

The Palaeozoic era has known two major ice-house periods (Fig. 5). An Ordovician-Silurian glaciation (~460 to ~430 My) is known from the widespread occurrence of glaciogenic sediments (Frakes et al., 1992; Page et al., 2007), although a shorter duration is envisaged by some (Brenchley et al. 1994, Finnegan et al. 2011). This seems related to the alleged 'paradox' that a long-lasting Ordovician glaciation is at odds with persistently high CO_2 pressures during that interval (Crowley and Baum 1995). The Late Palaeozoic glaciation spanned the entire Carboniferous and Permian periods, while its main phase occurred during the Late Carboniferous and Early Permian.

In Figure 5 the magnitude of both glaciations is indicated semi-quantitatively, based on the number of accounts of glaciogenic sediments in different regions on the globe (Frakes et al. 1992, Fielding et al. 2008). Note that the main phases of glaciation (~455-425 Ma, 330-290 Ma) started consistently ~35 My after narrowing of the arid-climate zones and lasted 30-40 My until the arid-climate zones widened again.

Our records suggest that arid-climate zones during the Palaeozoic conformed to either of two states (Fig. 3). The latitudinal width of the arid zones during the Cambrian, Devonian and Permian was approximately twice that during the Ordovician-Silurian and Carboniferous. Since the latter periods were ice-house periods, the present-day distribution of arid-climate zones as depicted in Figure 1 may be a relatively good analogue for the Ordovician-Silurian and Carboniferous. Today arid continental conditions occur roughly between 10 and 40 degrees north and south of the equator, and palaeogeographic reconstructions indicate that this was not much different during much of the geological past (Scotese 2001, Ziegler et al. 2003). As shown above, evaporite precipitation was at times much more widespread, and arid-climate sediments have even been encountered at equatorial latitudes (Scotese 2001, Ziegler et al. 2003, Chaboureau et al. 2012). Both periods in the Palaeozoic in which arid climate belts were very wide are 50-60 My long, and embedded within ~120 My long cycles. This was probably not coincidental and it may have resulted from significant reorganizations of atmospheric circulation, e.g. in relation to large-scale plate reorganizations (Ronov et al. 1980,

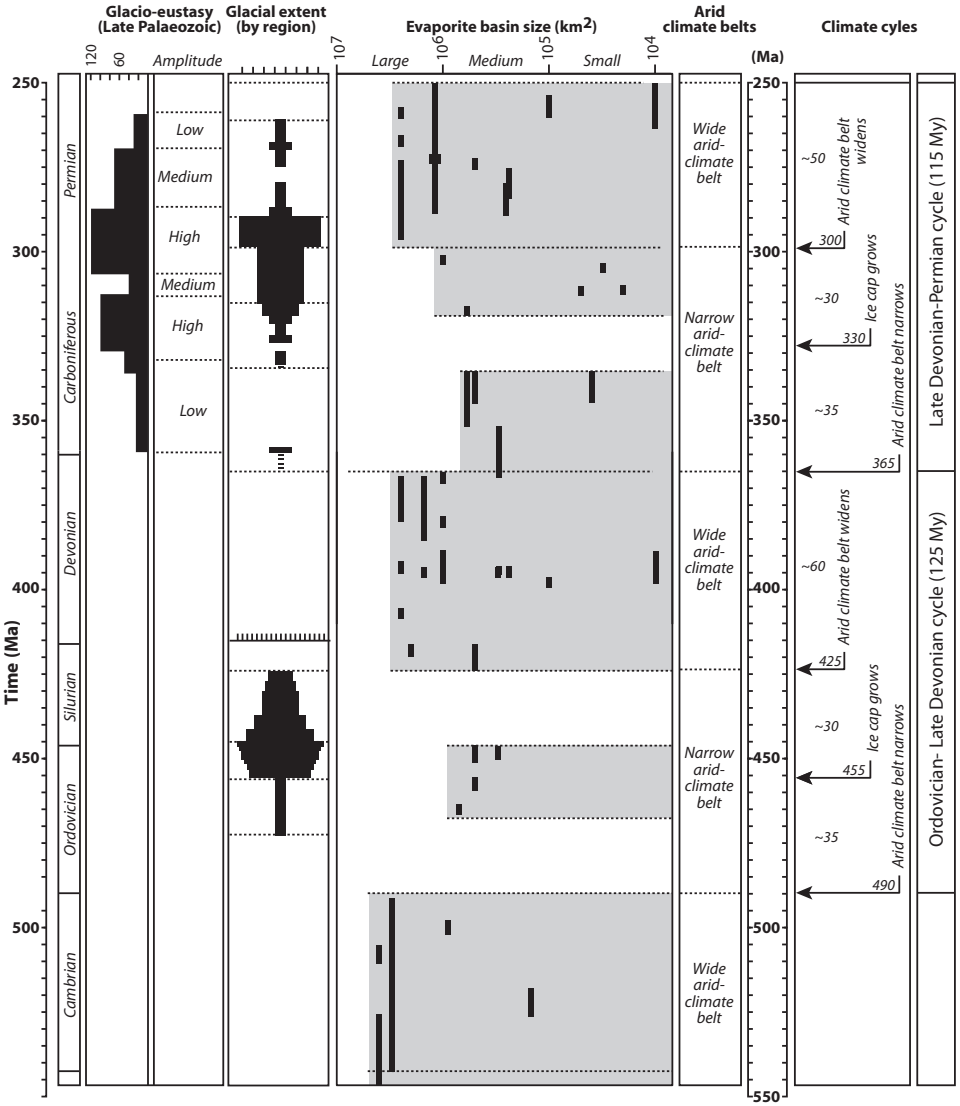

Figure 5 Comparison of glacial history and width fluctuation of arid-climate belts throughout the Palaeozoic, showing interpreted Ordovician-Late Devonian and Late Devonian-Permian climate cycles. Glacio-eustasy magnitude after Rygel (2008), glacial extent after Frakes et al. (1992) for the Early Palaeozoic and after Fielding et al. (2008) for the Late Palaeozoic.

Worsley and Nance 1986) or astronomical megacycles (Shaviv and Veizer 2003). This must have involved expansion of the Ferrell cells, with the consequent expansion of the arid-climate zones, at the expense of the Hadley and Polar cells. The two stable states, one of which is associated with a continental arid-climate zone twice as wide as the other, likely did not pass into one another, but involved a relatively sudden and drastic reorganisation of the entire circulation system.

Relation to palaeozoic temperature and pCO_2 trends

In Figure 6 the Palaeozoic climate cycles and glacial periods are compared with $\delta^{18}O$-derived tropical sea-surface (TSS) temperature data

(Came et al. 2007) and modelled pCO_2 pressure data (Berner 2003). Periods when arid-climate zones were wide were typically associated with rising tropical sea surface (TSS) temperatures and periods when arid-climate belts were narrow with declining TSS temperatures. Temperature maxima and minima occurred typically 10-15 My before the reorganization of atmospheric circulation. TSS temperature trends reflect global temperature trends and these large-scale trends are variably attributed to tectonic or galactic cycles (Veizer et al. 2000). Our data suggest that a long-term increase of global temperatures is associated with a mode of atmospheric circulation that results in widespread continental aridity. Conversely, a long-term decrease of global temperatures is associated with a mode of atmospheric circulation that results in restricted aridity.

The correlation between glacial history and TSS temperatures (as a function of global temperatures) is very strong, with greatest glacial extent consistently associated with the lowest temperatures (Fig. 6). Although it has been shown for the Palaeozoic that there is no correlation between modelled pCO_2 trends and other palaeoclimate indicators (Veizer et al. 2000), the development of the Late Palaeozoic glaciation is largely attributed to low pCO_2 during the Late Carboniferous and Early Permian (Montañez et al. 2007, Poulsen et al. 2007). Based on the available information there is no reason to conclude that pCO_2 variations played a big role in Palaeozoic glacial history; there is no obvious correlation between modelled pCO_2 trends and temperature, nor between pCO_2 and the occurrence of glaciogenic sediments. There is clear correlation, however, between the modelled pCO_2 trends and carbon burial rates (Berner 2003) and in particular the accumulation rate of coal. Levels of pCO_2 are clearly lowest when coal accumulation peaked during the Late Carboniferous and Permian. When glacial extent rapidly decreased during the early Permian, pCO_2 remained low and did not rise significantly until the end of the Permian (Royer 2006), which lines up with the early Triassic 'coal gap' and erosion of Permo-Carboniferous coals (Faure et al. 1995). This strong correlation, however, is not surprising since modelled pCO_2 is based primarily on carbon burial (Berner and Kothavala 2001). It is concluded that low CO_2 pressures during the Late Carboniferous and Permian period did not control glaciation, but instead the eustatic sea-level fluctuations associated with glaciation promoted the widespread accumulation of carbon in peat bodies (Bohacs and Suter 1997) thus causing declining CO_2 concentrations. This also explains the alleged Early Palaeozoic 'paradox' that Ordovician-Silurian glaciation was remarkable during a time of consistently high pCO_2 (Crowley and Baum 1995, Vandenbroucke et al. 2010, Finnegan et al. 2011). Land plants had not evolved yet. Therefore, sea-level fluctuations associated with the Ordovician-Silurian glaciation did not cause a withdrawal of atmospheric carbon through peat accumulation.

Relation to major extinction events and evolution of land plants

Palaeozoic history is pinpointed by a number of major biotic extinction events (Raup and Sepkoski 1982, McGhee et al. 2011), many of which define the period boundaries that subdivide the Palaeozoic time scale. These events are not instantaneous, but typically take a few million years (Rohde and Muller 2005).

There are seven Palaeozoic extinction events, three of which form part of the 'big five' (End Ordovician, Late Devonian and End Permian (Raup and Sepkoski 1982, see Figure 6). All extinction events line up in time with major changes in the surface-area record of evaporite basins, suggesting that they are associated with minor or major reorganisations of the atmospheric circulation system. The End-Cambrian, Late-Devonian and End-Permian events coincided with contractions of arid-climate zones from wide to narrow. The End-Ordovician and Serpukhovian (mid-Carboniferous) events coincided with transitions from halite precipitation in narrow arid-climate zones to temporary (global) cessation of halite precipitation, which possibly indicates further narrowing of arid-climate zones. The End-Silurian event is the only one associated with widening of arid-climate zones.

Extinction events have been attributed to a range of different causes, including glaciation, deglaciation, rapid rise of pCO_2, ocean overturning, sea-level fall, flood-basalt eruption events

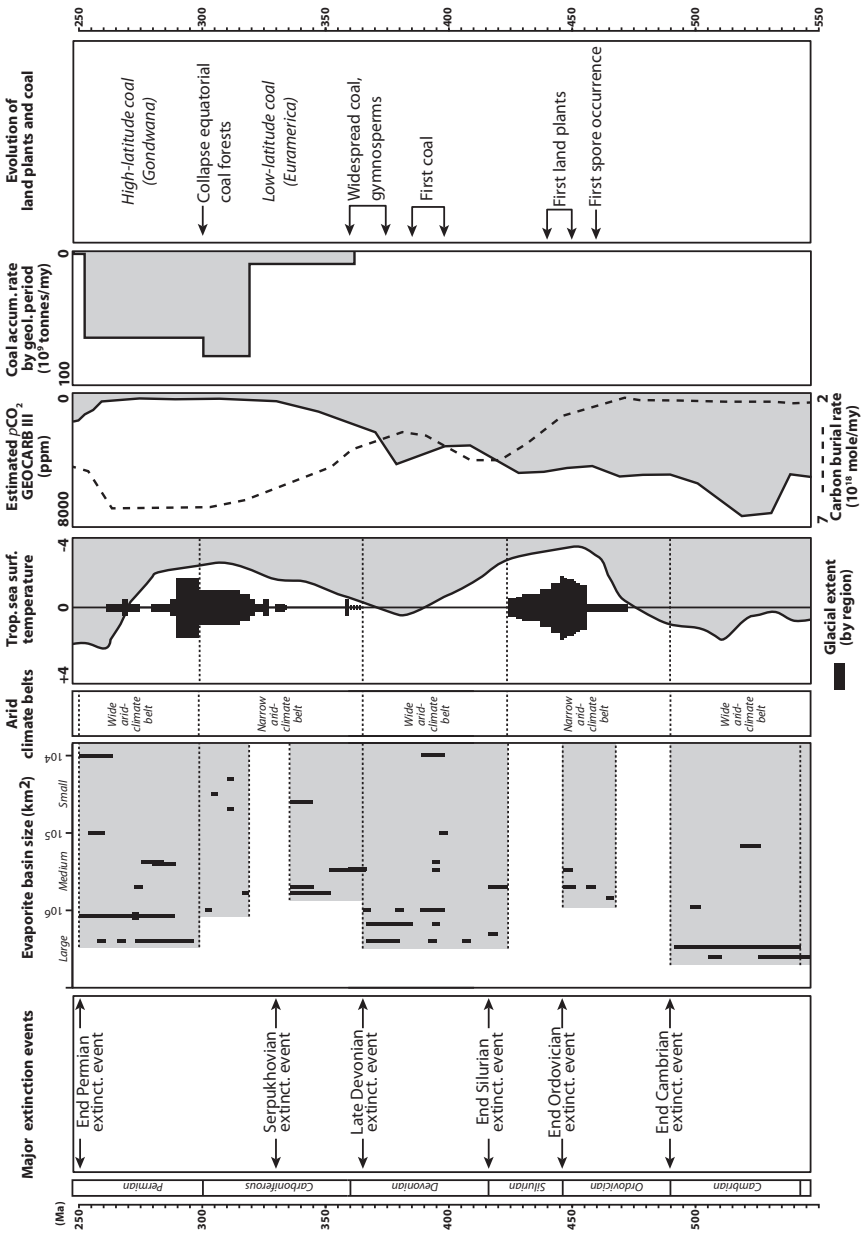

Figure 6 Integration of climate data with evolutionary trends and events for the Palaeozoic era. Tropical sea-surface temperature data from Came et al. (2007), estimated CO_2 pressure and carbon burial rate from Berner (2003). Extinction events and evolutionary trends for land plants and coal from various sources.

and ocean anoxia, with the notion that different explanations are given for different events. The observation that extinction events are synchronous with contractions of the arid-climate zone, leaves room for many of the above mentioned causes, either as primary or secondary drivers. The implications of reorganizations of the atmospheric circulation system on land are clear, affecting precipitation and evaporation patterns, temperature, wind directions and so forth. Hence, reorganizations of the circulation system will cause direct environmental stress and lead to major ecosystem shifts. Since atmospheric and oceanic circulation are intimately related, the ocean environment must be seriously affected as well, involving changes in temperature, current directions, deep- or intermediate-depth-water anoxia, ocean overturning and salinity.

We already briefly discussed how coal formation fits within the Palaeozoic climate history. The information in Figure 6 shows that more aspects of Palaeozoic coal formation and the evolution of land plants fit within that overall framework. Most extraordinary is the sudden demise of equatorial coal forests at the end of the Carboniferous (DiMichele et al. 2001) at the expense of arid-climate red beds. This is in agreement with the above interpretation that the arid-climate zone expanded at the Carboniferous-Permian transition. At the same time coal accumulation commenced at high-latitudes on the Gondwana continent (Michaelsen and Henderson 2000) and lasted until the end of the Permian, when global coal accumulation halted altogether (Retallack et al. 1996).

The first coals accumulated in the Middle Devonian, which is right in the middle of a period of widespread aridity when TSS temperatures were at a long-term maximum. However, this directly followed a period with a conspicuously high number of halite basins (Fig. 6), and it could therefore indicate the recovery from an extremely dry period and the expansion of wet conditions. Coal accumulation then accelerated during the latest Devonian, concurrent with a narrowing of the arid-climate zone, and hence expansion of the wet equatorial zone. During the Early Carboniferous coal accumulation was common along the palaeoequator and may have been promoted by glacio-eustatic sea-level fluctuations associated with the incipient Late Palaeozoic glaciation. When the magnitude of sea-level fluctuations increased at about 330 Ma (Fig. 5; Rygel et al. 2008) this probably resulted in accelerated carbon storage due to sea-level-controlled generation of accommodation space.

As mentioned above coal accumulation did not play a role in the Ordovician-Silurian glaciation because land plants had not evolved yet. The first evidence of incipient vegetation on land (spores) are from the Late Ordovician to Early Silurian (Davies et al., 2011). This is coincident with the peak of the Ordovician-Silurian glaciation (Fig. 6), suggesting that Early-Palaeozoic sea-level fluctuations contributed to the initiation of vegetation on land. First direct evidence of small sporophytes is from the Early Silurian (Davies et al., 2011), which indicates that land plants started to colonize the land when arid-climate zones narrowed and wet zones expanded at the end of the Ordovician.

Discussion and conclusions

As shown above the distribution of smaller and larger marine halite basins over time defines a Palaeozoic-climate chronology that is in harmony with the Ordovician-Silurian and Late Palaeozoic glaciations. The well-defined boundaries coincide with major biotic extinction events, indicating that the cycles relate to major events with global implications. The sharpness of these boundaries is attributed to fast transitions between two stable modes of atmospheric circulation. One of these modes is associated with wide arid-climate zones, which allows for halite precipitation in both small and large basins. The other mode is associated with narrow arid-climate zones; these are too small to allow basin-wide halite precipitation in large basins. It was estimated that the width of arid-climate zones on continents is generally about 1500-3000 km for wide arid-climate zones and about 850-1100 km for narrow arid-climate zones. These estimates are rough, but regardless of the accuracy the above results indicate that arid-climate zones doubled in size during times of extended aridity.

The climate cycles in the Paleozoic each lasted approximately 120 My. Detailed datasets of evaporite-basin size are not available for the Mesozoic and Cenozoic, so the continuation of

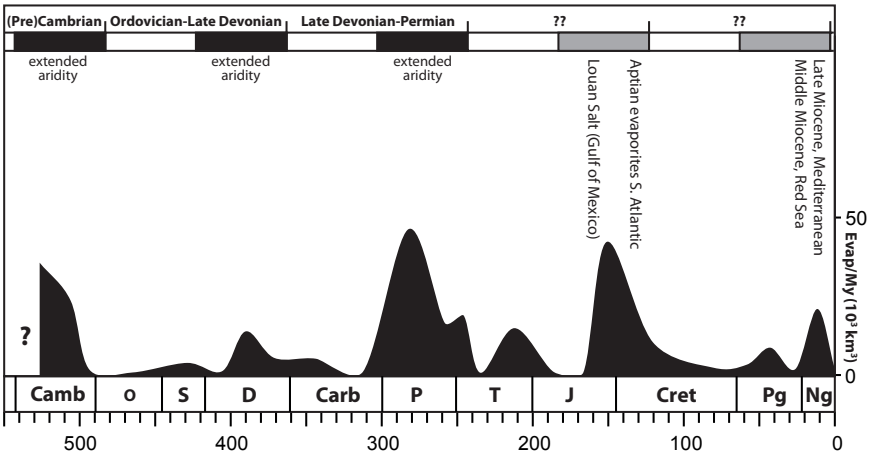

Figure 7 Evaporite accumulation over Phanerozoic time (Volume/My; calculated based on Ronov 1976). Black-and-white bars indicate climate cycles described in this study. Grey bars represent climate cycles extrapolated into the Mesozoic and Cenozoic based on a 120 My duration. Text labels refer to evaporite basins with large surface areas (Warren 2010, Chaboureau et al. 2012, Burke and White 1978).

a potential 120-My climate cyclicity based on basin size could not be verified in detail. However, major phases of evaporite precipitation occurred during the Middle Jurassic to Early Cretaceous, with extensive evaporites in the Gulf of Mexico and along the continental margins of the South Atlantic, and during the Eocene-Miocene with extensive evaporites in the Red Sea and the Mediterranean Sea (Burke and White 1978, Warren 2010, Chaboureau et al. 2012). This is in good agreement with predicted periods of extended aridity around 180-130 Ma and 60-10 Ma (Fig. 7).

The origin of long-term climate cycles is a matter of speculation. A common explanation involves plate-tectonic cycles (Ronov et al. 1980, Worsley and Nance 1986), which may control fluctuations in e.g. spreading rates of mid-ocean ridges or volcanism, thus influencing global sea level and atmospheric composition. Also astronomical causes have been suggested (Steiner and Grillmair 1973). Shaviv and Veizer (2003) noted that TSS temperatures correlate well with the 125-140 My passing of the solar system through the spiral arms of the Milky Way. Also the orbit of the Sun around the centre of the Milky Way could play a role, the 120 Ma climate cycle equating to half of the 240 My galactic year (Hess 2005). In this respect it is interesting to note that the TSS temperature pattern and glaciation history of the Ordovician-Late Devonian and Late Devonian-Permian climate cycles are mirror images at both sides of the Late Devonian temperature maximum.

Chapter 8

SYNTHESIS: SEDIMENTARY CYCLES IN COAL AND EVAPORITE BASINS AND THE RECONSTRUCTION OF PALAEOZOIC CLIMATE (WITH SPECIAL REFERENCE TO THE DEPOSITIONAL HISTORY OF NW EUROPE)

F.J.G. van den Belt

In this thesis the focus is on the origin of coal-clastic cycles (cyclothems) and evaporite cycles against a background of large-scale Palaeozoic climate and climate change. The chapters stand on their own, each dealing with different aspects of cyclical deposition. Together they cover the Late Palaeozoic depositional history of northwest Europe; from Pennsylvanian (Upper Carboniferous) coal-bearing fluvio-deltaic deposits, through Early Permian (Rotliegend) aeolian sandstones and evaporitic mudstones, to Late Permian (Zechstein) marine evaporites. Here the main conclusions of the individual chapters are summarized and synthesized in the scope of the large-scale depositional history of the Late Palaeozoic in northwest Europe.

Orbital control on cyclothem formation

Long ago it was recognized that Pennsylvanian coal-bearing facies in Euramerican basins are very cyclic, showing small-scale alternations of (marginal) marine shales, terrestrial shales and sands and coal beds. Depending on basin and location, cyclothem sequences consist of tens to hundred or more cycles. These sequences formed during the peak of the Late Palaeozoic glaciation and the cycles are numerous and persistent along more than 3000 kilometres of the Euramerican palaeoequator. Therefore cyclothem formation has since long been related to sea-level fluctuations caused by orbitally controlled waxing and waning of southern-hemisphere polar ice.

Consequently it has been attempted in many studies to link cyclothem formation to glacio-eustasy, but a clear picture of cycle periods did not emerge. In *chapter 2* it is shown that this is primarily the result of limitations of the methods used, as well as to the incompleteness of commonly condensed sequences in the classic study areas of the UK and USA.

Previous cyclothem studies were based on the concept that a cyclothem is the lithological reflection of orbitally controlled sea-level fluctuations, e.g. caused by eccentricity variations, and it was hardly taken into account that different orbital cycles interfere. It is shown that such interference results in splitting and merging of primary cycles and that the resultant short-term sea-level fluctuations are of highly variable duration, only incidentally matching one of the orbital periods. This not only hampers the determination of the duration of single cyclothems, but of long cyclothem successions as well.

In *chapter 2* this problem is solved by considering cyclothem composition. By plotting the ratio of the thickness of subaerial facies against the total thickness of subsequent cyclothems in a nearly 2 km thick cyclothem succession from a high-subsidence area in the Netherlands, the influence of long and short eccentricity cycles could be defined. The entire sequence, spanning the Late Langsettian (Westphalian A) to Late Bolsovian (Westphalian C), represents 2.9 My. Based on this information the average cyclothem duration (145 in total) turned out to be ~21 ky, which is slightly more than the ~19-ky average duration of the precession cycle in the Late Palaeozoic. This does not necessarily imply that many cyclothems represent precession cycles. The cyclothems have very variable durations, probably as the result of the interference of precession, obliquity and eccentricity-controlled sea-level fluctuations. The average duration of ~21 ky probably reflects that the amplitude of precession-driven sea-level fluctuations was large enough most of the time to split obliquity and eccentricity-driven fluctuations into precession-scale subcycles.

Comparison with a cyclothem sequence from a medium-subsidence area in Kentucky (USA) shows that there the same interval contains ap-

proximately 25% of the number of cyclothems observed in the high-subsidence area in the Netherlands, while these cyclothems have relatively comparable thicknesses. In other words, approximately 75% of the cycles have not been preserved or were never deposited due to limited accommodation space. Hence, those cyclothems, i.e. the occasionally preserved ones, are interpreted as similar short-term cycles, with a an duration in order of 20 ky, and the 100 ky estimate in previous studies includes the duration of missing cyclothems.

Influence of tectonics on cyclothem formation

Some authors have proposed that tectonics play a role in the process of cyclothem formation. Tankard (1986) concluded that cyclic pulses of thrusting and subsequent relaxation were entirely responsible for cyclic deposition in the Appalachian Basin. Klein and Willard (1989) viewed glacio-eustasy as the dominant factor but acknowledged that tectonics may have overprinted the eustatic signal and influenced the cyclothem composition by affecting its sandstone content.

In *chapter 3* the tectonic signal in a cyclothem sequence in Poland was isolated by analysing the fluvial sandstone content in relation to subsidence variations controlled by block faulting. It is shown that major fluvial sandstones were only deposited following normal-faulting events. These were probably triggered by thrust loading and resulted in the addition of accommodation space, the amount of which varied over short distances due to block faulting with differential subsidence, not only perpendicular to but also parallel to the faults.

The data show that the accommodation space created during thrust and fault activity was entirely filled by thick, laterally extensive fluvial sand bodies until a level depositional surface had been established again. Upon the cessation of tectonic activity, the depositional environment returned to a muddy fluvial floodplain with small, discontinuous fluvial channels. Hence, thrusting activity in the source area, accompanied by laterally variable subsidence, was responsible for the deposition of major sandstones, whereas regionally constant background subsidence in tectonically quiet periods is reflected in mudstone-dominated fluvial floodplain facies. When the major fluvial sandstone intervals are excluded, three stacked, 50 m thick coal-bounded cycles remain, pointing at overriding glacio-eustatic control.

Palaeogeographical and climatic controls on aeolian-dune and desert-lake cycles

Aeolian and arid-fluvial deposits of the Rotliegend (Permian) were laid down across large parts of Western and Eastern Europe not long after thick Pennsylvanian (Upper Carboniferous) cyclothem successions were formed in that area. A major unconformity, representing some 20 million years, separates the oldest Rotliegend from the youngest Carboniferous deposits. The connection with the ocean was lost, and in the early Permian deposition took place in a dried-out continental depression that may have been a few hundred metres below sea level.

In *chapter 4* aeolian-dune and desert-lake cycles in the western part of the Rotliegend Basin are described from the interval directly above the Carboniferous-Permian unconformity. The aeolian cycles are 5-7 m thick retrogradational sequences (occasionally twice as thick) from aeolian-dune-sandstone to desert-lake-mudstone. The desert-lake cycles are progradational cycles of comparable thickness that consist of mudstones deposits grading upward into mudflat and sandflat facies. Mapping has shown that the aeolian deposits were formed in a large E-W aligned palaeovalley in the Carboniferous substrate. The cycles were probably shaped by lake-level fluctuations. Aeolian dune bodies initially formed at the foot of the palaeohigh that defined the southern (landward) margin of the palaeovalley. When lake level rose, deposition of these dune sands retreated towards the margin, and older sands were drowned by the lake. Once the palaeovalley had been filled and levelled, further lake-level rise resulted in expansion of the lake far landward, not obstructed by palaeohighs, leading to the widespread deposition of desert lake mudstones. Following the rise of lake level, the depositional system progressively built out, filling the lake, and resulting in progradational cycle trends.

Rotliegend cyclical deposition is commonly attributed to orbitally controlled climate fluctuations. The cycle succession studied in *chapter 4* is relatively short and not well dated. Therefore

precise determination of cycle periods was not possible. Based on rough dating estimates the aeolian cycles are considered to be in the range of precession and obliquity cycles. Cycle interference, along the lines described in chapter 2, seems not to have played a role since subsequent cycles have fairly constant thickness. This suggests that lake level was controlled by local climate, dominated by a specific astronomical cycle, instead of eustatic-sea-level cycles which may be the resultant of a number of interfering multi-period sea-level fluctuations.

However, global sea level possibly had some influence in the Rotliegend Basin as indicated by the presence of a number of decametre-scale halite bodies in the basin centre. Although these bodies are typically interpreted as continental halite accumulations, it is tempting to view the Rotliegend Basin as a proto-marine-evaporite basin that experienced the occasional influx of sea water during highstands of global sea level. That would make the Rotliegend a transition phase ultimately leading to permanent marine flooding and basin-wide deposition of the Zechstein evaporites, the subject of chapters 5 and 6 and the next section.

Isostatic subsidence in evaporite basins

Especially since the publication of the deep-desiccated-basin theory, developed to explain the presence of thick Late Miocene evaporite bodies at the bottom of the Mediterranean Sea, certain evaporites have been viewed as the deposits of deep dried-out depressions. This concept is questioned here, one of the reasons being that it ignores that the precipitation of thick, high-density evaporite bodies (especially in the case of anhydrite) in a deep air-filled basin would cause extreme subsidence reactions. Thus, following the deposition of evaporite bodies (often many kilometres thick) a deep basin would remain. In the rock record, however, such evaporites are typically associated with shallow-water and terrestrial deposits.

In *chapter 5* some quantitative aspects of the interaction of deposition and isostatic subsidence in evaporite basins are described. The main conclusions are that these basins were much shallower than often assumed and that some of the more spectacular conditions in the classical model, such as repetitive gigantic waterfalls needed to re-flood the deep desiccated depression, are not required.

It was suggested in *chapter 5* (and published) that *individual* evaporite cycles are in isostatic equilibrium, i.e. that the subsidence response required to compensate for the depositional load takes place during deposition. In *chapter 6*, however, it is shown through modelling that evaporite deposition is so rapid that much of the required subsidence takes place after deposition. Hence, isostatic equilibrium does not apply to individual evaporite cycles but to the stack of cycles as a whole. The Zechstein evaporite succession is a particularly good example, because each cycle is about half as thick as its predecessor. This is exactly what is predicted; when a body of water is replaced by halite (density 2.2 g/cc) that gives a subsidence reaction of half the depth of the water body.

Self-regulatory formation of evaporite cycles

Evaporite cycles are tens to hundreds of metres thick, and are primarily composed of calcium sulphate (gypsum and/or anhydrite), halite and 'potash salts'. The bulk of the sulphate is present in basin-margin platforms, whereas the halite and potash salts are found in the central basin. The formation of evaporite cycles has been variably attributed to extra-basinal processes such as eustatic fluctuations and tectonic movements.

In *chapter 6* an intra-basinal mechanism is proposed and its validity tested using a numerical model. The mechanism concerns the basinward progradation of marginal sulphate platforms and how that affects the outflow of brines to the ocean. Evaporite basins are connected to the ocean by narrow corridors, typically a few tens of kilometres across. Results of the modelling exercise show that progradation of the sulphate platforms across the mouths of the ocean corridors may rapidly cause a reduction of the outflow until the point that the basin becomes halite-saturated. Especially basins with a large surface area, such as the Zechstein Basin with a surface area of ~1,000,000 km^2, may quickly reach halite saturation from which point onward the available accommodation space is quickly filled with halite and potash salts. This is because the evaporation area increases quadratically with

basin radius, while the basin circumference increases only linearly. This means that sulphate platforms prograde more rapidly in large basins, and therefore more quickly obstruct the ocean connection, the width of which is independent of basin size.

Results show, for the Zechstein case, that a 100-m-thick evaporite cycle would be precipitated in less than 100 ky. To form a similar cycle in a small basin such as the Paradox Basin (USA), with a surface area of ~25,000 km^2, almost 400 ky is needed. This means that the closure process in small basins is more likely to be interrupted by external events (e.g. sea-level rise), and it explains why basin-wide halite bodies are found primarily in giant basins such as the Zechstein Basin and the Mediterranean.

Long-term Palaeozoic climate cycles

The Palaeozoic long-term and large-scale climate history is, to a certain degree, reflected in the distribution of certain rock types in time and space, including coal and evaporites. In *chapter 7* the distribution of evaporite basins over time is analyzed, with an emphasis on variations of basin size. Basin-wide evaporites formed in very large basins during the Cambrian, Devonian and Permian and in small to medium-sized basins during the Ordovician-Silurian and Carboniferous. The transitions between periods of extensive and restricted evaporite precipitation were rapid, and it is shown that were controlled by contractions and expansions of the subtropical arid-climate zones. Calculations based on the surface area of halite-bearing evaporite basins indicate that the width of the arid climate zone shifted between 850-1100 km and 1500-3000 km. These fluctuations occurred in cycles of ~120 million years, which may have continued in the Mesozoic, possibly driven by tectonic or astronomical megacycles. It is shown that the major Palaeozoic extinction events, as well as the end-Carboniferous demise of equatorial coal forests coincided with major changes of the width of the arid-climate zones, in particular the change from extensive to restricted aridity.

In the Late Palaeozoic of northwest Europe these long-term climate cycles are reflected by the sudden termination of coal formation during the Asturian (Westphalian D), being replaced by arid fluvial depositional environments. During the Permian this was followed by occasional halite deposition in a continental setting, followed by the widespread precipitation of marine evaporites during the Late Permian.

REFERENCES

Aitken, J.F., and Flint, S.S. (1995) The application of high-resolution sequence stratigraphy to fluvial systems: a case study from the Upper Carboniferous Breathitt Group, eastern Kentucky, USA: Sedimentology, v. 42, 3-30.

Alexander, J., and Leeder, M.R. (1987) Active tectonic control of alluvial architecture, *in* Ethridge, F.G., Flores, R.M. and Harvey, M.D., eds., Recent developments in fluvial sedimentology: Tulsa, USA, SEPM Spec. Publ. 39, 243-252.

Algeo, T.J., and Wilkinson, B.H. (1988) Periodicity of mesoscale Phanerozoic sedimentary cycles and the role of Milankovitch orbital modulation: Journal of Geology, v. 96, 313-322.

Allen, J.L. (1993) Lithofacies relations and controls on deposition of fluvial-deltaic rocks of the Upper Pocahontas Formation in southern West Virginia: Southeastern Geology, v. 33, 131-147.

Almon, W.R. (1981) Depositional environment and diagenesis of Permian Rotliegendes sandstones in the Dutch sector of the southern North Sea, *in* Longstaffe, F.J., ed., Clays and the resource geologist: Edmonton, Mineralogical Association of Canada 7, 119-147.

Al-Zoubi, A., Shulman, H. and Ben-Avraham, Z. (2002) Seismic reflection profiles across the southern Dead Sea basin: Tectonophysics, 346, 61-69.

Anderson, R.Y., Dean, W.A., Kirkland, D.W., and Snider, H.I. (1972) Permian Castile varved evaporite sequence, West Texas and New Mexico: Geological Society of America Bulletin, v. 83, 59-86.

Bailey, R.J., and Clever, J.E. (2003) The Windermere gas field, Blocks 49/9b, 49/4a, UK Southern North Sea, *in* Gluyas, J.G. and Hichens, H.M., eds., United Kingdom Oil and Gas Fields; Commemorative Millennium Volume: London, Geological Society Memoir 20, 893-904.

Bailey, R.J., and Lloyd, D.A. (2001) A log correlation of the Rotliegend of the northern Cleaver Bank High: the search for controls on reservoir sand distribution: Petroleum Geoscience, v. 7, no. 4, 351-358.

Benson, R.H. (1972) Ostracods as indicators of threshold depth in the Mediterranean during the Pliocene, *in* Stanley, D.J., ed., The Mediterranean Sea: Stroudsburg, Pennsylvania, Dowden Hutchinson and Ross, 63-73.

Berger, A., and Loutre, M.F. (1994) Astronomical Forcing through Geological Time, *in* De Boer, P.L. and Smith, D.G., eds., Orbital Control and Cyclic Sequences, IAS Special Publication 19, 15-24.

Berner, R.A. (2003) The long-term carbon cycle, fossil fuels and atmospheric composition: Nature, v. 426, 323-326.

Berner, R.A., and Kothavala , Z. (2001) Geocarb III: A Revised Model of Atmospheric CO_2 over Phanerozoic Time: American Journal of Science, v. 301, no. 2, 182-204.

Blair, T.C., and Bilodeau, W.L. (1988) Development of tectonic cyclothems in rift, pull-apart, and foreland basins: Sedimentary response to episodic tectonism: Geology, v. 16, 517-520.

Blakey, R. (2012) Library of paleogeography: http://www.cpgeosystems.com/paleomaps.html.

Blanc, P.L. (2000) Of sills and straits: a quantitative assessment of the Messinian Salinity Crisis: Deep-Sea Research Part I-Oceanographic Research Papers, 47, 1429-1460.

Bohacs, K.M., and Suter, J. (1997) Sequence stratigraphic distribution of coaly rocks; fundamental controls and paralic examples: AAPG Bulletin, v. 81, 1612-1639.

Brenchley, P.J., Marshall, J.D., Carden, G.A.F., Robertson, D.B.R., Long, D.G.F., Meidla, T., Hints, L. and Anderson, T.F. (1994) Bathymetric and isotopic evidence for a short-lived Late Ordovician glaciation in a greenhouse period: Geology, v. 22, 295-298.

Bridge, J.S., and Leeder, M.R. (1979) A simulation model of alluvial stratigraphy: Sedimentology, v. 26, 617-644.

Bridge, J.S., and Mackey, S.D. (1993) A revised alluvial stratigraphy model, *in* Marzo, M. and Puigdefabregas, C., eds., Alluvial Sedimentation, IAS Special Publication 17, 319-336.

Bryant, M., Falk, P., and Paola, C. (1995) Experimental study of avulsion frequency and rate of

deposition: Geology, v. 23, 365-368.

Burger, K., Hess, J.C., and Lippolt, H.J. (1997) Tephrochronologie mit Kaolin-kohlentonsteinen; mittel zur Korrelation paralischer und limnischer Ablagerungen des Oberkarbons: Geologisches Jahrbuch, v. A 147, 3-39.

Burke, K. (1975) Atlantic evaporites formed by evaporation of water spilled from the Pacific, Tethyan and Southern oceans: Geology, v. 3, 613-616.

Burke, K., and White, G.W. (1978) Evaporites of northern South America and the opening of the Caribbean and Gulf of Mexico: Abstracts with Programs - Geological Society of America, v. 10, 374-375.

Busch, R.M., and Rollins, H.B. (1984) Correlation of Carboniferous strata using a hierarchy of transgressive-regressive units: Geology, v. 12, 471-474.

Busson, G., and Schreiber, B.C. (1997) Sedimentary Deposition in Rift and Foreland Basins in France and Spain (Paleogene and Lower Neogene), Columbia University Press, 479 p.

Butler, J.B. (1975) The West Sole Gas-Field, *in* Woodland, A.W., ed., Petroleum and the Continental Shelf of NW Europe, vol. I, Applied Science Publishers Ltd., Barking, 213-219.

Came, R.E., Eiler, J.M., Veizer, J., Azmy, K., Brand, U., and Weidman, C.R. (2007) Coupling of surface temperatures and atmospheric CO_2 concentrations during the Palaeozoic era: Nature, v. 449, 198-202.

Cameron, T.D.J., Crosby, A., Balson, P.S., Jeffery, D.H., Lott, G.K., Bulat, J., and Harrison, D.J., 1992, Upper Permian, *in* The Geology of the Southern North Sea: London, HMSO/British Geological Survey, 43-54.

Catacosimos, P.A., Daniel., P.A. and Harrison, W.B. (1990) Structure, stratigraphy and petroleum geology of the Michigan Basin, *in* Leighton, M.W. et al., eds., Interior cratonic basins, AAPG Memoir 51, 561-601.

Cercone, K.R. (1988) Evaporative sea-level drawdown in the Silurian Michigan Basin: Geology, 16, 387-390.

Chaboureau, A.-., Donnadieu, Y., Sepulchre, P., Robin, C., Guillocheau, F., and Rohais, S. (2012) The Aptian evaporites of the South Atlantic: a climatic paradox?: Climate of the Past, v. 8, 1047-1058.

Chesnut, D.R. (1997) Eustatic and tectonic control of the Lower and Middle Pennsylvanian strata of the Central Appalachian Basin, *in* Podemski, M., ed., Proceedings of the XIII International Congress on the Carboniferous and Permian: Proceedings of the Polish Geological Institute, v 177, 33-41.

Cita, M.B. (2001) The Messinian salinity crisis in the Mediterranean, *in* Briegel, U. and Xiao, W., eds., Paradoxes in Geology: Amsterdam, Elsevier Science, 353-360.

Clemmenson, L.B., Øxnevad, I.E.I., and De Boer, P.L. (1994) Climatic controls on ancient desert sedimentation: some Palaeozoic and Mesozoic examples from NW Europe and the Western Interior of the USA, *in* De Boer, P.L. and Smith, D.G., eds., Orbital Forcing and Cyclic Sequences, IAS Special Publication 19, 439-457.

Collinson, J.D., Jones, C.M., Blackbourn, G.A., Besly, B.M., Archard, G.M., and McMahon, A.H. (1993) Carboniferous depositional systems of the Southern North Sea. *in* Parker, J.R., ed., Petroleum Geology of Northwest Europe: Proceedings of the 4th Conference: London, Geological Society, 677-687.

Crouch, S.V., Baumgartner, W.E.L., Houlleberghs, E.J.M.J., and Walzebuck, J.P. (1996) Development of a tight gas reservoir by a multiple fracced horizontal well: Ameland-204, the Netherlands, *in* Rondeel, H.E., Batjes, D.A.J. and Nieuwenhuijs, W.H., eds., Geology of Gas and Oil under the Netherlands: Dordrecht, Kluwer Academic Publishers, 93-102.

Crowley, T.J., (1994) Pangean climates, *in* Klein, G.D., ed., Pangea: Paleoclimate, Tectonics, and Sedimentation during Accretion, Zenith, and Breakup of a Supercontinent, Geological Society of America Special Paper 288, 25-40.

Crowley, T.J., and Baum, S.K. (1995) Reconciling Late Ordovician (440 Ma) glaciation with very high (14x) CO_2 levels: Journal of Geophysical Research, v. 100, 1093-1101.

Crugnola, M.T., Renaud, P., and Lafont, F., (1996) Prediction of reservoir facies distribution, Saxonian Lower Slochteren Formation in the central part of the Dutch Offshore, EAGE, 58th Conference and Technical Exhibition, 3–7 June 1996, Amsterdam, abstract L041.

Davies, S.J. (2008) The record of Carboniferous

sea-level change, in low-latitude sedimentary successions from Britain and Ireland during the onset of the late Paleozoic ice age, Geological Society of America Special Paper 441, 187-204.

Davies, N.S., and Gibling, M.R. (2010) Paleozoic vegetation and the Siluro-Devonian rise of fluvial lateral accretion sets: Geology, v. 38, 51-54.

Davydov, V.I., Crowley, J.L., Schmitz, M.D., and Poletaev, V.I. (2010) High-precision U-Pb zircon age calibration of the global Carboniferous time scale and Milankovitch band cyclicity in the Donets Basin, eastern Ukraine: Geochemisty, Geophysics, Geosystems, v. 11, 1-22.

Davydov, V.I., Wardlaw, B.R., and Gradstein, F.M. (2004) The Carboniferous period, *in* Gradstein, F.M., Ogg, J.G. and Smith, A.G., eds., A geological time scale 2004, p. 222-248.

De Boer, P.L., and Smith, D.G. (1994) Orbital control and cyclic sequences, *in* De Boer, P.L. and Smith, D.G., eds., Orbital Control and Cyclic Sequences, IAS Special Publication 19, 1-14.

De Boer, P.L. (1991) Comment: Pennsylvanian time scales and cycle periods: Geology, v. 19, 408-409.

Diegel, F.A., Schuster, D.C., Karlo, J.F., Schoup, R.C., and Tauvers, P.R. (1995) Cenozoic structural evolution and tectonostratigraphic framework of the northern Gulf Coast continental margin, *in* Jackson, M.P.A., ed., Salt Tectonics: A Global Perspective, AAPG Memoir 65; 109-151.

DiMichele, W.A., Pfefferkorn, H.W., and Gastaldo, R.A. (2001) Response of Late Carboniferous and Early Permian plant communities to climate change: Annual Review of Earth and Planetary Sciences, v. 29, 461-487.

Doktor, M. (2007) Conditions of accumulation and sedimentary architecture of the Upper Westphalian Cracow Sandstone Series (Upper Silesia Coal Basin, Poland): Annales Societatis Geologorum Poloniae, v. 77, 219-268.

Drozdzewski, G. (1993) The Ruhr coal basin (Germany): structural evolution of an autochthonous foreland basin: International Journal of Coal Geology, v. 23, 231-250.

Einsele, G. (2000) Sedimentary Basins: Evolution, Facies and Sediment Budget: Berlin, Springer-Verlag, 792 p.

El Tabakh, M., Utha-Aroon, C., and Schreiber, B.C. (1999) Sedimentology of the Cretaceous Maha Sarakham evaporites in the Khorat Plateau of northeastern Thailand: Sedimentary Geology, v. 123, 31-62.

Eros, J.M., Montañez, I.P., Osleger, D.A., Davydov, V.I., Nemyrovska, T.I., Poletaev, V.I., and Zhykalyak, M.V. (2012) Sequence stratigraphy and onlap history of the Donets Basin, Ukraine: Insight into Carboniferous icehouse dynamics: Palaeogeography, Palaeoclimatology, Palaeoecology, v. 313–314, 1-25.

Ethridge, F.G., Wood, L.J., and Schumm, S.A. (1998) Cyclic variables controlling fluvial sequence development: problems and perspectives. in Shanley, K.W. and McCabe, P.J., eds., Relative Role of Eustasy, Climate, and Tectonism in Continental Rocks, SEPM Special Publication 59, 17-29.

Fabbri, A., and Curzi, P. (1979) The Messinian of the Thyrrhenian Sea: Seismic evidence and dynamic implications: Giornale di Geologia, v. 43, 215-248.

Falcon-Lang, H.J. (2001) Pennsylvanian tropical rain forests responded to glacial-interglacial rhythms, v. 32, 689-692.

Falcon-Lang, H.J., Heckel, P.H., Dimichele, W.A., et al. (2011) No major stratigraphic gap exists near the Middle–Upper Pennsylvanian (Desmoinesian–Missourian) boundary in North America: Palaios, v. 26, 125-139.

Faure, K., de Wit, M.J., and Willis, J.P. (1995) Late Permian global coal hiatus linked to ^{13}C-depleted CO_2 flux into the atmosphere during the final consolidation of Pangea: Geology, v. 23, 507-510.

Ferm, J.C., and Weisenfluh, G.A. (1989) Evolution of some depositional models in Late Carboniferous rocks of the Appalachian coal fields: International Journal of Coal Geology, v. 12, 259-292.

Fielding, C.R., Frank, T.D. and Isbell, J.L. (2008) The late Paleozoic ice age-A review of current understanding and synthesis of global-climate patterns: Geological Society of America Special Paper 441, p. 343-354.

Fielding, C.R. (1986) Fluvial channel and overbank deposits from the Westphalian of the

Durham coalfield, NE England: Sedimentology, v. 33, 119-140.

Fielding, C.R. (1984a) A coal depositional model for the Durham Coal Measures of NE England: Journal of the Geological Society, London, v. 141, 919-931.

Fielding, C.R. (1984b) Upper delta plain lacustrine and fluviolacustrine facies from the Westphalian of the Durham coalfield, NE England: Sedimentology, v. 31, 547-567.

Fielding, C.R., and Johnson, G.A.L. (1987) Sedimentary structures associated with extensional fault movement from the Westphalian of NE England: SEPM Special Publication 28, 511-516.

Finnegan, S., Bergmann, K., Eiler, J.M., et al., 2011, The magnitude and duration of Late Ordovician–Early Silurian glaciation: Science, v. 331, 903-906.

Flint, S., Aitken, J., and Hampson, G. (1995) Application of sequence stratigraphy to coal-bearing coastal plain successions: implications for the UK Coal Measures, *in* Whateley, M.K.G. and Spears, D.A., eds., *in* European Coal Geology, Geological Society Special Publication 82, 1-16.

Frakes, L.A., Francis, J.E., and Syktus, J.I. (1992) Climate modes of the Phanerozoic: Cambridge, U.K., Cambridge University Press, 288 p.

Gast, R.E., Dusar, M., Breitkreuz, C., et al. (2010) Rotliegend, *in* Doornenbal, J.C. and Stevenson, A.G., eds., Petroleum Geological Atlas of the Southern Permian Basin: Houten, EAGE, 101-121.

Gebhardt, U., Schneider, J., and Hoffmann, N. (1991) Modelle zur Stratigraphie und Beckenentwicklung im Rotliegenden der Norddeutschen Senke: Geologisches Jahrbuch, v. A127, 405-427.

Geluk, M.C. (2007) Permian, *in* Wong, T.E., Batjes, D.A.J. and De Jager, J., eds., Geology of the Netherlands: Amsterdam, Royal Netherlands Academy of Arts and Sciences, 63-83.

Geluk, M.C., and Mijnlieff, H.F. (2001) Controls on the distribution and thickness of Permian basal Upper Rotliegend sandstones, The Netherlands: probing the limits of the Rotliegend play area (abstract P522), in EAGE, 58th Conference and Technical Exhibition, 26–30 May 2001, Amsterdam, abstract P522.

George, G.T., and Berry, J.K. (1997) Permian (Upper Rotliegend) synsedimentary tectonics, basin development and palaeogeography of the southern North Sea: Geological Society, London, Special Publications, v. 123, 31-61.

George, G.T., and Berry, J.K. (1993) A new lithostratigraphy and depositional model for the Upper Rotliegend of the UK Sector of the Southern North Sea: Geological Society, London, Special Publications, v. 73, 291-319.

Gilbert, G.K. (1890) Lake Bonneville: Government Printing Office, Washington, 438 p.

Glennie, K.W. (1998) Lower Permian-Rotliegend, *in* Glennie, K.W., ed., Petroleum geology of the North Sea; basic concepts and recent advances.: Blackwell Science, Oxford, 137-173.

Glennie, K.W. (1997) Recent advances in understanding the southern North Sea Basin: a summary: Geological Society Special Publication 123, 17-29.

Glennie, K.W., and Provan, D.M.J. (1990) Lower Permian Rotliegend reservoir of the Southern North Sea gas province: Geological Society Special Publication 50, 399-416.

Goldhammer, R.K., Oswald, E.J., and Dunn, P.A. (1994) High-frequency, glacio-eustatic cyclicity in the Middle Pennsylvanian of the Paradox Basin: an evaluation of Milankovitch forcing, *in* De Boer, P.L. and Smith, D.G., eds., Orbital Forcing and Cyclic Sequences, IAS Special Publication 19, 243-283.

Gordon, W.A. (1975) Distribution by latitude of Phaneozoic evaporite deposits: Journal of Geology, v. 83, 671-684.

Gradstein, F.M., Ogg, J.G., and Smith, A.G. (2005) A Geologic Time Scale 2004: Cambridge, U.K., Cambridge University Press, 610 p.

Gradzinski, R., Doktor, M., and Slomka, T. (1995) Depositional environments of the coal-bearing Cracow Sandstone Series (Upper Westphalian), Upper Silesia, Poland: Studia Geologica Polonica, v. 108, 149-170.

Greb, S.F., and Chesnut, D.R., 1992, Transgressive channel filling in the Breathitt Formation (Upper Carboniferous), eastern Kentucky coal field, USA: Sedimentary Geology, v. 75, 209-221.

Greb, S.F., Eble, C.F., and Hower, J.C., 1999, Depositional history of the Fire Clay coal bed (Late Duckmantian), Eastern Kentucky, USA: International Journal of Coal Geology, v. 40, 255-280.

Greb, S.F., Eble, C.F., Hower, J.C., and Andrews, W.M. (2002) Multiple-bench architecture and interpretations of original mire phases—Examples from the Middle Pennsylvanian of the Central Appalachian Basin, USA: International Journal of Coal Geology, v. 49, 147-175.

Greb, S.F., Eble, C.F., and Hower, J.C. (2005) Subtle structural influences on coal thickness and distribution: Examples from the Lower Broas–Stockton coal (Middle Pennsylvanian), Eastern Kentucky Coal Field, USA: Geological Society of America Special Paper 387, 31-50.

Greb, S.F., Pashin, J.C., Martino, R.L., and Eble, C.F. (2008) Appalachian sedimentary cycles during the Pennsylvanian: Changing influences of sea level, climate, and tectonics, Geological Society of America Special Paper 441, 235-248.

Guion, P.D., and Rippon, J.H. (1995) The Silkstone Rock (Westphalian A) from the east Pennines, England: implications for sand body genesis: Journal of the Geological Society, London, v. 152, 819-832.

Guion, P.D., and Fielding, C.R. (1988) Westphalian A and B sedimentation in the Pennine Basin, UK, *in* Besly, B.M. and Kelling, G., eds., Sedimentation in a syn-orogenic basin compex: the Upper Carboniferous of northwest Europe, 153–177.

Guion, P.D., Fulton, I.M., and Jones, N.S. (1995) Sedimentary facies of the coal-bearing Westphalian A and B north of the Wales-Brabant High: Geological Society Special Publication 82, 45-78.

Hampson, G.J., Davies, S.J., Elliott, T., Flint, S.S., and Stollhofen, H. (1999) Incised valley fill sandstone bodies in Upper Carboniferous fluvio–deltaic strata: recognition and reservoir characterization of Southern North Sea analogues: Geological Society, London, Petroleum Geology Conference series, v. 5, 771-788.

Hardie, L.A. (1991) On the significance of evaporites: Annual Review of Earth and Planetary Sciences, v. 19, 131-168.

Hardie, L.A. (1967) The gypsum-anhydrite equilibrium at one atmosphere pressure: American Mineralogist, v. 52, 171-200.

Hardie, L.A., and Lowenstein, T.K. (2004) Did the Mediterranean Sea dry out during the Miocene? A reassessment of the evaporite evidence from DSDP Legs 13 and 42A cores.: Journal of Sedimentary Research, v. 74, 453-461.

Harvey, C.E., Weare, J.H., Hardie, L.A., and Eugster, H.P. (1980) Evaporation of seawater: calculated mineral sequences: Science, v. 208, p. 498-500.

Haszeldine, R.S., and Anderton, R. (1980) A braidplain facies model for the Westphalian B Coal Measures of north-east England: Nature, v. 284, 51-53.

Hays, J.D., Imbrie, J., and Shackleton, N.J. (1976) Variations in the Earth's Orbit: Pacemaker of the Ice Ages: Science, v. 194, 1121-1132.

Heckel, P.H. (2008) Pennsylvanian cyclothems in Midcontinent North America as far-field effects of waxing and waning of Gondwana ice sheets: Geological Society of America Special Paper 441, 275-289.

Heckel, P.H. (1986) Sea-level curve for Pennsylvanian eustatic marine transgressive-regressive depositional cycles along midcontinent outcrop belt, North America: Geology, v. 14, 330-334.

Hedemann, H.A., Maschek, W., Paulus, B., and Plein, E. (1984) Mitteilung zur lithostratigraphischen gleiderung des Oberrotliegenden im Nordwestdeutschen Becken: Deutsche Geologische Gesellschaft Nachrichten, v. 30, 100-107.

Hess, F.S. (2005) Earth Science: Geology, the Environment, and the Universe, Glencoe/McGraw-Hill, 348 p.

Hess, J.C., and Lippolt, H.J. (1986) $^{40}Ar/^{39}Ar$ ages of tonstein and tuff sanidines: new calibration points for the improvement of the Upper Carboniferous time scale: Chemical Geology, v. 59, 143-154.

Holster, W.T. (1979) Rotliegend evaporites, Lower Permian of Northwestern Europe, geochemical confirmation of the nonmarine origin: Erdöl und Kohle, Erdgas, Petrochemie, v. 32, 159-162.

Horne, J.C. (1978) Sedimentary responses to

contemporaneous tectonism, *in* Horne, J.C. and Ferm, J.C., eds., Carboniferous depositional envirnments: Eastern Kentucky and southern West Virginian: South Carolina, Columbia, 27-34.

Howell, J., and Mountney, N., (1997) Climatic cyclicity and accommodation space in arid to semi-arid depositional systems: an example from the Rotliegend Group of the UK southern North Sea: Geological Society Special Publication 123, 63-86.

Hsü, K.J., Cita, M.B., and Ryan, W.B.F. (1973) Late Miocene desiccation of the Mediterranean: Nature, v. 242, 240-244.

Hsü, K.J., Montadert, L., Bernoulli, D., et al. (1977) History of the Mediterranean salinity crisis: Nature, v. 267, 399-403.

Intergeos/TNO (1995) Geological and petrophysical study of the Markham field (report prepared for Energie Beheer Nederland B.V., Heerlen).

Jervey, M.T. (1988) Quantitative geological modeling of siliciclastic rock sequences and their seismic expression, *in* Wilgus, C.K., Hastings, B.S., Posamentier, H., Van Wagoner, J., Ross, C.A. and Kendall, C.G.S.C., eds., Sea-Level Changes: an integrated approach, SEPM Special Publication 42, 47-69.

Jones, N.S., and Glover, B.W. (2005) Fluvial sandbody architecture, cyclicity and sequence stratigraphical setting – implications for hydrocarbon reservoirs: the Westphalian C and D of the Osnabrück and Ibbenbüren area, northwest Germany, *in* Collinson, J.D., Evans, D.J., Holliday, D.W. and Jones, N.S., eds., Carboniferous hydrocarbon geology - The southern North Sea and surrounding onshore areas, Yorkshire Geological Society Occasional Publication 7, 57-74.

Jones, J.A., and Hartley, A.J. (1993) Reservoir characteristics of a braid-plain depositional system: the Upper Carboniferous Pennant Sandstone of South Wales: Geological Society, Special Publication 73, 143-156.

Jureczka, J., and Kotas, A. (1995) Coal deposits - Upper Silesian Coal Basin, *in* Zdanowski, A. and Zakowa, H., eds., The Carboniferous system in Poland: Warsaw, Proceedings of the Polish Geological Institute 148, 164-172.

Kallberg, P., Berrisford, P., Hoskins, B., Simmons, A., Uppala, S., and Lamy-Thepaut, S. (2005) Atlas of the atmospheric general circulation: Reading, U.K., European Centre for Medium-Range Weather Forecasts 19.

Kendall, A.C. (1992) Evaporites, *in* Walker, R.G. and James, N.P., eds., Facies models; response to sea level change: St. Johns, Newfoundland, Canada, Geological Association of Canada, 375-409.

Kendall, A.C., and Harwood, G.M. (1996) Marine evaporites: arid shorelines and basins, *in* Reading, H., ed., Sedimentary Environments: Processes, Facies and Stratigraphy: Oxford, Blackwell, 281-324.

Kendall, C.G.S.C., Lake, P., Weathers, D.H., Lakshmi, V., Althausen, J., and Alsharhan, A.S. (2003) Evidence of rain shadow in the geologic record: repeated evaporite accumulation at extensional and compressional plate margins, *in* Sharhan, A.S., Wood, W.W., Goudie, A.S., Fowler, A. and Abdellatif, E.M., eds., Desertification in the Third Millennium: Lisse, The Netherlands, Swets and Zeitlinger, 45-52.

Klein, G. (1990) Pennsylvanian time scales and cycle periods: Geology, v. 18, 455-457.

Klein, G., and Kupperman, J.B., (1992) Pennsylvanian cyclothems: methods of distinguising tectonically induced changes in sea level from climatically induced changes: Geological Society of America Bulletin, v. 104, 166-175.

Klein, G., and Willard, D.A. (1989) Origin of Pennsylvanian coal-bearing cyclothems of North America: Geology, v. 17, 152-155.

Kotas, A. (1994) Coal-bed methane potential of the Upper Silesian Coal Basin, Poland: Proceedings of the Polish Geological Institute, v. 142, 81 p.

Krijgsman, W., Hilgen, F.J., Raffi, I., Sierro, F.J., and Wilson, D.S. (1999) Chronology, causes and progression of the Messinian salinity crisis: Nature, v. 400, 652-655.

Krijgsman, W., and Meijer, P.T. (2008) Depositional environments of the Mediterranean "Lower Evaporites" of the Messinian salinity crisis: Constraints from quantitative analyses: Marine Geology, v. 253, 73-81.

Langford , R., and Chan, M.A. (1988) Flood surfaces and deflation surfaces within the Cutler Formation and Cedar Mesa Sandstone (Permian), southeastern Utah: Geological Society

of America Bulletin, v. 100, 1541-1549.

Leeder, M.R., and Gawthorpe, R.L., 1987, Sedimentary models for extensional tilt-block/half-graben basins: Geological Society Special Publication 28, 139-152.

Leeder, M.R., Mack, G.H., Peakall, J., and Salyards, S.L. (1996) First quantitative test of alluvial stratigraphic models: Southern Rio Grande rift, New Mexico: Geology, v. 24, 87-90.

Lucia, F.J. (1972) Recognition of evaporite-carbonate shoreline sedimentation: SEPM Special Publication 16, 160-191.

Lyons, P.C., and Wagner, R.H. (1995) The Stephanian of North America: Early 1900s controversies and problems. in Lyons, P.C., Morey, E.D. and Wagner, R.H., eds., Historical perspective of early twentieth century Carboniferous paleobotany: Boulder, Colorado, Geological Society of America Special Paper 185, 293-314.

Lyons, P.C. and 7 others (1992), An Appalachian isochron: a kaolinized Carboniferous air-fall volcanic-ash deposit (tonstein): Geological Society of America Bulletin, v. 104, 1515-1527.

Lyons, P.C., Krogh, T.E., Kwok, Y.Y., Davis, D.W., Outerbridge, W.F., and Evans Jr., H.T. (2006) Radiometric ages of the Fire Clay tonstein [Pennsylvanian (Upper Carboniferous), Westphalian, Duckmantian]: A comparison of U–Pb zircon single-crystal ages and $^{40}Ar/^{39}Ar$ sanidine single-crystal plateau ages: International Journal of Coal Geology, v. 67, 259-266.

Mack, G.H., and James, W.C. (1993) Control of basin symmetry on fluvial lithofacies, Camp Rice and Palomas Formations (Plio-Pleistocene), southern Rio Grande rift, USA, *in* Marzo, M., and Puigdefabregas, C.. eds., Alluvial Sedimentation, IAS Special Publication 17, 439-449.

Mackey, S.D., and Bridge, J.S. (1995) Three-dimensional model of alluvial stratigraphy; theory and applications: Journal of Sedimentary Research, v. 65, 7-31.

Manzi, V., Lugli, S., Ricci Lucchi, F., and Roveri, M. (2005) Deep-water clastic evaporites deposition in the Messinian Adriatic foredeep (northern Apennines, Italy): did the Mediterranean ever dry out?: Sedimentology, v. 52, 875-902.

Martin, J.H., and Evans, P.F. (1988) Reservoir modeling of marginal aeolian/sabkha sequences, Southern North Sea (UK Sector): SPE 1988 Annual Technical Conference and Exhibition, Houston, Texas, paper 18155.

Mawson, M., and Tucker, M.E. (2009) High-frequency cyclicity (Milankovitch and millennial-scale) in slope-apron carbonates: Zechstein (Upper Permian), North-east England: Sedimentology, v. 56, 1905-1936.

Maynard, J.R., and Gibson, J.P., (2001) Potential for subtle traps in the Permian Rotliegend of the UK Southern North Sea: Petroleum Geoscience, v. 7, 301-314.

Maynard, J.R., and Leeder, M.R. (1992) On the periodicity and magnitude of Late Carboniferous glacio-eustatic sea-level changes: Journal of Geological Society of London, v. 149, 303-311.

McCabe, P.J. (1984) Depositional Environments of Coal and Coal-Bearing Strata, *in* Rahmani, R.A. and Flores, R.M., eds., Sedimentology of Coal and Coal-Bearing Sequences, IAS Special Publication 7, 11-42.

McGhee, G.R., Sheehan, P.M., Bottjer, D.J., and Droser, M.L. (2012) Ecological ranking of Phanerozoic biodiversity crises: The Serpukhovian (early Carboniferous) crisis had a greater ecological impact than the end-Ordovician: Geology, v. 40, 147-150.

Menning, M., Weyer, D., Drozdzewski, G., Van Amerom, H.W.J., and Wendt, I. (2000) A Carboniferous time scale 2000: discussion and use of geological parameters as time indicators from Central and Western Europe: Geologisches Jahrbuch, v. A156, 3-44.

Michaelsen, P., and Henderson, R.A. (2000) Facies relationships and cyclicity of high-latitude, Late Permian coal measures, Bowen Basin, Australia: International Journal of Coal Geology, v. 44, 19-48.

Mijnlieff, H.F., and Geluk, M.C. (2011) Palaeotopography-governed sediment distribution—a new predictive model for the Permian Upper Rotliegend in the Dutch sector of the Southern Permian Basin, *in* The Permian Rotliegend of the Netherlands, Grotsch, J. and Gaupp, R., eds., SEPM Special Publication 98, 147-159.

Montañez, I.P. and 8 others (2007) CO_2-forced climate and vegetation instability during Late Paleozoic deglaciation: Science, v. 315, 87-91.

Myres, J.C., Jones, A.F., and Towart, J.M. (1995) The Markham Field: UK Blocks 49/5a and 49/10b, Netherlands Blocks J3b and J6: Petroleum Goescience, v. 1, 303-309.

Nadon, G.C. (1998) Magnitude and timing of peat-to-coal compaction: Geology, v. 26, 727-730.

Neev, D. and Emery, K.O. (1967) The Dead Sea depositional processes and environments of evaporites: Geological Survey of Israel Bulletin 41, 147 p.

Nesteroff, W.D. (1973) Mineralogy, petrography, distribution and origin of the Messinian Mediterranean evaporites, *in* Ryan, W.B.F., Hsu, K.J. and Cita, M.B., eds., Initial report DSDP Leg 13, 673-694.

NLOG (2010) Public online database - oil and gas exploration and production in the Netherlands and the Dutch sector of the North Sea continental shelf: http://www.nlog.nl.

Norman, S.E., and Chase, C.G. (1986) Uplift of the shores of the western Mediterranean due to Messinian desiccation and flexural isostacy: Nature, v. 322, 450-451.

Northrup, C.J. and Snyder-Walter, S. (2000) Transpressional and transtensional tectonics of the southern Ural Orogen: AAPG Annual meeting expanded abstracts, 107-108.

Nurmi, R.D., and Friedman, G.M. (1977) Sedimentology and depositional environments of basin-center evaporites, Lower Salina Group (Upper Silurian), Michigan Basin, *in* Fisher, J.H., ed., Reefs and Evaporites; Concepts and Depositional Models, AAPG Memoir 5, 23-52.

Ochsenius, C. (1877) Die Bildung der Steinsalzlager und ihrer Mutterlaugensalze: Halle, Pfeffer.

Orszag-Sperber, F., Harwood, G., Kendall, A. and Purser, B.H. (1998) A review of the evaporites of the Red Sea-Gulf of Suez rift, *in* Purser, B.H. and Bosence, D.W.J., Sedimentation and Tectonics of Rift Basins: Red Sea-Gulf of Aden, Chapman and Hall, London, 409-426.

Page, A.A., Zalasiewicz, J.A., Williams, M. and Popov, L.E. (2007) Were transgressive black shales a negative feedback modulating glacioeustasy in the Early Palaeozoic Icehouse? *in* Williams M.M. et al., eds., Deep Time Perspectives on Climate Change: Marrying the Signal from Computer Models and Biological Proxies, Geological Society of London, 123-156.

Parrish, J.T., Ziegler, A.M., and Scotese, C.R. (1982) Rainfall patterns and the distribution of coals and evaporites in the Mesozoic and Cenozoic: Palaeogeography, Palaeoclimatology, Palaeoecology, v. 40, 67-101.

Peterson, J.A. and Hite, R.J. (1969) Pennsylvanian evaporite-carbonate cycles and their relation to petroleum occurrence, Southern Rocky Mountains, AAPG Bulletin, v. 53, 884-908.

Posamentier, H.W., and Allen, G.P. (1993) Variability of the sequence stratigraphic model: effects of local basin factors: Sedimentary Geology, v. 86, 91-109.

Poulsen, C.J., Pollard, D., Montañez, I.P., and Rowley, D. (2007) Late Paleozoic tropical climate response to Gondwanan deglaciation: Geology, v. 35, 771-774.

Raup, D.M., and Sepkoski, J.J. (1982) Mass Extinctions in the Marine Fossil Record: Science, v. 215, 1501-1503.

Raymo, M.E., Ruddiman, W.F., Shackleton, N.J., and Oppo, D.W. (1990) Evolution of Atlantic-Pacific $\delta^{13}C$ gradients over the last 2.5 m.y.: Earth and Planetary Science Letters, v. 97, 353-368.

Reed, J.M. (1994) Probable Cretaceous-to-Recent rifting in the Gulf of Mexico Basin: Journal of Petroleum Geology, 17, 429-444.

Retallack, G.J., Veevers, J.J., and Morante, R. (1996) Global coal gap between Permian–Triassic extinction and Middle Triassic recovery of peat-forming plants: Geological Society of America Bulletin, v. 108, 195-207.

Rice, C.L., Currens, J.C., Henderson, J.A., and Nolde, J.E. (1987) The Betsie Shale Member - a datm for exploration and stratigraphic analysis of the lower part of the Pennsylvanian in the central Appalachian Basin: U.S. Geological Survey Bulletin, v. 1834, 17 p.

Richter-Bernberg, G. (1985) Zechstein-Anhydrite: Facies und Genese: Geologisches Jahrbuch, v. 85, p. 1-82.

Riley, N.J., and Turner, N. (1995) The Correlation

of mid-Westphalian marine bands between the central Appalachian Basin (USA) and the United Kingdom, *in* Podemski, M., Dybova-Jachowicz, S., Jaworowski, K., Jureczka, J. and Wagner, R., eds., The XIII International Congress on the Carboniferous and Permian: Krakow, Polish Geological Institute, 122 p.

Rippon, J.H. (1996) Sand body orientation, palaeoslope analysis and basin-fill implications in the Westphalian A-C of Great Britain: Journal of the Geological Society, London, v. 153, 881-900.

Rodríguez-López, J.P., Meléndez, N., De Boer, P.L., and Soria, A.R. (2012) Controls on marine–erg margin cycle variability: aeolian–marine interaction in the mid-Cretaceous Iberian Desert System, Spain: Sedimentology, v. 59, 466-501.

Rohde, R.A., and Muller, R.A. (2005) Cycles in fossil diversity, v. 434, 208-210.

Ronov, A.B. (1976) Global carbon geochemistry, volcanism, carbonate accumulation, and life: Geochemistry International, v. 13, 172-195.

Ronov, A.B., Khain, V.E., Balukhovsky, A.N., and Seslavinsky, K.B. (1980) Quantitative analysis of Phanerozoic sedimentation: Sedimentary Geology, v. 25, 311-325.

Royer, D.L. (2006) CO_2-forced climate thresholds during the Phanerozoic: Geochimica et Cosmochimica Acta, v. 70, 5665-5675.

Ruddiman, W.F. (2006) Orbital changes and climate: Quaternary Science Reviews, v. 25, 3092-3112.

Ryan, W.B.F. (1976) Quantitative evaluation of depth of western Mediterranean before, during and after Late Miocene salinity crisis.: Sedimentology, v. 23, 791-813.

Rygel, M.C., Fielding, C.R., Frank, T.D. and Birgenheier, L.P. (2008) The magnitude of Late Paleozoic glacioeustatic fluctuations: a synthesis: Journal of Sedimentary Research, v. 78, 500-511.

Sannemann, D., Zimdars, J., and Plein, E. (1978) Der basale Zechstein (A2-T1) zwischen Weser und Ems: Zeitschrift der Deutschen Geologischen Gesellschaft, v. 129, 33-69.

Schreiber, B.C., and Hsü, K.J. (1980) Evaporites, *in* Hobson, G.D., ed., Developments in Petroleum Geology 2: Amsterdam, Elsevier, p. 87-138.

Scotese, C.R. (2001) Atlas of Earth History, PALEOMAP Project: Arlington, Texas, University of Texas at Arlington, 52 p.

Scott, M. (1985) This is the sea, *on* The Waterboys: This is the Sea, Chrysalis Records, London, track 9: 6:31 min.

Shanley, K.W., and McCabe, P.J. (1994) Perspectives on the sequence stratigraphy of continental strata: AAPG Bulletin, v. 78, p. 544-568.

Sharples, D.M., Myres, J.C., Morgan, C.L., and Kuzemko, N.C.J. (1994) The Markham Field, a trans-median development, in Society of Petroleum Engineers, European Petroleum Conference, SPE paper 028839.

Shaviv, N.J., and Veizer, J. (2003) Celestial driver of Phanerozoic climate?: GSA Today, v. 13, 4-10.

Siesser, W.G. (1978) Leg 40 Results in relation to continental shelf and onshore geology, *in* Bolli, H.M. and Ryan W.B.F., Initial Reports of the Deep Sea Drilling Project, 965-979.

Sonnenfeld, P. (1985) Models of Upper Miocene evaporite genesis in the Mediterranean region, *in* Stanley, D.J. and Wezel, F.C., eds., Geological evolution of the Mediterranean Basin: New York, Springer-Verlag, 323-346.

Sonnenfeld, P. (1984) Brines and Evaporites: Orlando, Academic Press, 613 p.

Sonnenfeld, P., and Kendall, C.G.S.C. (1989) Marine evaporites; genesis, alteration, and associated deposits: Geology, v. 17, 573-574.

Stanley, M.S. (1986) Earth and life through time: W.H Freeman and company, New York, 690 p.

Steiner, J., and Grillmair, E., March (1973) Possible Galactic Causes for Periodic and Episodic Glaciations: Geological Society of America Bulletin, v. 84, 1003-1018.

Stevenson, G.M. and Baars, D.L. (1986) The paradox; a pull-apart basin of Pennsylvanian age. *in* Peterson, J.A., ed., Paleotectonics and Sedimentation, AAPG Memoir 41, 513-539.

Tankard, A.J. (1986) Depositional response to foreland deformation in the Carboniferous of eastern Kentucky: AAPG Bulletin, v. 70, 853-868.

Tay, P.L., Lonergan, L., Warner, M., and Jones, K.A. (2002) Seismic investigation of thick evaporite deposits on the central and inner unit of the Mediterranean Ridge accretionary complex: Marine Geology, v. 186, 167-194.

Taylor, J.C.M. (1998) Upper Permian, Zechstein, *in* Glennie, K.W., ed., Petroleum Geology of the North Sea; Basic Concepts and Recent Advances.: Oxford, Blackwell, 174-210.

Tucker, M.E. (1991) Sequence Stratigraphy of Carbonate Evaporite Basins - Models and Application to the Upper Permian (Zechstein) of Northeast England and Adjoining North-Sea: Journal of the Geological Society, v. 148, p. 1019-1036.

Tucker, R.M., and Cann, J.R. (1986) A model to estimate the depositional brine depth of ancient halite rocks: Implications for ancient subaqueous evaporite depositional environments: Sedimentology, v. 33, 401-412.

Van Adrichem Boogaert, H.A., and Kouwe, W.F.P. (1993) Stratigraphic Nomenclature of the Netherlands: Haarlem, Mededelingen Rijks Geologische Dienst 50.

Van Asselen, S., Stouthamer, E., and Smith, N.D. (2010) Factors controlling peat compaction in alluvial floodplains: a case study in the cold-temperate Cumberland marshes, Canada: Journal of Sedimentary Research, v. 80, 155-166.

Van Bergen, F., Krzystolik, P., van Wageningen, N., et al. (2009) Production of gas from coal seams in the Upper Silesian Coal Basin in Poland in the post-injection period of an ECBM pilot site: International Journal of Coal Geology, v. 77, 175-187.

Van Bergen, F., Pagnier, H., and Krzystolik, P. (2006) Field experiment of enhanced coalbed methane-CO_2 in the upper Silesian basin of Poland: Environmental Geosciences, v. 13, 201-224.

Van den Belt, F.J.G., and De Boer, P.L. (2007) A shallow-basin model for 'saline giants' based on isostasy-driven subsidence, in Nichols, G., Williams, E., and Paola, C., eds., Sedimentary Processes, Environments and Basins, IAS Special Publication 38, 241-252.

Van der Baan, D. (1990) Zechstein reservoirs in the Netherlands: Geological Society Special Publication 50, 379-398.

Van der Laar, J.G.M., and Fermont, W.J.J. (1989) On-shore palynology of the Carboniferous of the Netherlands: Mededelingen Rijks Geologische Dienst, v. 3, 35-52.

Van Hulten, F.F.N. (2007) Exploration risk reduction from gas field information, the Netherlands (extended abstract): EAGE, 69th Conference and Technical Exhibition, London, abstract C-036.

Van Wees, J.-D., Stephenson, R.A., Ziegler, P.A., et al. (2000) On the origin of the Southern Permian Basin, Central Europe: Marine and Petroleum Geology, v. 17, 43-59.

Vandenbroucke, T.R.A., Armstrong, H.A., Williams, M. et al. (2010) Polar front shift and atmospheric CO_2 during the glacial maximum of the Early Paleozoic Icehouse: Proceedings of the National Academy of Sciences, v. 107, 14983-14986.

Veevers, J.J., and Powell, C.M., 1987, Late Paleozoic glacial episodes in Gondwanaland reflected in transgressive–regressive depositional sequences in Euramerica: Geological Society of America Bulletin, v. 98, 179-196.

Veizer, J., Godderis, Y., and François, L.M. (2000) Evidence for decoupling of atmospheric CO_2 and global climate during the Phanerozoic eon: Nature, v. 408, 698-701.

Verdier, J.P. (1996) The Rotliegend sedimentation history of the southern North Sea and adjacent countries, *in* Rondeel, H.E., Batjes, D.A.J. and Nieuwenhuijs, W.H., eds., Geology of Gas and Oil under the Netherlands: Dordrecht, Kluwer Academic Publishers, 45-56.

Villeneuve, M. (2004) Radiogenic isotope geochronology, *in* Gradstein, F.M., Ogg, J.G. and Smith, A.G., eds., A geological time scale 2004, Cambridge, Cambridge University Press, 87-95.

Visser, W.A. (1955) The Upper Permian in the Netherlands: Leidse Geologische Mededelingen, v. 20, 186-194.

Volozh, Y.A., Antipov, M.P., Brunet, M.-., Garagash, I.A., Lobkovskii, L.I., and Cadet, J.-. (2003) Pre-Mesozoic geodynamics of the Precaspian Basin (Kazakhstan): Sedimentary Geology, v. 156, 35-58.

Wanless, H.R., and Shepard, F.P. (1936) Sea level and climatic changes related to late Paleozoic cycles: Geological Society of America Bulletin, v. 47, 1177-1206.

Warren, J.K. (2006) Evaporites: Sediments, Resources and Hydrocarbons: Berlin, Springer-Verlag, 1036 p.

Warren, J.K. (2010) Evaporites through time:

Tectonic, climatic and eustatic controls in marine and nonmarine deposits: Earth-Science Reviews, v. 98, 217-268.

Waters, C.N., and Condon, D.J. (2012) Nature and timing of Late Mississippian to Mid-Pennsylvanian glacio-eustatic sea-level changes of the Pennine Basin, UK: Journal of the Geological Society, London, v. 169, 37-51.

Watts, A.B. (2001) Isostasy and Flexure of the Lithosphere: Cambridge, Cambridge University Press, 458 p.

Weisenfluh, G.A., and Ferm, J.C. (1984) Geologic controls on deposition of the Pratt seam, Black Warrior Basin, Alabama, U.S.A., *in* Rahmani, R.A. and Flores, R.M., eds., Sedimentology of Coal and Coal-Bearing Sequences, IAS Special Publication 7, 317-330.

Weller, J.M. (1930) Cyclical sedimentation of the Pennsylvanian period and its significance: Journal of Geology, v. 38, 97-135.

Wilkinson, B.H., Merrill, G.K., and Kivett, S.J., 2003, Stratal order in Pennsylvanian cyclothems: Geological Society of America Bulletin, v. 115, 1068-1087.

Williams-Stroud, S. (1994) The evolution of an inland sea of marine origin to a non-marine saline lake: the Pennsylvanian Paradox Salt.: SEPM Special Publication 50, 293-306.

Worsley, T.R., Nance, R.D., and Moody, J.B. (1986) Tectonic cycles and the history of the earth's biogeochemical and paleoceanograhic record: Paleoceanography, v. 1, 233-263.

Yang, C., and Kouwe, W.F.P. (1995) Wireline log-cyclicity analysis as a tool for dating and correlating barren strata: an example from the Upper Rotliegend of the Netherlands: Geological Society Special Publication 89, 237-259.

Zdanowski, A., and Zakowa, H. (1995) The Carboniferous system of Poland: Warsaw, Proceedings of the Polish Geological Institute 148, 215 p.

Zharkov, M.A. (1981) History of Paleozoic Salt Accumulation: Berlin, Springer-Verlag, Berlin, 308 p.

Zharkov, M.A. (1984) Paleozoic salt bearing formations of the world. Springer-Verlag, Berlin, 427 p.

Ziegler, P.A. (1990) Geological Atlas of Western and Central Europe. Shell Internationale Petroleum Maatschappij, Den Haag, 239 p.

Ziegler, A.M., Eshel, G., Rees, P.M., Rothfus, T.A., Rowley, D.B., and Sunderlin, D. (2003) Tracing the tropics across land and sea: Permian to present: Lethaia, v. 36, 227-254.

SAMENVATTING

Sedimentaire cycli in steenkoolbekkens

Het is precies een eeuw geleden dat de Amerikaanse geoloog Udden voor het eerst de sterk cyclische afzettingen in het Carboon van het oosten van de Verenigde Staten beschreef: afwisselingen van mariene kleien, terrestrische kleien en zanden, en steenkoollagen. Deze koolhoudende sedimentaire cycli werden later *cyclothemen* gedoopt. Het Carboon van NW Europa, waaronder de steenkoollagen in Zuid Limburg, bestaat uit vergelijkbare cyclothemen, terwijl de gebieden tijdens het Carboon (~300 miljoen jaar geleden) zo'n drieduizend km van elkaar waren verwijderd.

De verklaring is dat beide gebieden in die tijd rond de evenaar lagen, waar tropische begroeiïng de vorming van dikke veenpakketten mogelijk maakte. Begraving tot enige kilometers diep in de aardkorst gedurende de daarop volgende miljoenen jaren zorgde ervoor dat deze veenpakketten werden omgezet in steenkool.

Steenkool komt veel voor in de aardkorst, maar nooit in de hoeveelheden die we kennen uit het Carboon. Dit heeft alles te maken met de mega-ijstijd die toen plaatsvond en verantwoordelijk was voor versnelde veenafzetting. Tijdens ijstijden beweegt de zeespiegel als gevolg van smelten en aangroeien van ijs, en een stijgende zeespiegel bevordert de vorming en de preservatie van veen omdat het stijgende water de plantenresten afsluit van zuurstof en daarmee de afbraak door bacteriën en ander microleven sterk afremt.

Het smelten en aangroeien van ijskappen wordt in sterke mate bepaald door de hoeveelheid zonneenergie die de aarde absorbeert en die o.a. varieert omdat de baan van de aarde om de zon niet constant van vorm is. Deze fluctueert tussen cirkelvormig en elliptisch (eccentriciteit) met een periode van *ca*. 100 duizend jaar. Daarnaast verandert de hoek die de aardas maakt met het baanvlak van de aarde (obliquiteit) met een periode van ongeveer 40 duizend jaar, en maakt de aardas een tollende beweging met een periode van ongeveer 20 duizend jaar (precessie).

De verwachting van geologen was dat de diktevariaties in opeenvolgende cyclothemen de zeespiegelbewegingen zouden reflecteren, maar de vele studies die daaraan de laatste eeuw zijn gewijd hebben dat niet kunnen bewijzen.

In *hoofdstuk 2* wordt aangetoond dat cyclothemen wel degelijk door astronomisch gecontroleerde zeespiegelvariaties worden gecontroleerd, maar dat door interferentie van een aantal zeespiegelfluctuaties, ieder met haar eigen vaste periode, de dikte van de uiteindelijke cyclothemen niet *kan* overeenkomen met de periode van precessie, obliquiteit of eccentriciteit (toeval uitgezonderd). Deze periodes kunnen echter wel zichtbaar gemaakt worden door de variatie in de samenstelling van de opeenvolgende cyclothemen te bepalen. Dit is gedaan voor cyclothemen uit de ondergrond van Limburg en uit die studie blijkt dat zeespiegelfluctuaties ten tijde van het Carboon o.a. gekenmerkt werden door grootschalige variaties met een periode van 95 duizend jaar en 413 duizend jaar. Dat signaal is gebruikt om vast te stellen dat de belangrijkste Europese koolperiode (het Westfaal) ongeveer 7 miljoen jaar heeft geduurd.

In *hoofdstuk 3* is gekeken naar de mate waarin tectonische activiteit (zoals breukbewegingen en gebergtevorming) in en rond bekkens waar veenvorming plaatsvond de registratie van het zeespiegelsignaal in de cyclothemenopeenvolging heeft verstoord. Daartoe is het gesteentepakket uit een aantal boringen in een steenkolenmijn in Zuid Polen met elkaar vergeleken. In dit gebied kantelde de ondergrond tijdens sedimentatie, waardoor de gesteentekolom binnen hetzelfde tijdsinterval op sommige plaatsen significant dikker is dan op andere plaatsen. Er is aangetoond dat op iedere plek de hoeveelheid klei en kool gelijk is en dat alle extra daling heeft geresulteerd in de afzetting van zand. Wanneer deze zandsteenhoeveelheid van de rest van de opeenvolging wordt afgetrokken, blijven de cyclothemen over, zoals deze zouden zijn geweest wanneer alleen zeespiegelcontrole belangrijk was geweest.

De observatie dat 100% van de door kanteling ontstane afzettingsruimte gevuld is met zand is niet in overeenstemming met bestaande modellen (70-90%) en leidt tot een ongebruikelijke,

maar eenvoudige verklaring. Door kanteling ontstaat een gradient, met een component in de stroomafwaartse richting, waardoor fijnkorrelig sediment (dat weinig stromingsenergie nodig heeft om in suspensie te blijven) een tijd lang in het geheel niet afgezet wordt.

Sedimentaire cycli in evaporietbekkens

Evaporietcycli zijn opeenvolgingen van zouten die zijn ontstaan door indamping van voormalige binnenzeeën. Het gaat vooral om anhydriet ('gips'), haliet (keukenzout) en 'potas'. In de Nederlandse ondergrond bevindt zich het Zechstein zout, dat zich uitstrekt van Engeland tot Polen, en gevormd werd tijdens het Perm (~250 miljoen jaar geleden), toen dit deel van Europa ten noorden van de evenaar lag in de subtropische, aride klimaatszone.

Bestaande modellen verklaren niet goed waarom evaporietpakketten uit herhalingen van steeds dezelfde zouten bestaan; ze zijn niet eenduidig en gaan uit van toevallige, vaak extreme omstandigheden, die niet in overeenstemming zijn met het wereldwijd veelvuldig voorkomen van evaporiet-lichamen.

Een veelgebruikt model is dat van de *diepe, uitgedroogde zee*. Stelt u zich de Middellandse Zee voor, zes miljoen jaar geleden, en zo'n drie kilometer diep. Wanneer de toch al nauwe Straat van Gibraltar door tektoniek verder zou worden gesloten, zou de geblokkeerde aanvoer van zeewater resulteren in het geleidelijk verdampen van de Middellandse Zee en zouden de opgeloste zouten neerslaan op de bodem. Dit proces zou zich echter tientallen malen moeten herhalen om het kilometers-dikke zoutpakket te vormen. Vanuit tektonisch oogpunt is dit moeilijk te verklaren.

Daarnaast houdt het model geen rekening met het effect van de afzetting van een enorme gesteentemassa op een buigzame aardkorst. Volgens dit 'isostatisch effect' zou de afzetting van dikke pakketten zout gevolgd moeten worden door een sterke daling van de aardkorst, waardoor na evaporietafzetting een diep bekken zou moeten achterblijven. Voor de Middellandse Zee is dit geen onoverkomelijk probleem (het is immers een kilometers diepe zee), maar in de regel worden evaporieten niet afgedekt door diep-water sedimenten.

In *hoofdstuk 5* wordt aangetoond dat de isostatische daling al tijdens afzetting plaats vindt, wat inhoudt dat een groot deel van de benodigde afzettingsruimte door de evaporietneerslag zelf gecreëerd wordt, en diepe depressies in het geheel niet nodig zijn. In *hoofdstuk 6* is dit idee verder uitgewerkt. Daarin wordt aannemelijk gemaakt dat de typische cycliciteit die in veel evaporietbekkens wordt waargenomen, waarbij iedere cyclus half zo dik is als de voorafgaande, het gevolg is van isostatische compensatie tussen twee opeenvolgende cycli, en dat tektonische bekkendaling in het geheel niet bijdraagt aan de dikte van het evaporiet pakket.

In *hoofdstuk 6* wordt een eenvoudig mechanisme beschreven dat zonder enige invloed van buiten de vorming van evaporietcycli in het bekken verklaart. Wanneer er maar een smalle verbinding bestaat met de oceaan, en een bekken zich grotendeels in een droge klimaatszone bevindt, zal langs de bekkenrand gips neerslaan omdat water door verdamping het bekken verlaat en er voortdurend vers zeewater uit de oceaan wordt aangevoerd. Modelresultaten laten zien dat dit ervoor kan zorgen dat de oceaanverbinding geleidelijk wordt afgeknepen, waardoor de afvoer van zout water in toenemende mate gehinderd wordt en het bekken steeds zouter wordt. Dit leidt er uiteindelijk toe dat niet alleen gips, maar na verloop van tijd ook haliet en daarna potas zouten neerslaan, resulterend in de typische evaporietcyclus.

Paleozoische klimaatsreconstructie

In *hoofstuk 7* worden veen- en evaporietafzetting gedurende het Paleozoicum (542-251 miljoen jaar geleden) bestudeerd vanuit het perspectief van grootschalige klimaatontwikkeling. Uit de verdeling van grote evaporietbekkens over de tijd blijkt dat de breedte van de subtropische klimaatgordel heeft gevarieerd tussen ~1000 km en ~2000 km volgens cycli van ongeveer 120 miljoen jaar. De overgangen tussen deze twee situaties vallen samen met massa extincties, wat suggereert dat deze extincties klimaatgedreven zijn. Tijdens de Laat-Paleozoïsche klimaatcyclus valt de overgang van een smalle naar een brede droge gordel samen met de abrupt relocatie van veenbossen van de equatoriale naar de gematigde klimaatzone.

ABOUT THE AUTHOR

Frank van den Belt was born on 2 November 1969 in Zwolle, the Netherlands. After receiving his Atheneum B diploma in 1989, he studied geology at the Department of Earth Sciences of Utrecht University. He graduated on a thesis on the reservoir architecture and cyclicity of Pennsylvanian coal-bearing fluvio-deltaics in Kentucky (USA) in 1995.

Over the years Frank has worked as a reservoir geologist at Shell's research lab in Rijswijk (KSEPL), Panterra Geoconsultants in Warmond/Leiderdorp and TNO/Geological Survey of the Netherlands He studied sedimentary rocks across the globe, including the Cenozoic of the Niger Delta; the Permian of Oman; the Neogene of NE Spain; the Pennsylvanian and Permo-Triassic of Kazachstan; the Pennsylvanian of Kentucky (USA), Ukraine and Poland, and almost the entire Phanerozoic in the North Sea Basin.

Frank works as an independant geological consultant and teaches chemistry, physics and science at a secondary school in Epe. He is a guest researcher at the sedimentology research group of the Department of Earth Sciences, Utrecht University.

John's Creek road cut near Pikeville, US-119 exit Bent Branch/Phelps, 1 September 2009 (Photograph: T. van Hoof)

PUBLICATIONS

Peer-reviewed journals and book chapters

F.J.G. van den Belt and F.F.H. van Hulten (2011) *Sedimentary architecture and paleogeography of Lower Slochteren aeolian cycles from the Rotliegend desert-lake margin (Permian), the Markham area, Southern North Sea*, *in* The Permian Rotliegend of the Netherlands (eds. J. Grotsch and R. Gaupp), SEPM Special Publication 98, 161-176.

F.J.G. van den Belt and P.L. De Boer (2007) *A shallow-basin model for 'saline giants' based on isostasy-driven subsidence*, *in* Sedimentary processes, environments and basins (eds. G.Nichols, E. Williams and C. Paola), IAS Special Publication 38, 241-252.

J.P. Barde, P. Chamberlain, M. Galavazi, P. Gralla, J. Harwijanto, J. Marsky and F.J.G. van den Belt (2002) *Sedimentation during halokinesis: Permo-Triassic reservoirs of the Saigak Field, Precaspian Basin, Kazakhstan*, Petroleum Geoscience, v. 8, 177-187.

E.S. Dvorjanin, A.P. Samoyluk, M.G. Egurnova, N.Y. Zaykovsky, Y.Y. Podladchikov, F.J.G. van den Belt and P.L. de Boer (1996) *Sedimentary cycles and paleogeography of the Dnieper Donets Basin during the late Visean-Serpukhovian based on multiscale analysis of well logs*, Tectonophysics, v. 268, 169-187.